

Evaluation of the Food-Energy-Water nexus through case studies in the United States and East Africa

Submitted in partial fulfillment of the requirements for

the degree of

Doctor of Philosophy

In

Engineering and Public Policy

Jorge L. Izar-Tenorio

B.S., Chemical Engineering, Autonomous University of San Luis Potosi
M.S. Sustainable Energy Technology, Delft University of Technology

Carnegie Mellon University
Pittsburgh, PA

May 2021

© Copyright 2021
Jorge L. Izar-Tenorio
All Rights Reserved

Acknowledgments

I am grateful to my advisor, Paulina, for allowing me to study at a top-tier university and for entrusting me with a salary and a challenging task. I would also like to thank my co-advisor, Nathan Williams, who pushed me to explore my limits and ultimately develop comprehensive solutions. To the rest of my committee, Mitch Small, Jay Taneja, and Vijay Modi, for their valuable time and insights and their dedication to my research. A special acknowledgment to Mike Griffin, who took me under his wing during my first year of the Ph.D. program and helped me ace the qualifier examinations. To him, Pauli, and Nathan, I am forever grateful for their tutoring as they have been instrumental in my scientific development process. They continue to inspire me with their patience, guidance, and dedication to my training.

I want to thank professors Christine Costello and Bart Nijssen for their cooperation and insights during this thesis's first part within the RIPS project context. A special acknowledgment to Yifan Cheng, who provided me with the datasets I requested from him for Chapter 2 of this thesis. Similarly, I want to mention my fellow students from the RIPS and e-GUIDE teams for providing valuable feedback on my work. I think of Michael Craig, Francisco Fonseca, Mike Roth, Peter Tschofen, and Aman Tyagi, to mention a few.

My gratification to Vicky Finney, Debbie Kuntz, Adam Loucks, Kim Martin, and the rest of the EPP staff because they are the silent stars in the department and keep the ship afloat in ways that are not always evident. They are always willing to help, especially during the 2020 global pandemic, and helped students focus solely on research by making our lives easier with administrative procedures.

I would also like to acknowledge the National Science Foundation's financial support via Grant Number EFRI-1441131, the Rockefeller Foundation's support, and the College of Engineering at Carnegie Mellon University via a Dean's Fellowship.

Finally, I would like to thank my parents, Juan and Ina, my siblings, Ana and Juan, my grandma, Valencia, and my aunts, Alma and Velia. Your continued support and patience helped me stay grounded and focused in difficult times. Your loving kindness and living example continue to be a source of inspiration in my personal and professional journey. For that and for much more, I love you all very much.

Abstract

The demand for systems and infrastructure that can equitably and efficiently provide food, energy, and water is central to economic development and sustainable growth. Diverse conditions such as growing population, climate change, and access constraints pose a formidable challenge for industrialized and non-industrialized countries. Industrialized countries' food and energy systems face the threat of unsustainable practices and competition for resources from multiple productive sectors. Meanwhile, the least developed countries struggle with inadequate access to modern agricultural, water, and energy technologies to provide food efficiently and securely. This thesis aims to identify and quantify food production impacts on energy and water consumption via case studies in the United States and East Africa. In both cases, I use integrated biophysical models to estimate the effects of food production (e.g., chicken broiler meat and irrigated crop yields) on energy and water resources consumption using climatological data inputs. For the case study in East Africa, I also assessed the financial viability of pressurized irrigation on a subnational level. Findings suggest that projected future climate change temperatures by mid-century will increase energy demand for cooling, reduce energy demand for heating, and substantially increase water withdrawals for evaporative cooling for industrial chicken broiler production in the Eastern U.S. The results for the case in East Africa indicate that the techno-economic potential of small-scale pressurized irrigation is highest for horticulture, maize, and potato crops grown with improved seeds and at least moderate fertility levels. My results suggest that food production impacts on energy and water demand are climate and site (or geography) dependent. These factors' relative importance depends on operational practices (e.g., input selection), technology types and costs, and fuel prices.

Table of Contents

Acknowledgments	iii
Abstract.....	v
1. Introduction.....	1
2. Impacts of projected climate change scenarios on heating and cooling demand for industrial broiler chicken farming in the Eastern U.S.	5
2.1. Introduction and Motivation	6
2.2. Materials and Methods.....	10
2.1.1. Steady-State Thermodynamic Model	12
2.1.2. Climate Projections.....	13
2.1.3. Analysis Of Simulation Outputs	14
2.3. Results and Discussion	16
2.3.1. Annual Energy Demand for Heating and Cooling.....	16
2.3.2. Seasonal Energy Demand for Heating and Cooling	20
2.3.3. Water Withdrawals for Cooling.....	23
2.3.4. Regression Slopes, ANOVA and ANCOVA Results	25
2.4. Conclusions.....	26
3. Effects of small-scale pressurized irrigation systems on primary productivity and electricity demand in East African countries through an integrated modeling approach... 29	
3.1. Introduction.....	30
3.1.1. Commonly used modeling approaches	31
3.2. Materials and Methods.....	33
3.2.1. AquaCrop model: simulating yields and net irrigation requirements	36
3.2.2. Irrigation model	40
3.2.3. Hydrology model	41
3.2.4. Analysis of Results	44
3.3. Results and Discussion	44
3.3.1. Yield Increase and Water for Irrigation Requirements.....	44

3.3.2.	Electricity Requirements.....	49
3.3.3.	Implications on Productivity and Food Security	52
3.4.	Limitations of the study	52
3.5.	Conclusions.....	54
4.	Techno-economic analysis of small-scale pressurized irrigation in Ethiopia, Rwanda, and Uganda.....	57
4.1.	Introduction.....	58
4.2.	Materials and Methods.....	60
4.2.1.	Levelized Cost of Irrigation (LCOI).....	61
4.2.2.	Irrigation Potential and Implications by District	62
4.2.3.	Sensitivity Analysis	63
4.3.	Results and Discussion	63
4.3.1.	Levelized Cost of Irrigation (LCOI).....	63
4.3.2.	Irrigation Potential by District	66
4.3.3.	Electricity Consumption Potential	69
4.3.4.	Sensitivity Analysis	69
4.4.	Limitations of the study	71
4.5.	Conclusions.....	71
5.	Conclusions.....	74
	References.....	78
	Appendix A. Supplemental Information for Chapter 2.....	98
A.1.	Materials and methods	98
A.1.1.	Steady-state thermodynamic model.....	98
A.1.2.	General Circulation Models (GCM).....	103
A.2.	Additional Results.....	104
A.2.1.	Analysis of Regression Slopes and Statistical Significance	104
A.2.2.	Analysis of Variance (ANOVA).....	116
A.2.3.	Analysis of Covariance (ANCOVA)	119

A.2.4.	Validation of Results.....	119
A.2.5.	Energy Demand for Heating and Cooling	120
A.2.6.	The effect of insulation and bird density on HVAC demand under climate change 125	
Appendix B.	Supplemental Information for Chapters 3 and 4.....	128
B.1.	Materials and methods	128
B.1.1.	AquaCrop model.....	128
B.1.2.	Irrigation model	135
B.1.3.	Hydrology model	136
B.2.	Additional Results.....	139
B.2.1.	Demand for Inputs: Annual Electricity Requirements for Irrigation per Hectare	139
B.2.2.	Hydrology model: Water Balance	141

List of Tables

Table 3.1. Summary of data and parameter inputs used in the modeling framework.	42
Table 3.2. Annual average (2010-2019) range of electricity demand for irrigation across districts or woredas measured in kilowatt-hours per additional metric ton of fresh weight.	50
Table 4.1. Calculated 2000-2016 range of crop prices from FAOSTAT.	62
Table 4.2. Sensitivity analysis for electricity prices measured as LCOI percent change with respect to the base case with an electricity price of 0.5 US\$ per kilowatt-hours.	69
Table A.1. Values assumed for the different parameters required to calculate the thermal heat fluxes in a single-story broiler house.	103
Table A.2. Names of the twenty general circulation models (GCMs) used in our study.	103
Table A.3. Regression slopes for cooling for early (2010 to 2045) and full (2010 to 2095) periods per GCM and RCP climate change scenario.	106
Table A.4. Regression slopes for heating demand for early (2010-2045) and late (2010-2095) periods per GCM and RCP climate change scenario.	107
Table A.5. Comparison matrix for ratios of regression slopes for cooling demand 2010-2095 across GCMs for RCP 8.5 scenario	108
Table A.6. Comparison matrix for ratios of regression slopes for cooling demand 2010-2095 across GCMs for RCP 4.5 scenario	109
Table A.7. Comparison matrix for ratios of regression slopes for heating demand 2010-2095 across GCMs for RCP 8.5 scenario	110
Table A.8. Comparison matrix for ratios of regression slopes for heating demand 2010-2095 across GCMs for RCP 4.5 scenario	111
Table A.9. Comparison matrix for ratios of regression slopes for cooling demand 2010-2045 across GCMs for RCP 8.5 scenario	112
Table A.10. Comparison matrix for ratios of regression slopes for cooling demand 2010-2045 across GCMs for RCP 4.5 scenario	113

Table A.11. Comparison matrix for ratios of regression slopes for heating demand 2010-2045 across GCMs for RCP 8.5 scenario	114
Table A.12. Comparison matrix for ratios of regression slopes for heating demand 2010-2045 across GCMs for RCP 4.5 scenario	115
Table A.13. ANOVA probability values (p-values) for treatment effects by 2045 and 2095 per RCP.....	116
Table A.14. Percent of the variability of heating and cooling (response variables) explained by the linear model within periods 2010-2045 and 2010-2095 for RCP 8.5 and RCP 4.5.....	119
Table A.15. Simulated-cell location’s coordinates and associated 2017 state-level broiler chicken production per reported by USDA.....	125
Table B.1. Nonconservative characteristics of small-scale, low-yield crop varieties, as used in AquaCrop.....	128
Table B.2. Nonconservative characteristics of improved, high-yield crop varieties, as used in AquaCrop.....	130
Table B.3. Coordinate points, elevation above sea level, and depth to groundwater for Rwanda’s districts.....	132
Table B.4. Coordinate points, elevation above sea level, and depth to groundwater for Uganda’s districts.....	133
Table B.5. Parameter values used in the mathematical formulation of the model to estimate electricity demand for pumping. Assumed and calculated values after Fipps (2017).....	135

List of Figures

Figure 2.1. Schematic of heat fluxes as modeled.....	11
Figure 2.2. Annual average estimated energy consumption per thousand pounds of broiler weight produced in Gainesville, Georgia, for a) cooling (electricity), and b) heating (propane) for RCPs 8.5 and 4.5. The horizontal axis depicts the year of estimation from 2018 to 2090; the vertical axis shows the annual spreads and average estimated energy consumption per thousand pounds of broiler weight across the 20 GCMs. (Note the different magnitudes and units of the y-axis in plots a and b). The tables in each panel provide percent changes in energy demand w.r.t. 2018 by mid- and late century.	18
Figure 2.3. Annual average HVAC energy consumption per thousand pounds of broiler weight in 2018 (first row) and 2095 (second and third rows) under two RCPs. The first row depicts 2018; the second row depicts 2095 under RCP 4.5; and the third row depicts 2095 under RCP 8.5. Note the different scales and units on the panels. The left-hand panel measures electricity consumption for cooling in kWh per 1,000 lb of broiler weight. The middle panel measures propane consumption for heating in gallons per 1,000 lb of broiler weight. The right-hand side panel measures total (i.e., combined heating and cooling) energy in kJ per 1,000 lb of broiler weight. 19	
Figure 2.4. Average estimated electricity demand for cooling and propane demand for heating per thousand pounds of broiler weight produced at different months of flock initiation per RCP scenario. The horizontal axis depicts the year of estimation from 2018 to 2095; the vertical axis shows the average estimated energy for cooling and heating consumption per thousand pounds of broiler weight. Every line represents a sequence of 78-point estimates (2018-2095), each one calculated as the average of the 28 to 31 flocks initiated in each month. Note the different scales of the y-axis for kWh of cooling vs gal of propane for heating.....	22
Figure 2.5. Annual average estimated water withdrawal for evaporative cooling per thousand pounds of broiler weight produced for RCP 8.5, and RCP 4.5 scenarios. The horizontal axis depicts the year of estimation from 2018 to 2090; the vertical axis shows the annual mean and ranges of estimated water withdrawal for evaporative cooling per thousand pounds of broiler weight produced across the 20 GCMs.	24
Figure 3.1. Method chart for the modeling framework.	34

Figure 3.2. Map of the study region and land cover use in Ethiopia, Rwanda, and Uganda. 35

Figure 3.3. Seasons and climate (rainy and dry) in Ethiopia, Rwanda, and Uganda..... 40

Figure 3.4. Annual average yields over ten years (2010-2019) of simulated crop growth for improved cultivars with 100% fertility. The maps measure the yield increase from rainfed to irrigated crops for the same cultivar and fertility level in metric tons of fresh weight per hectare of land cultivated. Note that the scale of the color scheme is different for different crops. The geographical scale of each country's map is different for better appreciation. 47

Figure 3.5. Annual average water for irrigation per additional ton over ten years (2010-2019) of simulated crop growth for improved cultivars with 100% fertility level. The maps measure the volume of water from rainfed to irrigated crops grown with the same cultivar and fertility level in millimeters per metric ton of fresh weight. Note that the scale of the color scheme is different for different crops. The geographical scale of each country's map is different for better appreciation. 48

Figure 3.6. Annual average electricity for irrigation per additional ton over ten years (2010-2019) of simulated crop growth for improved cultivars with 100% fertility levels. The maps measure this effect by comparing rainfed and irrigated crops grown with the same cultivar and fertility level in kilowatt-hours per metric ton of fresh weight. Note that the scale of the color scheme is different for different crops. The geographical scale of each country's map is different for better appreciation. 51

Figure 3.7. Effects of small-scale irrigation on annual yields for crops grown with four fertility levels in Ethiopia, Rwanda, and Uganda. 52

Figure 4.1. Levelized Cost of Irrigation (LCOI) over ten years (2010-2019) for 690 districts in Ethiopia, 30 in Rwanda, and 80 in Uganda. The vertical axis shows the four fertility levels (FERT) at 25%, 50%, 85, and 100%. The horizontal axis shows the annualized costs of the irrigation system per additional yield due to irrigation in US\$ per metric ton. Black vertical dashed lines represent (from left to right) the minimum, mean, and maximum annual crop prices for each country in US\$ per ton (FAOSTAT, 2019) from 2000 to 2016. The first three panels of each row (from left to right) represent staple crops, and the remaining two panels are horticulture crops. Note that the values on the x-axis are different for staple and horticulture crops..... 65

Figure 4.2. Map of irrigation potential for improved cultivars grown with 100% fertility. On the right-hand side, the three plots serve as bivariate legends. The x-axis shows water availability (in mm/ha/yr) while the y-axis displays the Levelized cost of irrigation, LCOI (in US\$ per metric ton). Note that districts with LCOI costs above 1,000 US\$/ton are shown in gray. The labels under each country's maps display the market price per crop (US\$ per metric ton) derived from FAO [120]. Note that the geographical scale of each country's map is different for better appreciation..... 68

Figure A.1. Histogram of Standardized Residuals and Normal Q-Q Plots for Heating Demand for climate change scenarios RCP 8.5 and RCP 4.5..... 117

Figure A.2. Histogram of Standardized Residuals and Normal Q-Q Plots for Cooling Demand for climate change scenarios RCP 8.5 and RCP 4.5. Note the big upper tail on both RCPs. 118

Figure A.3. Magnitude of change in average annual HVAC energy consumption per thousand pounds of broiler weight produced in 2095 with respect to 2018 on selected broiler-producing states. Note the different scales and units on the panels. Left-hand panel measures changes in electricity for cooling in kWh per 1,000 pounds of broiler weight. Middle panel measures changes in gallons of propane for heating per 1,000 pounds of broiler weight. Right-hand side panel measures changes of combined heating and cooling energy per 1,000 pounds of broiler weight. Note that the magnitude of energy changes is roughly twice as high for RCP 8.5 than for RCP 4.5 for most states..... 123

Figure A.4. Ratio of annual average HVAC energy consumption in 2095 with respect to 2018 in 22 major broiler-producing states across GCMs and RCPs. A ratio of one indicates no energy consumption difference between the two years. Note that energy for cooling ratios are all greater than one (increases) and energy for heating ratios are all smaller than one (decreases). 124

Figure A.5. Estimated net present costs (NPC) of operational energy costs at varying insulation levels from 2018 to 2050 for two broiler house sizes. The horizontal axis depicts the insulation value, R, in English units. Note that the lowest level of insulation depicted, R-4, implies no insulation. The vertical axis shows the net present costs of energy and insulation combined to 2050 in 2018 US\$ per thousand pounds of broiler weight produced. The 440' x 42' house represents the most common house size, housing around 20,000 chickens per batch. The 700' x 66' house represents a modern size with about 50,000 chickens per batch. The energy prices (for

electricity and propane) are varied parametrically to represent possible future scenarios. The current pricing in the U.S. is closer to price 2, with the price of electricity around US \$0.020/MJ and the price of propane around US \$0.015/MJ [96]..... 127

Figure B.1. Deficit irrigation strategy with root zone depletion not dropping more than 25% of the readily available soil water (RAW). Note the that % RAW is a range between field capacity and the threshold to stomatal closure. (Screenshot from AquaCrop standalone version 6.0). ... 131

Figure B.2. Annual average electricity consumption for irrigation per hectare for five crops in Ethiopia. Green-filled areas represent protected areas not considered for agricultural production. Blue regions represent water bodies. 139

Figure B.3. Annual average electricity consumption for irrigation per hectare for five crops in Rwanda and Uganda. Green-filled areas represent protected areas not considered for agricultural production. Blue regions represent water bodies..... 140

Figure B.4. Projected annual average water availability for Ethiopia (top row), Rwanda (middle row), and Uganda (bottom row). This water balance measures the weighted difference of water recharge minus simulated irrigation. Note that the size of the countries is not in the same geographical scale. Also, note that the ranges of our estimated average water values are different for each country. 141

1. Introduction

“We take for granted the things we need the most.”

Humanity faces the challenge of ensuring access to food, energy, and water (FEW) for a growing global population. As the world aims to transition toward the age of sustainable development, it is imperative to enact resource-efficient strategies that ensure economic growth and adequate livelihoods. Over the next several decades, the demand for systems and infrastructure that can reliably and efficiently provide these three vital resources poses a formidable challenge.

Increasingly efficient and responsive technologies (e.g., renewable energy, heat pumps, modern irrigation) can help tackle some of these challenges. However, additional research efforts need to provide a new understanding of FEW systems' interdependences under different challenging conditions such as extreme weather or geological/geographical limitations.

The world population is expected to grow from 7.7 billion in 2019 to 9.7 billion by 2050 [1], increasing urban areas from 55% in 2018 to 68% in 2050 [2]. Moreover, countries in Sub-Saharan Africa (SSA) project to account for more than half (1.05 billion) of the additional 2 billion people in population growth expected by 2050 [1]. Most of the projected other half are concentrated in Central and Southern Asia and the United States of America [1]. Estimates project that the world will need 53% more food [3], 50% more energy [4], and 30% more freshwater [5] to meet the expected demand increases by 2050.

Currently, agriculture accounts for 70% of global water withdrawals and industry for another 22%, primarily for power plant and manufacturing cooling [6]. About 90% of global power generation is water intensive. In some European countries and the United States, half of the

country-level freshwater withdrawals are for power plant cooling [7]. Meanwhile, the food production and agricultural supply chain sectors account for about 30% of global energy use [8], including processes like fertilizer production, crop harvesting, or post-harvest processing. Estimates from 2016 suggest that 14% of the food produced globally is lost before reaching the retail stage [9], while 2011 estimates indicate that about one-third of all the food produced never gets consumed (i.e., it is lost or wasted) [8]. Water technologies also require energy with different processes such as groundwater extraction, potable water production (e.g., desalination), or water delivery and transport (e.g., irrigation), becoming increasingly energy-intensive [10]. The use of crops as biofuels leads to competition for available land to grow food to feed humans or to supply energy as fuels for industrial purposes [11], with evidence suggesting that, in some areas, biofuels contribute to increased market volatility and higher food prices [12]. Moreover, more than 2 billion people experienced some form of food insecurity in 2018, with about one-third of these people living in Sub-Saharan Africa [13].

The challenges surrounding the food-energy-water (FEW) nexus have varying degrees of complexity and range across multiple layers from ensuring access to services to environmental and economic implications across different geopolitical and temporal scales [14], [15]. Efforts toward quantifying components and impacts of the FEW nexus require understanding the linkages between biophysical, social, and governance systems [16] and interweaving various disciplinary sciences [17]. A couple of review papers of the FEW nexus literature [18], [19] reveal that most studies focus on quantifying impacts on a single element of the nexus either in industrialized [20], [21] or least developed nations [14], [15] or both [22], [23] under specific conditions such as climate change [14], [15], [24]. Numerous analyses of the nexus strongly favor quantitative approaches via case studies at the national or subnational levels [14]-[24].

Infrastructure systems in industrialized countries are becoming increasingly vulnerable and unsustainable with the competition for resources from multiple productive sectors such as power generation and food production [16], [17], [25]. Meanwhile, most increased demands will occur in the least developed countries due to the high population increases expected in the future [1] and the path towards urbanization, industrialization, and modernization required for economic growth [2], [3], [26], [27]. Many industrialized and non-industrialized countries could greatly benefit from quantitative research that evaluates the complex FEW nexus' impacts and interdependencies to inform decision-making. These insights can contribute to the betterment of livelihoods and economic growth while also providing crucial support for investors, public planners, and policymakers. The opportunity to provide sound scientific insights and learn how to build robust infrastructure systems capable of efficiently and equitably delivering our vital resources—with their intrinsic effects on human health and livability—motivates this thesis.

This thesis contributes to the existing literature through prospective examinations of interdependent FEW systems to inform relevant stakeholders in the food and energy sectors. Specifically, this thesis investigates how food production affects energy and water consumption via case studies in industrialized and least developed countries. For one of the cases, I also provide insights about the potential double dividend of electricity and agriculture with its correspondent implications economic and biophysical implications.

The first case study in Chapter 2 is based on a paper published in the Journal of Cleaner Production [28]. It evaluates the impacts of projected climate change scenarios on the chicken broiler production's heating and cooling energy requirements in Eastern U.S. states. For this study, I developed a thermodynamic model that uses downscaled hourly temperature data under

moderate (RCP 4.5), and business-as-usual (RCP 8.5) projected climate change scenarios to simulate the heat flows occurring in modern industrial chicken coops from 2010 to 2100. This topic's selection is relevant because the U.S. is currently the world's largest producer (with about 20% of total) and second-largest exporter (after Brazil) of chicken meat. The U.S. produces more meat (in weight) from chicken than beef, veal, and swine combined [29]. Moreover, 2020 was the first year that chicken meat's global production was larger than beef, veal, or swine [29], becoming the meat of choice worldwide.

The second case study is the subject of Chapters 3 and 4, where I investigate the benefits and opportunities for co-investment in electricity and small-scale irrigation infrastructure in East Africa. This study presents an integrated assessment model that combines simplified irrigation and hydrology models with an existing biophysical crop growth model. These models use publicly available meteorological data from 2010 to 2019 to quantify yield gaps, electricity needs, and groundwater recharge for various crops and fertility scenarios. Chapter 3 introduces the energy requirements and effects of small-scale irrigation. Chapter 4 extends this study by performing the corresponding techno-economic assessment. The selection of this topic is relevant because SSA is the global region with the highest projected population growth by 2050 [1], while electricity access and uptake, together with agricultural modernization, play a vital role in the path toward economic growth [26], [27].

2. Impacts of projected climate change scenarios on heating and cooling demand for industrial broiler chicken farming in the Eastern U.S.

Abstract

Industrial poultry production is a resource-intensive activity due to specific indoor temperature requirements to ensure optimal chicken growth. The energy consumption to maintain this ideal microclimate demands substantial operating expenses that are subject to climate conditions. As such, energy demand for heating and cooling (HVAC) for commercial broiler chicken production may be influenced by increased temperatures that occur due to climate change. This study focuses on evaluating the effects of climate change on future HVAC demands in a typical commercial broiler house in the Eastern U.S. To estimate such demands, I developed a simplified thermodynamic model that uses downscaled air temperature as input. These inputs stemmed from twenty General Circulation Models (GCM) for business-as-usual (RCP 8.5) and moderate (RCP 4.5) climate change scenarios. My results indicate that increased temperatures from climate change scenarios by mid-century will increase energy demand for cooling by $5.5 \pm 1.8\%$ (RCP 4.5) and $6.6 \pm 2.1\%$ (RCP 8.5), and reduce energy demand for heating by $9.0 \pm 3.2\%$ (RCP 4.5) and $10.3 \pm 3.7\%$ (RCP 8.5) with respect to 2018. Furthermore, my results suggest that warmer temperatures under climate change will substantially increase water withdrawals for evaporative cooling. However, there may be a point where cooling pads may not be efficient enough to cool down chickens and other innovative alternatives may be required. Such changes could include the use of air conditioning units, which would further increase electricity demand.

Efficiency improvements that could mitigate some of the negative changes in energy demand could include increasing the size of the house, modifying the production schedule to minimize energy use, and adding insulation.

This chapter is published as **Izar-Tenorio, J.L., P. Jaramillo, W.M. Griffin, M. Small.** **“Impacts of projected climate change scenarios on heating and cooling demand for industrial broiler chicken farming in the Eastern U.S.”** *Journal of Cleaner Production*, vol. 255, pp. 1-8, 2020.

2.1. Introduction and Motivation

Numerous integrated models and studies have been developed to assess the impact of economic activities on greenhouse gas emissions and climate change (e.g., [30], [31]). The impact of climate change on economic, natural, and human resources is recognized as an important part of this assessment, requiring an understanding of the reciprocal impacts of modified climate on buildings (especially the energy requirements for their heating and cooling), agriculture, energy supply, and other sectors [32]-[36]. In this study, I focus on the potential impact of climate change on resource requirements for heating and indoor cooling facilities for an important part of the agricultural food supply, poultry production.

Poultry is a major part of the global meat market. Global meat consumption is expected to increase from 330 to 455 million tons per year by 2050 in response to projected population growth and dietary shifts towards higher-protein foods [37], [38]. Indeed, poultry production is expected to meet nearly 40% of the increase in global meat demand [38]. Increasing and sustaining food production at this level will likely result in increased resource use, particularly

energy. Climate change that leads to increased temperatures could further modify the resource needs of poultry production.

The United States (U.S.) accounts for roughly 20% of global poultry production, with nearly 9 billion chickens raised every year, making it the largest producing country in the world [39]. Similarly, the U.S. poultry industry accounts for 48% of the U.S. total meat production, which includes beef and pork production [40]. Poultry production resulted in \$65 billion in revenue in 2017 [41].

Currently, nearly 80% of U.S poultry production occurs in the U.S. Southeast due to favorable climate conditions and proximity to processing facilities [42]. However, under climate change, this region is expected to experience increased temperatures and decreased water availability that could be exacerbated by simultaneous population growth and land-use change [43]. Such climate impacts could negatively affect broiler production by potentially increasing cooling energy and water demand in the summer months. This negative impact, however, might be offset by reduced heating demand during winter.

Most U.S. industrial broiler¹ operations grow chickens indoors. The time to slaughter (or harvest) ranges between six to nine weeks of bird age [44] with an average market age of 49 days and an average bird weight of over six pounds [45], [46]. It is common practice to operate broiler houses at full capacity with flocks (or batches) of birds of uniform size. Doing so enables better control of the microclimate inside the barn and improves efficiency [45].

¹ 'Broiler' is the term used for chickens raised specifically for meat production.

Broilers are particularly susceptible to temperature stress due to their limited capacity to respond to temperature changes. Birds regulate their internal temperatures through panting, resting more, drinking more water, and reducing physical activity. Inappropriate temperature control often results in mortality or reduced weight gain and growth rate [47], [48]. Industrial broiler production thus involves controlling the indoor microclimate, which is driven by the thermal flows occurring inside the broiler house and the requirements of the birds throughout their growth stages. The first two weeks of the chicks' life, when they are unable to adequately self-regulate their metabolic processes, are critical to the productivity of the brood [47]. During this time, room temperature is kept between 32-35°C to help the chicks maintain optimal body temperature. At 20 days of age, the chicks can regulate their body temperature and tolerate lower temperature, usually around 21°C [49], [50], [47].

Throughout their life, birds are a source of heat flow to the house. Birds use feed as an energy source for growth and metabolic functions, including increased "meat" weight and maintaining body temperature [51], [52]. An adult bird may produce as much energy as a 25-watt light bulb in a day [52]. Indeed, the heat released by the chickens to its surroundings is a major source of heat for the house. Heating, ventilation, and air conditioning (HVAC) systems are also used to control the temperature in the broiler house. During brooding and in winter, propane is typically used to heat the houses, while mechanical ventilation is used for cooling in the summer [47].

Mechanical ventilation is also used in the winter to circulate air and remove harmful gases that accumulate in the house. In places where summer temperatures are too high for ventilation alone to maintain the inside temperature below a certain threshold, industrial broiler houses use different forms of active cooling. The most common active cooling practice in the industry is to use evaporative cooling pads [45]. These units rely on the latent heat of evaporation of water to

draw heat from outside-sourced ventilation air via a heat exchanger. Most farms use these systems when temperatures exceed 30 °C for periods of more than 2-3 hours.

In the past, efforts to model animal production focused on providing design guidelines or validating observed indoor microclimate data for animals grown in confinement. The International Commission of Agricultural and Biosystems Engineering (CIGR) developed best-practice heuristics to engineer the microclimates in animal houses. CIGR used point-estimate parameters for heat and moisture production for a variety of animals in European countries. Other work includes models to find the operational parameters for automated temperature control systems for livestock housing [53]. Finally, other research relied on empirical models to predict the indoor microclimate of pig facilities [54], [55].

A growing body of research aims to predict potential vulnerabilities and impacts of future climate change on global agricultural production systems [56], [57], and global livestock production [58]-[60]. Some work has focused on evaluating climate adaptation measures for agricultural systems [61], [62]. The work of other scholars who focused on regional impacts to specific livestock products is also available. For example, Hahn et al. [63] developed algorithms to measure extreme summer weather and heat stress impacts on cattle in the U.S. Mader et al. [64] derived a model to estimate production (weight gain or milk production) changes for swine and beef cattle in response to climate-induced temperature increases. Other authors focused on econometric-based approaches. For instance, Key et al. [65] developed an econometric model for the USDA to measure economic impacts of heat stress on milk production from U.S. livestock. Similarly, St. Pierre et al. [66] used an econometric model to estimate animal mortality and economic losses from heat stress in U.S. livestock industries.

Prior research on broiler chickens focused on measuring the energy efficiency of broiler houses [44], [50] with observed data. Other scholars developed computational models that estimate direct energy consumption to calibrate measurement devices and, ultimately, improve energy efficiency in broiler houses [67]. Finally, some researchers have also investigated broiler behavioral changes in response to heat stress and provided management and adaptation alternatives to mitigate such effects [68], [69].

I extend the prior research by evaluating the indoor environment of contemporary broiler houses and quantifying operating resource (energy and water) requirements under climate-induced temperature changes in the Eastern U.S. This work uses the temperature projections from twenty General Circulation Models (GCM) and a simplified steady-state thermodynamic model that relies on air temperature as the input to estimate future energy and water requirements for temperature control in industrial broiler chicken house in the Eastern U.S.

2.2. Materials and Methods

This work focuses on evaluating the impacts of projected climate change on the energy demand for heating and cooling in a single-story industrial broiler house. Industrial farms typically comprise four to six houses, with the average house growing 5.5 flocks of nearly 20,000 chickens per batch every year [45], [46]. Propane furnaces typically provide heating, while a combination of mechanically ventilated and cooling water systems provide cooling. Due to the lack of publicly available empirical time series energy consumption data in broiler operations, I developed a simplified thermodynamic model for this work. Specifically, I developed a single story, well-mixed, steady-state thermodynamic model with a simplified characterization of thermal heat flows occurring in a typical house to estimate heating and cooling requirements.

Figure 2.1 includes a schematic of the thermal flows captured in the model. I then ran the thermodynamic model using downscaled humidity and temperature data from the Coupled Model Intercomparison Project Phase 5 (CMIP5) [70], representing a business as usual scenario and a moderate climate change scenario.

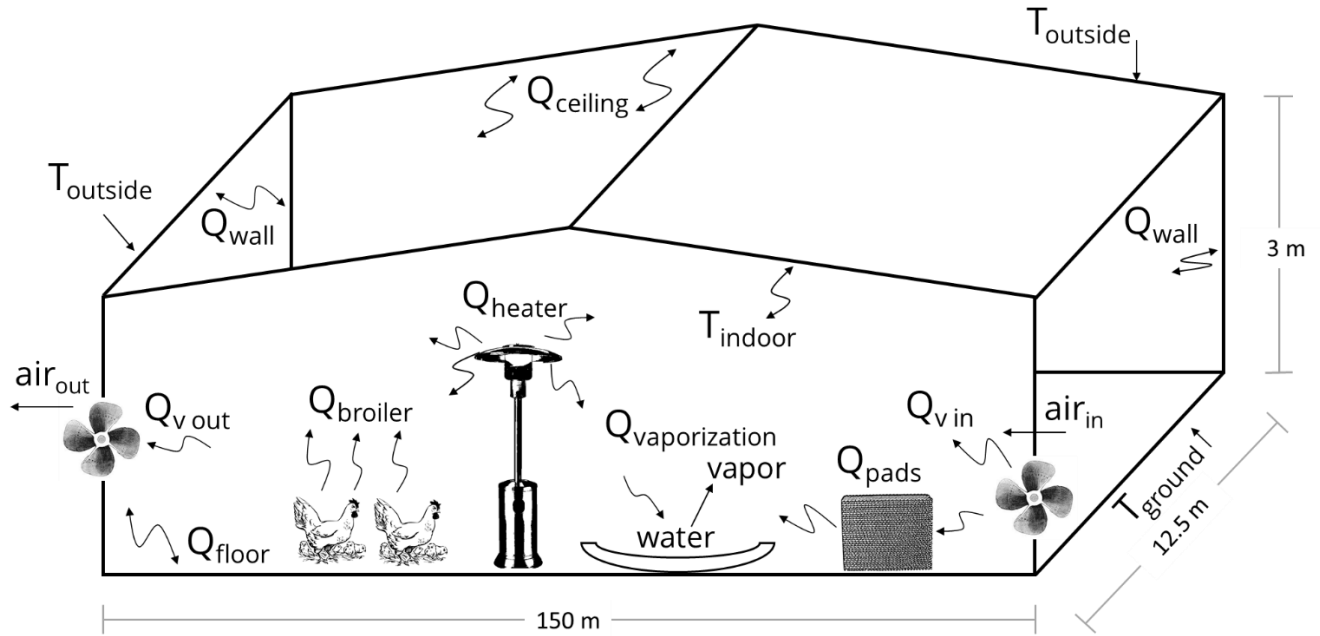


Figure 2.1. Schematic of heat fluxes as modeled.

The model assumes sequential periods of steady-state conditions over hourly time steps of a single batch of about 20,000 chickens. I assumed the average market age (or harvest time) for each batch is 49 days [45]. I ran these simulations for all possible starting dates of flock initiation using consecutive days as time steps. For instance, the first simulation starts on January 1st and ends on February 18th. The second simulation starts on January 2nd and ends on February 19th. The last simulation starts on December 31st and ends on February 17th of the next year. Therefore, any given year has 365 simulations.

While the required indoor temperature needs to be constant daily, the outside air temperature can fluctuate noticeably throughout the day. As a result, using an hourly resolution in the simulation improves the accuracy of my estimates for HVAC consumption. Indeed, a comparison of the simulation results with empirical annual energy consumption for chicken houses in Kentucky in 2011 [71], and Arkansas in 2013 [72] confirms that hourly simulations are more accurate than daily simulations. Specifically, I find that the daily resolution slightly overestimates the energy for ventilation and considerably underestimates the energy for heating and the water for cooling. Temperature fluctuations across seasons of the year further exacerbate this trend.

2.1.1. Steady-State Thermodynamic Model

For this analysis, I developed a steady-state thermodynamic model to simulate the microclimate and estimate HVAC consumption of a chicken broiler house. This model relies on a linear relationship between the required targeted indoor temperature and the age of the bird (in days). I assumed that one-day-old chicks enter the house at a temperature of 32 °C, with subsequent reductions of 0.5 °C per day until the temperature in the house reaches 21 °C [49], [47], [50]. Brooding typically occurs in smaller spaces in order to be more energy efficient [46]. Thus, the model simulates energy consumption during brooding by adjusting the area used according to the age of the chicken, following common industry guidelines. These assumptions include using half of the house area for chicks of up to one week of age; three-quarters of the house for chickens between one and two weeks of age; and full house size for broilers older than two weeks of age [73], [46]. To do the thermal heat balances, I use publicly available data reported by the Applied Broiler Research Farm (ABRF) of the University of Arkansas to approximate equations for the

live body weight (as a function of bird age) and the daily water use per bird. I relied on research by Sakomura et al. [51] to simulate hourly metabolic energy per bird.

Similarly, the simulations for the latent heat of vaporization production rely on the work by McKibbin and Wilkins [74]. I then calculated the overall energy balance using the method described by Hamilton et al. [50] and CIGR [75]. Finally, the model simulates heat transfer and infiltration losses in buildings based on Fourier's Law, as described by Geankoplis [76]. 0 includes the mathematical formulation of the thermodynamic model.

2.1.2. Climate Projections

Representative Concentration Pathways (RCP) developed by the IPCC describe a range of climate outcomes resulting from human greenhouse gas (GHG) emissions by 2100. The cumulative measure of such anthropogenic emissions, expressed in watts per square meter, is known as total radiative forcing. Each RCP represents emissions trajectories that lead to different radiative forcing by 2100. RCP 4.5, for example, represents a trajectory that leads to radiative forcing of 4.5 W/m², while RCP 8.5 leads to a radiative forcing of 8.5 W/m² by 2100 [77]. For this work, I relied on climate models under RCP 4.5 and 8.5. RCP 8.5 represents a business-as-usual scenario, and RCP 4.5 represents an intermediate emissions mitigation scenario. I selected a 12x12 km cell in Gainesville, Georgia (34.3 N, 83.8 W) as the location for the baseline analysis. This location captures the range of temperatures occurring in states with the highest broiler production in the U.S. (e.g., Georgia, Arkansas, Alabama, and North Carolina). I then ran additional simulations with simulated temperature data for different states to evaluate if climate change could lead to different spatial patterns for energy consumption and water withdrawals for thermal control in broiler houses.

Air temperature information used to run the thermodynamic model at these locations came from simulations with twenty General Circulation Models (GCMs) for the two RCP scenarios from CMIP5 [70]. CMIP5 provides data downscaled to spatial grids at a 12x12 km resolution using the Multivariate Adaptive Constructed Analogs (MACA) method described by Abatzoglou [78]. Hourly meteorological data came from the University of Washington Computational Hydrology group (UW Hydro), who downscaled the CMIP5 data to an hourly resolution using the Mountain Microclimate Simulation Model (MTCLIM) algorithm by Bohn et al. [79]. In total, I ran the model using hourly air temperature data from forty climate simulations (based on twenty GCMs for each of the two RCPs, 4.5 and 8.5) from 2010 to 2099. By using an ensemble of outputs from twenty GCMs for two RCPs, I aimed to account for the range of uncertainties in climate model signals. Section A.1.2 (Table A.2) provides a summary of the GCMs used in this analysis.

2.1.3. Analysis Of Simulation Outputs

Under climate change, the rate of temperature increase is projected to accelerate through the 21st Century [80], [56]. I thus measured the relative variability of each of the scenarios by mid- and late-twenty-first century with respect to (w.r.t.) the baseline year 2018. As previously noted, for each year, I ran 365 simulations, each representing a flock entering the house every consecutive day in a year. To present results, I averaged the simulation outputs over all flocks grown in any given year to obtain a point estimate per year for each of the forty climate simulations. This paper shows these point estimates as the running annual average energy demand normalized by thousand pounds of broiler weight produced. By using 20 GCMs I can show the spread of possible outcomes that account for uncertainties in the climate models [81]. By using annual averages, my results mask the effects of seasonal differences. I also present results for changes in

monthly averages to highlight the climate impacts on seasonal energy demand for thermal control in broiler production. It is important to note that this research does not attempt to produce detailed energy consumption forecasts that broiler producers can use for operating purposes. Instead, the average results in this paper are meant to highlight energy consumption patterns that may arise as a result of climate change and rely on the assumption that houses are operated continuously throughout the year.

To evaluate the significance of the simulation results across all climate scenarios, I performed a two-way analysis of variance (ANOVA). I used the year and the GCMs as treatments, while the response variables were the corresponding average annual energy consumption estimates (i.e., cooling, heating, and total). I also performed an analysis of covariance (ANCOVA) to evaluate the significance of results for auto-correlated data. The ANOVA and ANCOVA results allow us to evaluate the significance of the changes observed in model outputs by mid- and late-twenty-first century. Detailed information about the ANOVA and ANCOVA analysis is available in sections A.2.2 and A.2.3.

When comparing specific years to the baseline, I used a running average over 11 years to summarize the simulation outputs. GCM results are not meant to represent specific years in the future, but rather represent climate trends. So, for example, GCM data reported for 2045 is meant to be representative of climate trends in the 2040s, but the specific values from the climate model for that particular year could happen in 2044 or 2046. The point estimate I report for 2045 is thus the running average of simulation results over the period 2040-2050 (i.e., an average of eleven years).

2.3. Results and Discussion

2.3.1. Annual Energy Demand for Heating and Cooling

The model developed in this study uses the housing specifications described in Table A.1 of Appendix A. I simulated energy use for HVAC for a single house growing 20,328 chickens per flock, with 49 days of harvest age, and 6.26 pounds of market weight. The results of this analysis are consistent with the energy results reported by publicly available studies for chicken houses in Kentucky in 2011 [71], and Arkansas in 2013 [72]. More information about validation of results is available in section A.2.4.

Figure 2.2 shows that the energy demand for cooling increases, while the energy demand for heating energy decreases throughout the century under both climate scenarios for the base case in Gainesville, Georgia. Each bolded line represents the ensemble of point average estimates across the 20 GCMs over time. Shaded regions are the ranges (minimum and maximum) of running averages across the 20 GCMs. The tables within each panel provide percent changes in energy demand w.r.t. 2018 by mid- and late century for the base case in Gainesville, Georgia. Note that the energy demand between the two RCP scenarios in both panels diverges around the year 2040. After this year, energy demands under RCP 8.5 increase (cooling) or decrease (heating) sharply, while energy demand under RCP 4.5 remains relatively stable.

Figure 2.3 shows that the trends of cooling increases and heating reductions depicted in Figure 2.2 are spatially consistent under the two climate scenarios. These results suggest that Northern states (e.g., Minnesota, Wisconsin, Michigan) may see the largest decrease in energy demand for heating and the smallest increase in energy demand for cooling under both RCPs. These results also indicate that the magnitude of energy demand reductions for heating is larger than the

magnitude of the increased energy demand for cooling, particularly in Northern states. More information about the magnitude of HVAC energy use change and HVAC energy ratios w.r.t. 2018 are available in Figure A.3 and Figure A.4. Additionally, housing design specifications can influence the energy demand. For instance, the results of a parametric study on insulation indicate that adding insulation may be a good business investment. However, there is an optimum level of insulation for each location or, in other words, for different weather patterns. More details are available in Figure A.5 of section A.2.6.

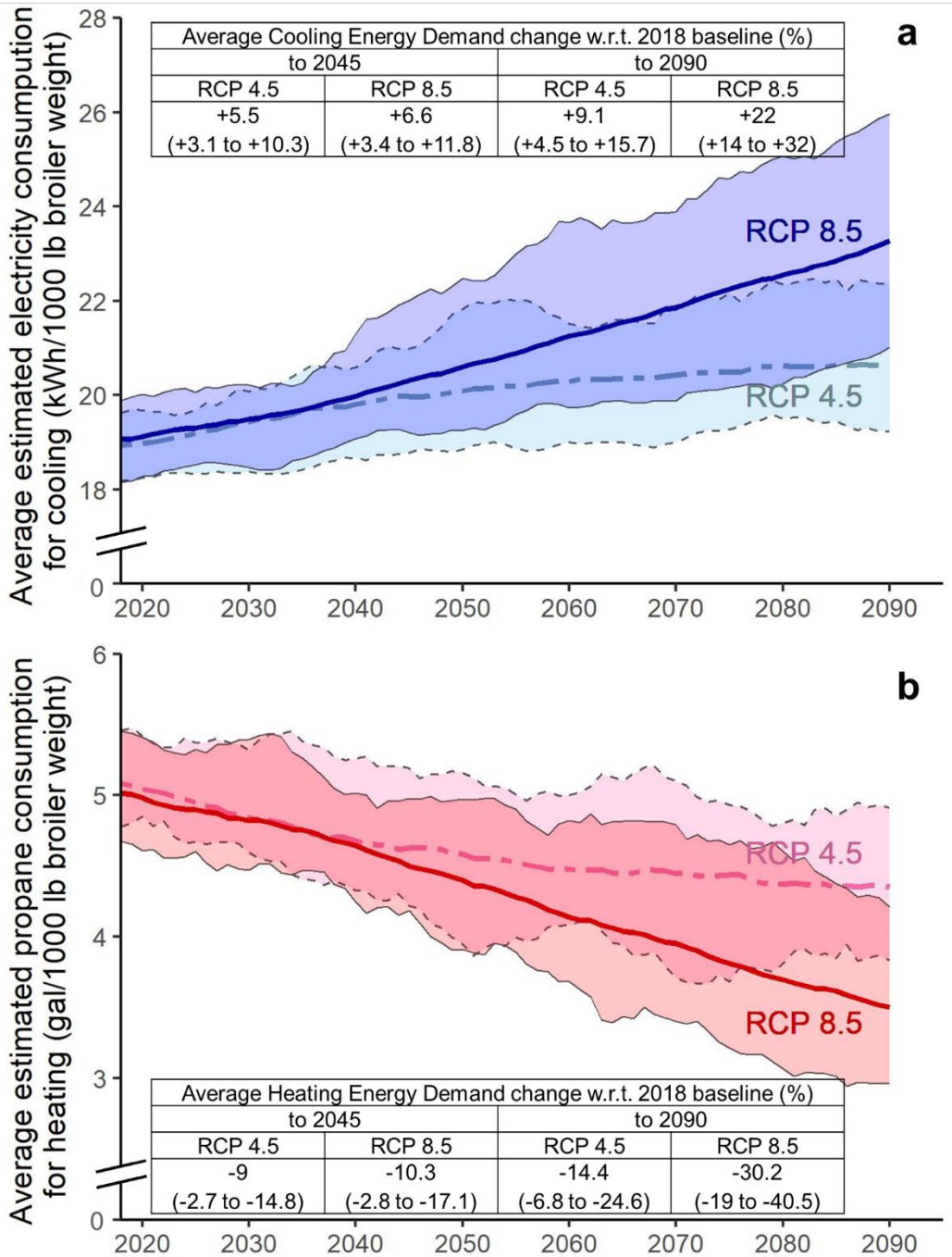


Figure 2.2. Annual average estimated energy consumption per thousand pounds of broiler weight produced in Gainesville, Georgia, for a) cooling (electricity), and b) heating (propane) for RCPs 8.5 and 4.5. The horizontal axis depicts the year of estimation from 2018 to 2090; the vertical axis shows the annual spreads and average estimated energy consumption per thousand pounds of broiler weight across the 20 GCMs. (Note the different magnitudes and units of the y-axis in plots a and b). The tables in each panel provide percent changes in energy demand w.r.t. 2018 by mid- and late century.

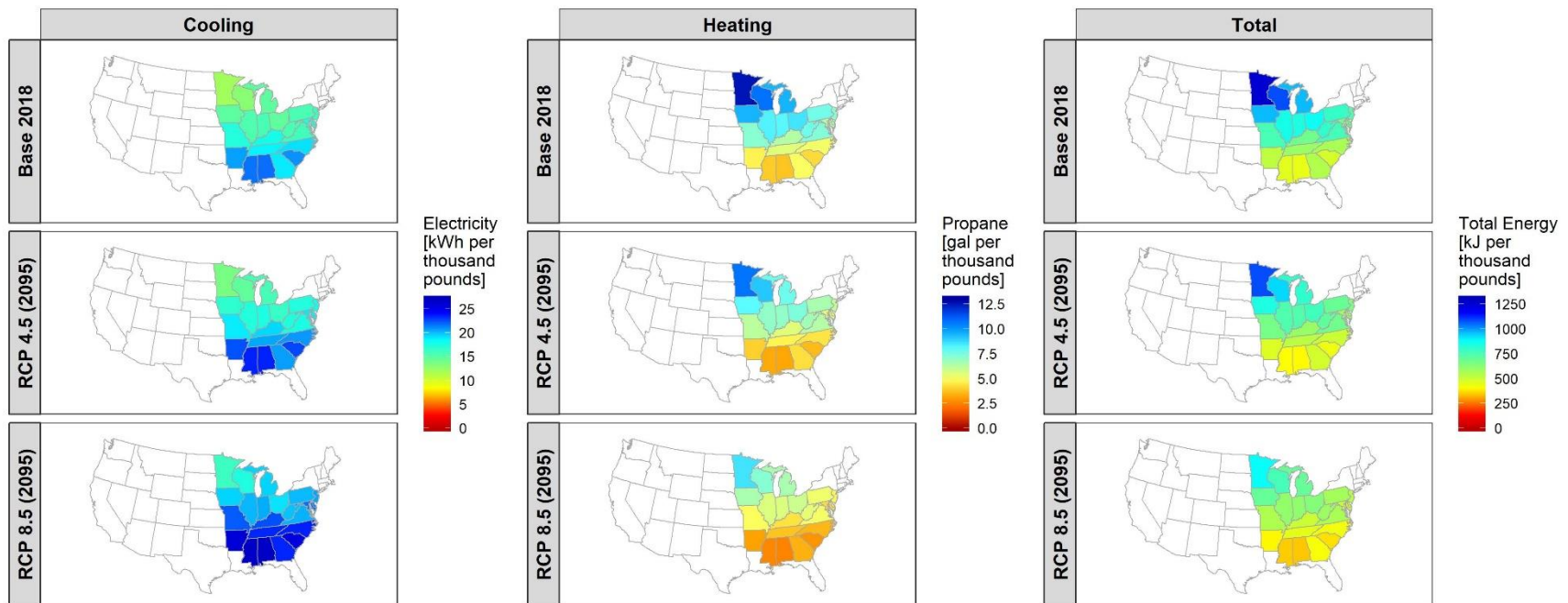


Figure 2.3. Annual average HVAC energy consumption per thousand pounds of broiler weight in 2018 (first row) and 2095 (second and third rows) under two RCPs. The first row depicts 2018; the second row depicts 2095 under RCP 4.5; and the third row depicts 2095 under RCP 8.5. Note the different scales and units on the panels. The left-hand panel measures electricity consumption for cooling in kWh per 1,000 lb of broiler weight. The middle panel measures propane consumption for heating in gallons per 1,000 lb of broiler weight. The right-hand side panel measures total (i.e., combined heating and cooling) energy in kJ per 1,000 lb of broiler weight.

2.3.2. Seasonal Energy Demand for Heating and Cooling

Baby chicks are more sensitive to cold stress than to heat stress during brooding [47], so they require more temperature control during winter. The results in the previous section assume that production is steady year-round. This assumption implies that producers grow a similar number of batches in winter and summer. However, farmers may opt to grow fewer batches during wintertime, when chicks are more sensitive to temperature stress. In this section, I disaggregate changes in energy demand by month of flock initiation.

Figure 2.4 shows seasonal energy consumption trends for flocks entering the barn at different months of the year. Each line comprises a sequence of point estimates for a given month over multiple years. These lines depict the average electricity demand for cooling and propane demand for heating to grow a thousand pounds of broiler weight for chickens (i.e., flocks) entering the house at any day of the given month. Every line is comprised of yearly point estimates for each month. For instance, the line pertaining to the month of July is a sequence of 78-point estimates (2018-2095), each one calculated as the average of the 31 flocks grown in July. Colder months (November to February) demand the lowest energy for cooling and the highest energy for heating. Note the different units used for electricity (kWh) and propane (gal) consumption. Observe also that RCP 8.5 results in greater changes on seasonal energy demand over time than does RCP 4.5.

These trends could have unmodeled implications. For instance, the increased cooling demand could result in current cooling technologies (such as evaporative cooling pads) being ineffective in case of extreme heat. Under such circumstances, producers could opt for technological changes such as using air conditioning [52], or behavioral changes such as migrating to other

geographical latitudes with less extreme climate. The decreased heating demand could lead producers to grow more chickens during winter (if they do not do that already). As a result, changes in production patterns would more than likely result in changes in the overall energy demand of broiler houses. Therefore, this section aims to highlight that climate-induced temperature increases may lead to changes in production behavior rather than to suggest specific solutions in the face of climate change.

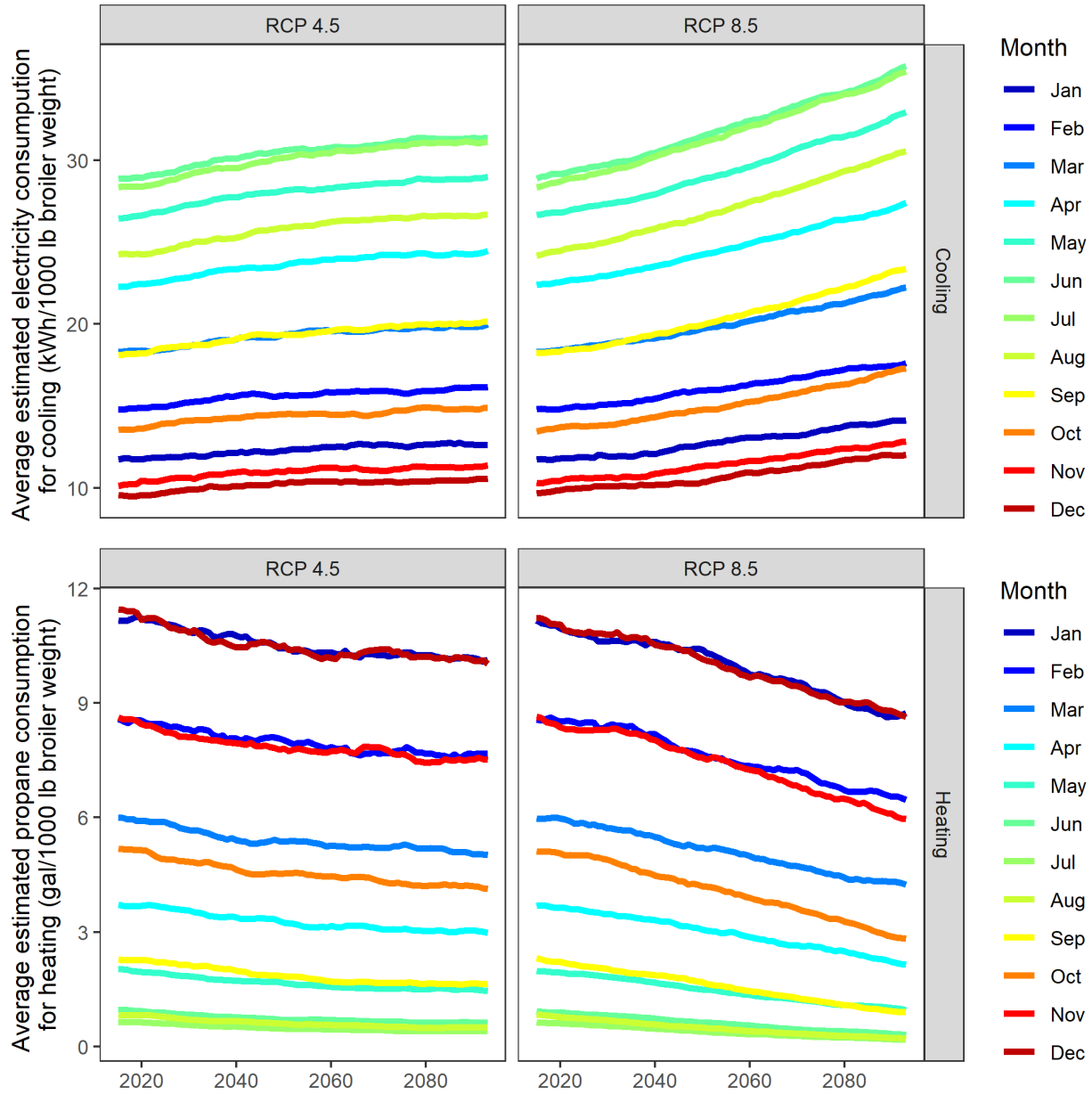


Figure 2.4. Average estimated electricity demand for cooling and propane demand for heating per thousand pounds of broiler weight produced at different months of flock initiation per RCP scenario. The horizontal axis depicts the year of estimation from 2018 to 2095; the vertical axis shows the average estimated energy for cooling and heating consumption per thousand pounds of broiler weight. Every line represents a sequence of 78-point estimates (2018-2095), each one calculated as the average of the 28 to 31 flocks initiated in each month. Note the different scales of the y-axis for kWh of cooling vs gal of propane for heating.

2.3.3. Water Withdrawals for Cooling

Since the energy demand for cooling involves the operation of evaporative cooling pads, increased summer temperatures result in increased water withdrawal requirement. Since most water used in the cooling pads is lost thorough evaporation, water withdrawals are likely reflective of consumptive water demand in these systems [71]. Figure 2.5 shows the resulting annual average estimated water withdrawal for evaporative cooling per thousand pounds of broiler weight produced. The red line represents the business-as-usual RCP 8.5 scenario and the blue line shows the moderate RCP 4.5 scenario. Note that the effect of the two climate scenarios is the same for the first few years until around 2040, when the effect of RCP 8.5 results in an increasing trend that diverges from the more “stable” moderate scenario, RCP 4.5. This suggests that warmer temperatures will substantially increase the demand for evaporative cooling. However, there may be a point where cooling pads may not be efficient enough to cool down chickens and other innovative alternatives may be required.

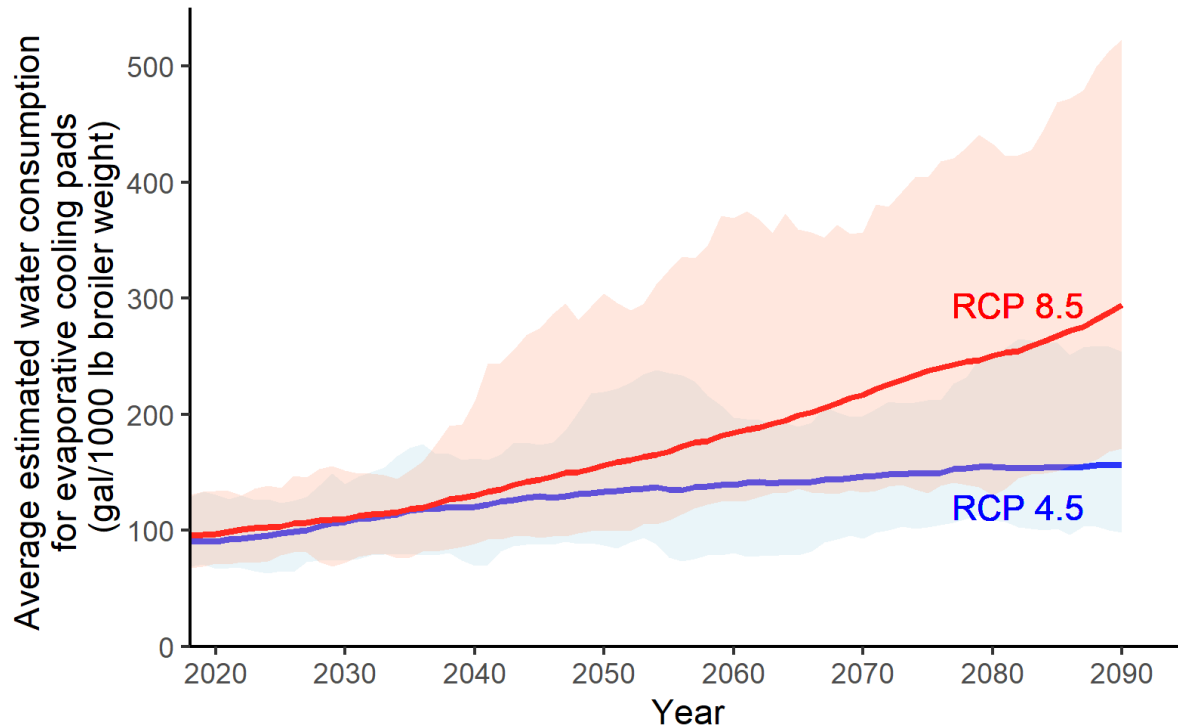


Figure 2.5. Annual average estimated water withdrawal for evaporative cooling per thousand pounds of broiler weight produced for RCP 8.5, and RCP 4.5 scenarios. The horizontal axis depicts the year of estimation from 2018 to 2090; the vertical axis shows the annual mean and ranges of estimated water withdrawal for evaporative cooling per thousand pounds of broiler weight produced across the 20 GCMs.

One factor that may affect this demand for water for cooling is the starting operating temperature of the evaporative cooling pads system. My model assumes that the evaporative cooling pad systems start operating when outside temperatures reach 28°C, which is a conservative estimate. Industry experts suggest that evaporative cooling systems may start operating when outside temperatures reach 33 °C without affecting chicken growth or health [84]. This operating change may significantly reduce cooling energy demand. However, this change often needs to occur in combination with tunnel ventilation systems to create the desired air velocity at broiler level and, in turn, a windchill effect [71].

Adult birds release larger amounts of heat into the house than baby chicks. Large chickens are also not particularly resistant to prolonged high temperatures. As a result, evaporative cooling pads may not efficiently chill heavier chickens in high-density houses during extended periods of very high temperatures (beyond 35 °C). Therefore, under expectations of extended high temperatures from climate change, evaporative cooling pads with tunnel-ventilated systems may no longer be cost-effective (Fairchild 2012). Under these circumstances, broiler producers may have to explore other cooling alternatives such as using air conditioning [52] or increasing the insulation [83]. A switch to air conditioning for cooling in broiler production would likely lead to increased electricity demand beyond what I estimated in this paper.

2.3.4. Regression Slopes, ANOVA and ANCOVA Results

To evaluate if the effect of climate change on projected energy demand was significant, I first calculated the slopes of the results for each GCM through linear regression for early (2010 to 2045) and full (2010 to 2095) periods per RCP. I found that the changes projected by the twenty models are indeed statistically significant for both periods and RCPs. The analysis shows that energy demands change more steeply after mid-century under RCP 8.5 and remain relatively more stable under RCP 4.5. I also compared linear regression slopes for cooling and heating energy demands per GCM and RCP for the early and full periods. The resulting comparison matrices show a consistent trend produced by different GCMs. Cooling slopes are positive, and heating slopes are negative. However, there are indeed differences in the magnitude of ratios across the ensemble of GCMs. Detailed information about the regression slopes analysis is available in section A.2.1.

In order to find statistical inference validity of the variability of the simulations, I measured the effect of the treatment (i.e., GCM and Year) on the response variable (i.e., heating or cooling) through a two-way ANOVA without replacement, allowing for interactions. The ANOVA test resulted in extremely low p-values ($<10^{-32}$) for both RCPs when comparing heating or cooling demand changes by mid- and late century with 2010 as the baseline year. This p-value is evidence of a statistically significant effect of the two treatments on the response variable. An additional ANCOVA model tested for homogeneity of regression slopes of the different GCMs per RCP for the same 2010-2045 and 2010-2095 periods. For the two RCPs and the two periods, p-values of the 'Year' treatment are all below 10^{-13} , while p-values of the 'GCM' treatment are all below 10^{-29} . These levels of significance validate the hypothesis that differences in energy demand over time (i.e., by mid- and late century) are due to the effect of treatments (i.e., climate change). More information about ANOVA and ANCOVA models and test results is available in sections A.2.2 and A.2.3.

2.4. Conclusions

In considering the results of this work, it is important to acknowledge the limitations and caveats of the modeling approach used. My model did not include technological improvements for energy efficiency (for heating and cooling) over time because the goal is to evaluate the effects of projected climate change scenarios under current technological conditions. For the same reason, I did not consider the inclusion of breeds with potentially increased heat tolerance over time via genetic modification, which may also affect energy demands.

Concerns about energy efficiency and animal-welfare could result in changes to standard industry practices. These changes could include: 1) increasing the size of broiler houses,

currently fewer than 3% of all the broiler farmhouses in the U.S. encompass modern sizes of more than 25,000 square feet [45]. 2) Increasing the level of insulation of barns. 3) Reducing the number of batches grown in winter, when propane consumption is highest (from 6 to 10 times higher than in summer, see Figure 2.4). 4) Modifying bird density, currently set to no more than two birds per square foot with an average of 1.1 bird per square foot [46]. 5) Limiting genetic modifications to grow market-weight chickens in less time (currently, chickens are grown in as little as 38 days). Future work could focus on evaluating the energy implication of such changes in production practices.

While I focused the discussion on the effect of changes in energy and water demand, such changes may have unmodeled implications. My results show that water demand for cooling could increase significantly, which creates an additional vulnerability should water resource constraints in the region increase due to climate change [43]. Similarly, the increase in electricity demand for cooling during summer could have implications for the power system, which will likely face other climate-induced constraints, including increased demand from other sectors, water flow restrictions, and capacity deratings for existing power plants [84].

The results in this paper are meant to be indicative of potential trends in energy consumption for poultry production under climate change. The results are not meant to serve as forecasts to be used to make decisions about changes in the operation of individual production facilities. Such decisions would require more refined models of the specific conditions of each facility and would, for example, account for the actual growing schedule the individual producer uses. Nonetheless, my results suggest that climate change may lead to a reduction in energy demand for heating and an increase in energy demand and water withdrawals for cooling in broiler houses.

While previous work evaluated the environmental impacts of livestock production [85]-[87], there has been limited work to understand the reciprocal impacts of climate change on livestock production. Such impacts could create new risks for the sustainability of broiler production. My work highlights that climate will indeed affect the operations of broiler production by changing the resource requirement for temperature control in broiler houses. My work thus contributes to the body of research by expanding the understanding of the interactions between climate and food production systems.

3. Effects of small-scale pressurized irrigation systems on primary productivity and electricity demand in East African countries through an integrated modeling approach

Abstract

Agriculture is the backbone of East Africa's economy, with contributions of up to 50% of the Gross Domestic Product (GDP) in some countries. Most farmers rely on traditional, small-scale subsistence farming with low fertilizer use and low-yield seeds. Simultaneously, less than 3% of the total cultivated area employs any form of irrigation, mostly non-pressurized. Meanwhile, electricity providers frequently struggle with low and unpredictable demand, challenging their ability to recover rural areas' investments. The adoption of electricity for small-scale irrigation can increase agricultural productivity and improve electricity utility financial sustainability. This study evaluates the effects of small-scale pressurized irrigation on primary productivity and electricity demand in East African countries for three staple crops and two horticulture crops. To study these effects, I develop simplified engineering-based irrigation and hydrology models and combine them with a biophysical crop growth model using district-level agrometeorological, soil, and crop physiology data as inputs. My results indicate that small-scale pressurized irrigation can significantly increase yields in regions with enough water to sustainably irrigate horticulture and staples such as maize and potato, especially those grown with improved seeds and fertility levels greater than 50%. Meanwhile, the electricity demand for irrigation hinges upon the amount of water required and the depth to the groundwater table and is highest in districts of Ethiopia, then Uganda, and Rwanda. Summarizing, this Chapter shows that climatic

zone, fertility, and soil characteristics are the most critical biophysical drivers of yield gaps across countries.

3.1. Introduction

Agriculture is the backbone of East Africa's economy, contributing up to 50% of the Gross Domestic Product and employing more than 80% of the workforce in some countries [97]. More than 95% of the agricultural holdings in East Africa are smaller than ten hectares (ha) (i.e., small-scale) and rely on traditional farming practices. Less than 4% of the total cultivated area in East Africa employs some form of irrigation [98], while fertilizer use (2-14 kilograms per hectare) is among the lowest in Sub-Saharan Africa (SSA), where average fertilizer use is 16 kg/ha (the lowest in the world) [99]. Simultaneously, electricity providers in the region struggle with low and unpredictable demand, which challenges their ability to recover infrastructure investments in rural areas. Additionally, according to FAO, the perishability of food (post-harvest losses) in the region exceeds 30%, and the informal nature of markets alongside corresponding value chains poses a significant challenge for further economic development and food security [100], [101].

Activities in agricultural value chains include multiple operations in primary production (inputs, seeds), processing (post-harvest), distribution, and storage. Numerous studies reveal the potential benefits of strengthening agricultural value chain activities in Africa. Schaffnit-Chatterjee [97] suggests investing in agricultural value chains is key to sustained economic growth, poverty reduction, and food security in SSA. Banerjee et al. [102] identify irrigation and post-harvest processing as the most promising out of 13 major agricultural value chain activities to boost productivity and support economic growth in SSA through improved access to modern electricity

services. Daly et al. [103] pinpoint strategies for enhancing the efficiency of maize's post-harvest processing and storage activities that could enhance economic growth through high-quality exports and ensure food security for Rwanda and Uganda. Furthermore, case studies by Nordhaus et al. [26] found that "meaningful universal electrification occurred as part of a broad process of economic development and modernization, driven by a virtuous cycle of energy consumption, urbanization, industrialization, and agricultural modernization." These observations support the idea that the development of electricity and agricultural systems should go hand in hand in the pursuit of rural development.

Despite its vast water resources, farmers in SSA withdraw only 3% of renewable water resources for irrigation [97], [98]. The limited use of irrigation is due to high capital costs, poorly developed supply chains, and lack of knowledge about irrigation schemes' benefits and technologies [104]-[106]. Along with irrigation and post-harvest processing, fertilizers and improved seed varieties could further enhance agricultural productivity [107]. This Chapter evaluates small-scale pressurized irrigation systems' effects on primary productivity and resource requirements (i.e., water and electricity) in Ethiopia, Rwanda, and Uganda based on agronomic, economic, and hydrologic factors.

3.1.1. Commonly used modeling approaches

Statistical and biophysical crop growth models are the two most common approaches to estimating agricultural yield variability as a function of water use. Compared to biophysical models, statistical models require fewer model parameters and, at least in theory, can handle model uncertainties more transparently [108]. However, some issues may arise with the collinearity of weather variables and the assumption that data is perfectly measured [109].

Schlenker and Lobell [110] use a statistical model to show that higher yields correlate positively with precipitation for most SSA countries' crops. Lobell and Burke [108] assess panel regression models' effectiveness and find that statistical models seem to be more appropriate at national scales.

Most of the studies that included irrigation or nutrient inputs used biophysical crop growth models. El-Sharif et al. [111] showed that incorporating soil moisture data from the U.S. into the DSSAT crop model improved the accuracy of crop yield forecasts and irrigation requirements. Castañeda-Vera et al. [112] evaluated irrigated winter wheat growth in semi-arid Spain using four crop growth models (i.e., AquaCrop, CERES-Wheat, CropSyst, and WOFOST). They found comparable results when water is non-limiting but significant differences under arid conditions compared to actual measured data. Folberth et al. [113], [114] used the EPIC crop growth model to show that nutrient, irrigation, and cultivar inputs are the main constraints to improved maize yields in SSA. In general, statistical models are less accurate than the more mechanistic crop growth models because of the insufficient quantity and quality of training data, especially at subnational scales, in SSA [108], [109]. Perhaps more importantly, statistical models tend to assume that maximum yields are already achieved and often ignore yield-limiting factors such as nutrient inputs or irrigation [114].

Only a handful of studies have quantitatively evaluated the technical feasibility of pressurized irrigation systems and nutrient inputs together. Blanc [115] studied irrigation requirements for different crops globally under projected future climate change. Rosegrant et al. [116] and You et al. [117] focused on finding the profitability (i.e., internal rate of returns) of irrigation systems in African countries using an entropy-based crop model. Sheahan and Barrett [107] used surveys to

show that modern inputs such as fertilizer, irrigation, and soil quality can explain productivity differences at subnational levels. Meanwhile, Gheewala et al. [118] and Mekonnen and Hoekstra [119] examined differences in major crops' water footprint intensity in selected countries.

None of these prior studies assessed irrigation's electricity requirements, which is a critical input often lacking in agricultural areas in East Africa. Similarly, these studies focused mainly on national scales and failed to include agricultural inputs such as fertility or soil characteristics.

This Chapter contributes to the literature by assessing the interaction of several critical inputs on crop yields, including electricity demand for irrigation, soil texture, fertility levels, cultivar type, and water availability for irrigation. For this purpose, I use an integrated approach that combines irrigation and hydrological models (that I developed based on engineering relations) with an existing biophysical crop growth model.

3.2. Materials and Methods

This Chapter's modeling framework combines a biophysical crop growth model, AquaCrop, with a simplified engineering-based irrigation model to estimate yields, electricity for pumped irrigation, and water use for irrigation. First, I use AquaCrop to predict crop yields and net irrigation requirements using agrometeorological (climate), soil, and crop physiology data as inputs. To estimate electricity demand for irrigation per hectare, I use as inputs AquaCrop's net irrigation estimates, the groundwater depth, and pressurized irrigation system parameters, as illustrated in Figure 3.1. These irrigation system parameters include the length and material of

pipes, the number and type of fittings, and the pump's volumetric flow rate.

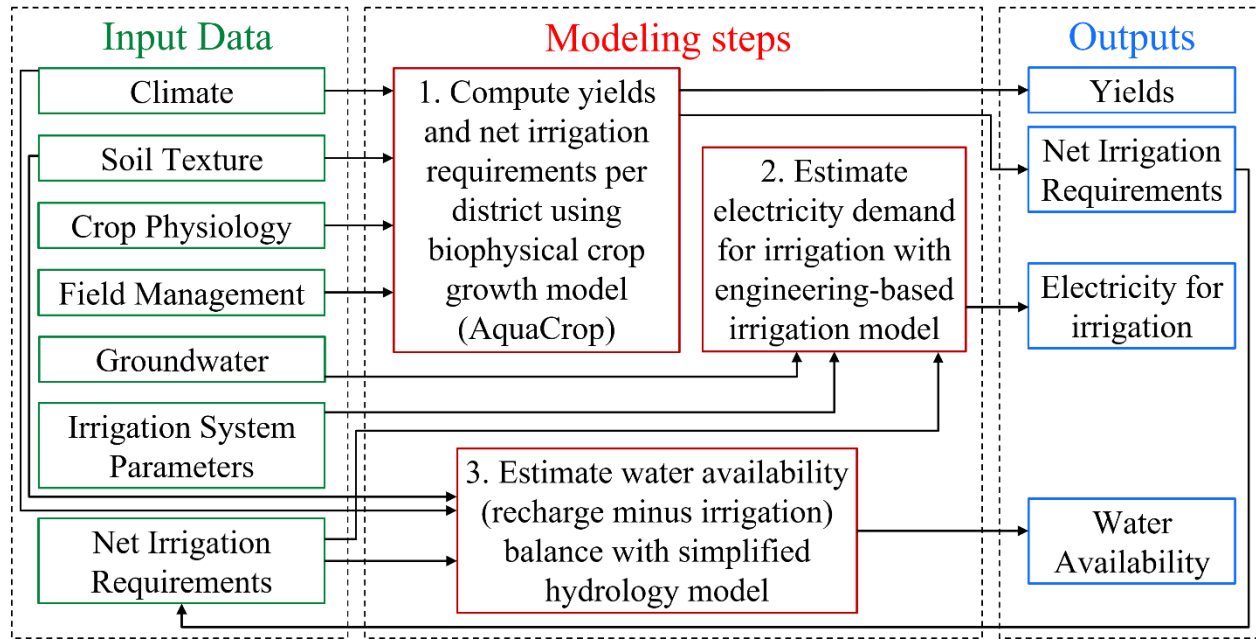


Figure 3.1. Method chart for the modeling framework.

I run simulations at a district-level resolution for each country, taking the centroid coordinates (i.e., latitude, longitude, and elevation) as representative of each district. Subnational scales are more appropriate than national levels because differences in the microclimate and the microenvironment are more discernible at higher resolutions. The administrative boundaries include 690 districts (called woredas) in Ethiopia, 30 districts in Rwanda, and 80 districts in Uganda, with an average district size of 1,600 km², 800 km², and 2,500 km², respectively. I select three staples and two horticulture crops for simulation in each country based on their relative national importance and productivity levels [120]. The selected crops are beans, maize, potato, tomato, and onions in Rwanda and Uganda, and maize, wheat, teff, tomato, and onion, in Ethiopia. The first three represent staple crops, while the last two represent horticulture crops.

Figure 3.2 shows a map of the study region and land cover in Ethiopia, Rwanda, and Uganda. More information about the centroid coordinates is available in Appendix B.

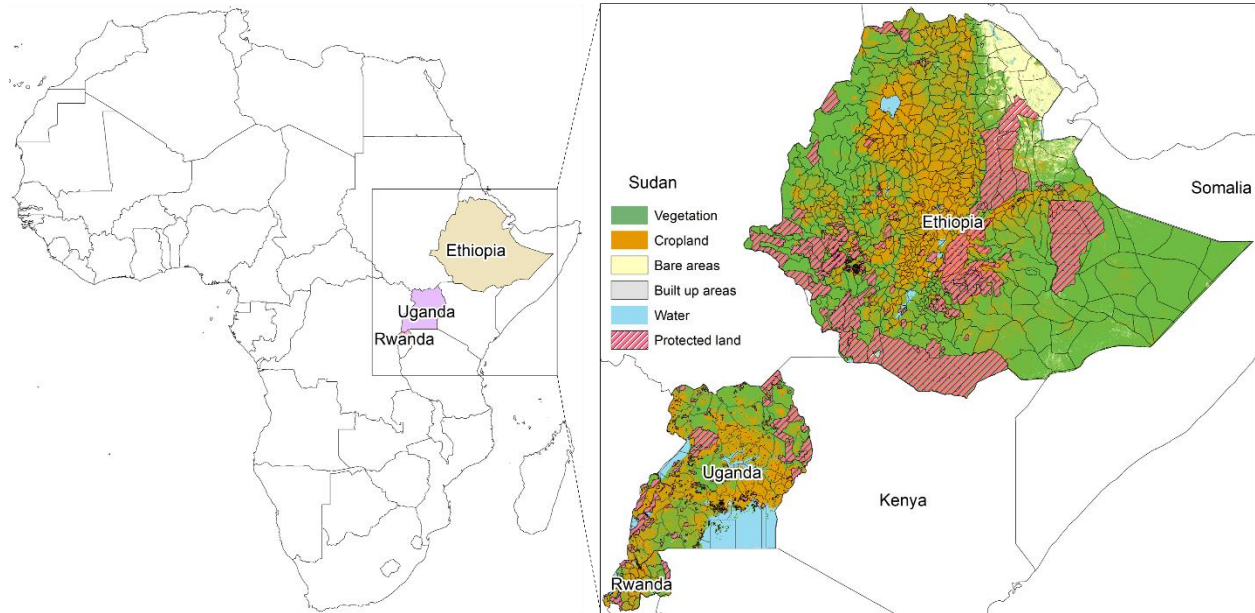


Figure 3.2. Map of the study region and land cover use in Ethiopia, Rwanda, and Uganda.

To perform the simulations described in Figure 3.1, I made some general assumptions. First, I assume fixed planting dates for each country. Second, I assume that the power source for irrigation is electricity. Third, water for irrigation comes from groundwater, with no cost for rights or license to extract water without considering water quality or salinity. Fourth, I model the different cultivars' phenology parametrically and do not consider changes over time. Fifth, I model the irrigation system as a function of the depth to groundwater without considerations for topography or slopes. The irrigation system assumes constant values for model parameters (available in the SI), such as the pump's operating pressure or the pipe's physical characteristics. Finally, I assume irrigation in 100% of each district's simulated hectare of planted land.

3.2.1. AquaCrop model: simulating yields and net irrigation requirements

AquaCrop is a water-driven crop growth model developed by the Food and Agriculture Organization of the United Nations (FAO). It simulates biomass (B) production as a function of a water productivity parameter (WP^*), transpiration (Tr), and reference evapotranspiration (ET_0). Instead of using leaf area index (LAI), AquaCrop relies on the more readily available green canopy cover (CC) as the basis to calculate transpiration and express foliage development. Yield production (Y) is a function of the final biomass production (B) and a harvest index (HI). The model requires climate, crop, soil, field management inputs from the user and relies on fundamental and often complex biophysical processes seeking a balance between simplicity, accuracy, and robustness [121].

3.2.1.1. *Climate Data*

I use daily agrometeorological data from the NASA POWER database on a $0.5^\circ \times 0.5^\circ$ resolution for various parameters. These parameters include the minimum and maximum temperature, mean precipitation, mean relative humidity (or dew/frost point temperature), wind speed, and top-of-atmosphere shortwave downward solar radiation [122] for the years 2010 to 2019.

3.2.1.2. *Soil Texture*

I use remote-sensed soil data on a 1 km x 1 km from the Harmonized World Soil Database (HWSD) version 1.2 [123]. I use each country's district-level shapefile to extract soil data over the district's polygon area, assigning the aggregated average soil texture composition (sand, silt, and clay) over the district polygon area as representative of that district's soil. Then, I use pedotransfer functions from Saxton et al. [124] to estimate hydraulic soil characteristics using the

soil texture composition as input. These calculated characteristics include the number and depth of soil horizons (cm), the soil water content at saturation, the volume of water at field capacity, the volume of water at the permanent wilting point, and the saturated hydraulic conductivity.

3.2.1.3. *Crop Physiology*

AquaCrop requires crop physiology data specifying canopy growth characteristics in two modes: calendar days or growing-degree-days (GDD). The calendar days mode uses a specific growth cycle length with a fixed number of days to reach each phenological stage (e.g., emergence, senescence, flowering, maturity). The GDD mode adjusts the time to reach phenological stages by subtracting the crop's base and mean temperatures as a means to quantify the crop's accumulated heat. AquaCrop requires calibrated conservative and non-conservative crop parameters to define crop cultivars. A crop cultivar is the plant variety used for cultivation, either by selective breeding or not. Conservative parameters in AquaCrop are standard for most cultivars and do not usually require further modification. Non-conservative parameters (e.g., phenological stages) may vary by geolocation and specific crop variety [121], [125].

In this study, I model three staples and two horticulture crops (i.e., high value) per country with two cultivars per crop. The three staple crops are beans, maize, and potato, in Rwanda and Uganda, maize, teff, and wheat, in Ethiopia. The horticulture crops are onion and tomato. In total, I model fourteen different varieties (two cultivars per crop) by modifying non-conservative parameters related to phenology, transpiration, biomass production, yield formation, and stresses [126]. Of these fourteen varieties, I model ten in GDD-mode and four in calendar mode.

AquaCrop includes pre-calibrated template crop files for different crops. I rely on AquaCrop's pre-calibrated template crop files as the basis to build tailored low- and high-yield cultivar files

for all but one of the seven crops considered in our study. For the remaining crop (onion), I created a crop physiology file using data from Agbemabiese et al. [127] and Karuku and Mbindah [128]. A summary of the different cultivars' parameter values is available in Table B.1 and Table B.2.

3.2.1.4. Field Management and Atmospheric Data

AquaCrop permits the user to choose among different soil fertility levels, weed control, and watering modes (e.g., rainfed, irrigation). AquaCrop uses a semi-quantitative approach to evaluate nutrient deficiencies (i.e., soil fertility). This approach expresses soil fertility as the maximum relative dry aboveground biomass ratio with respect to (w.r.t.) biomass grown in stress-free conditions, hence a percentage. In this sense, AquaCrop's soil fertility affects biomass production due to stresses on canopy development and biomass water productivity [129]. This study uses four fertility levels (in percentage terms), assuming no mulches and no weed interference. The literature reviewed seemed to indicate that incorporating the latter two parameters does not add significant value to the simulation and may vary from farm to farm. I model watering levels in deficit irrigation mode as a conservative measure to reduce water consumption without compromising yields. I choose this level of irrigation in order to maximize the evapotranspiration water productivity as AquaCrop's full irrigation mode may lead to excessive water use [130]. A graphical depiction of this strategy is available in Figure B.1. The atmospheric data measures the CO₂ concentration level per year using the default values provided by AquaCrop.

3.2.1.5. Initialization of AquaCrop simulation

Before starting the simulation, I determine the planting date for each season per country:

- Ethiopia has two main rainy seasons called the *belg* and *meher*, which run from February to June and June to October, respectively [131]. More than 90% of grain production occurs in *meher*, with grains accounting for around 88% of the country's planted areas [132]. Meanwhile, the dry season runs from mid-October to January. For this analysis, I assume that the dry season begins on October 15 and the rainy season on June 1.
- The National Institute of Statistics of Rwanda (NISR) distinguishes three agricultural seasons. Season A, or the long rainy season, begins in September and ends in February of the following year. The short rainy season B starts in March and ends in May. The dry season, or Season C, goes from May to October [133]. Based on data from the statistical yearbook of the Seasonal Agriculture Survey 2019 of Rwanda [134], I assume the start of the dry season on May 1 and the rainy season on September 15.
- Uganda's dry spells go from December to February and from June to July. There are two brief rainy seasons from mid-March to May and from September to November. Based on the Annual Agricultural Survey 2018 [135], Uganda's rainy season runs between March and August, while its dry season runs from mid-November to February. I assumed the dry season to start on November 10 and the rainy season to begin on March 15.

Figure 3.3 depicts the rainy and dry seasons in the three countries.

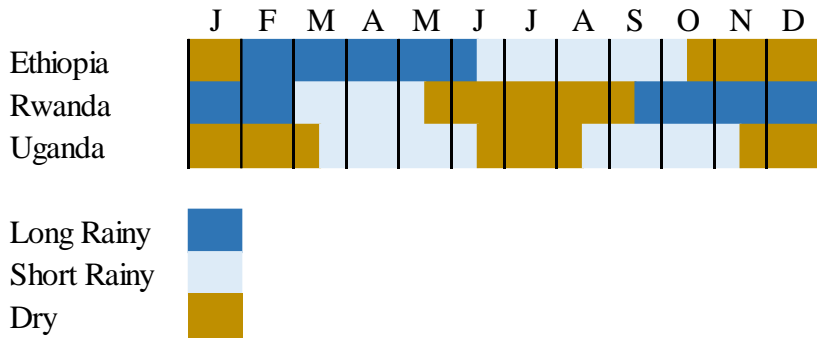


Figure 3.3. Seasons and climate (rainy and dry) in Ethiopia, Rwanda, and Uganda

Hence, I run simulations for 1,600 scenarios per country's district corresponding to ten years (2010 to 2019), five crops from a pool of seven (beans, maize, potato, teff, wheat, tomato, and onion), four fertility levels (low, moderate, near-optimal, non-limiting), two water management modes (irrigation, rainfed), two planting seasons (dry and rainy), and two cultivar varieties per crop (low- and high-yield). The resulting variables of interest from these simulations are yield (metric tons per hectare or t/ha) and irrigation water demand (mm/ha).

3.2.2. Irrigation model

To estimate electricity demand for irrigation, I build a model based on Bernoulli's principle [76] and the methods described by Duke [136] and Fipps [137]. This model assumes that the electricity for irrigation E_{irr} (kWh/ha) is a function of AquaCrop's simulated mass of irrigation water demand m_{irr} (kg/ha), the volumetric flow rate Q (m^3/s), the pipe's diameter D (m), the total dynamic head TDH (m) (including the depth to groundwater), the acceleration of gravity g ($= 9.81 m/s^2$), and the pump's efficiency η (%), as shown in Eq. 3.1. More information on the parameter values used is available in Table B.5.

$$E_{irr} = \frac{m_{irr} \left(\frac{1}{2} \left(\frac{4Q}{\pi D^2} \right)^2 + g * TDH \right)}{\eta} \quad Eq. 3.1$$

3.2.2.1. Groundwater Data

I characterize each country's available water resources assuming that the source of water is groundwater. This assumption is appropriate because groundwater is available virtually anywhere in our selected subnational spatial resolution. I did not consider surface water because it is site-specific, depends on topography, and is even more prone to pollution than groundwater [138]. Moreover, accounting for surface water's competing end uses (e.g., public supply) is out of this study's scope. I rely on publicly available data on a 0.05° x 0.05° resolution from the British Geological Survey [139] to estimate groundwater depth. Like the geoprocessing I did for soil data, I use each country's district-level shapefile to extract and assign the average depth to groundwater (*DTW*) over a district's polygon area as representative of that district's *DTW*.

3.2.3. Hydrology model

I develop a simplified hydrological model following the methods in Rodríguez-Huerta et al. [140] and Alley et al. [141]. The model assumes that monthly groundwater recharge (ΔR) occurs when precipitation (P) exceeds evapotranspiration (ET_o), and the soil-moisture (S) equals the soil-moisture storage capacity (STC). Otherwise, ΔR is zero. The reduced form version (*Eq. 3.2*) of this model states that for any month i ,

$$\Delta R = \begin{cases} (P_i - ET_{o_i}) - (STC - S_{i-1}), & \text{if } P_i \geq ET_{o_i} \text{ and } S_i = STC \\ 0, & \text{otherwise} \end{cases} \quad Eq. 3.2$$

The complete mathematical formulation and assumptions of the model are available in section B.1.3. As a validation step, I find that our 10-year annual average results for Rwanda (6,785 Mm³/yr) are about the same as the surface water runoff calculation (6,822 Mm³/yr) reported by [142] for the Rwandan National Water Resources Master Plan.

Finally, the model measures yearly water availability (*WaterAvail*) through a weighted mass water balance of groundwater recharge (*R*) minus simulated irrigation (*I*) for year *j* as:

$$WaterAvail_j = w_1 R_j - w_2 I_j \quad Eq. 3.3$$

It would be misguided to directly compare irrigation and recharge because irrigation occurs only on arable land, while groundwater recharges over virtually the country's entire surface. To better reflect water availability on nearby areas to farmers, I assigned weights to each variable to represent the arable land's ratio to the total surface area. The first weight, w_1 , is a base weight equaling one for all three countries. The second weight, w_2 , represents the fraction of arable land to the total country area and equals 0.2 for Ethiopia [143], 0.5 for Rwanda [144], and 0.33 for Uganda [145]. This weight allocation implicitly assumes that each simulated hectare (in each district) of planted land has 100% irrigation. Therefore, a positive *WaterAvail* value indicates more water available than the irrigation water demanded. In this sense, *WaterAvail* represents the volume of water available after irrigation. More details are available in section B.1.3.

summarizes the definitions, data inputs, and parameter values used to run the three models. Table 3.1 summarized the definitions, data inputs, and parameter values used to run the three models.

Table 3.1. Summary of data and parameter inputs used in the modeling framework.

Data type	Input Data or Parameter	Used in	Resolution	Source
------------------	--------------------------------	----------------	-------------------	---------------

Climate	<p>Minimum and maximum temperature, mean relative humidity or dew point temperature (T_{dew}), wind speed, solar irradiance, latitude, longitude, and elevation (above sea level) → used to calculate evapotranspiration (ET_o) with Penman-Monteith's equation.</p> <p>Precipitation (P)</p>	AquaCrop, Hydrology model	Daily, 50 km x 50 km	NASA POWER (Stackhouse, 2012)
Soil	<p>Depth, Texture in % sand, % silt, % clay = used to calculate hydraulic soil water content at saturation (SAT), volume of water at field capacity (FC), volume of water at permanent wilting point (PWP), saturated hydraulic conductivity (k_{sat}), available water capacity (AWC), soil-moisture (S), soil-moisture storage (ΔS), and soil-moisture storage capacity (STC). In conjunction with P and ET_o, ΔS and STC are used to calculate groundwater recharge (ΔR).</p>	AquaCrop, Hydrology model	Once, 1 km x 1 km	Harmonized World Soil Database (HWSD) v1.2 (FAO/IIASA/IRRI/ISSCAS/JRC, 2012)
Crop Physiology	<p>Conservative and non-conservative parameters for the specific type of cultivar, including phenology and planting dates</p>	AquaCrop	N/A	AquaCrop pre-calibrated files modified after 18 literature papers (see SI)
Field Management	<p>Rainfed or irrigated mode; fertility levels: low (25% or 33%, for potato), moderate (50%), near-optimal (85%), and unlimited (100%); no mulches and perfect weed management.</p>	AquaCrop	N/A	AquaCrop
CO₂	<p>Atmospheric CO₂, in ppm (default)</p>	AquaCrop	Yearly, Global	AquaCrop
Groundwater	<p>Depth to groundwater table (DTW)</p>	Irrigation model	Once, 5 km x 5 km	MacDonald et al. (2012)

Irrigation System Parameters	AquaCrop's simulated net irrigation requirements (I), volumetric flow rate (Q), pipe's diameter (D), total dynamic head (TDH) including depth to groundwater (DTW), acceleration of gravity (g), pump's efficiency (η) = used to calculate electricity demand for irrigation (E_{irr})	Irrigation model	N/A	AquaCrop's simulation, Geankoplis (1998), Fipps (2017)
-------------------------------------	---	------------------	-----	--

3.2.4. Analysis of Results

This chapter's first set of results shows the annual average yield increase per hectare, water for irrigation per metric ton, and electricity demand for irrigation per metric ton. All of them were calculated using the additional annual yield due to irrigation. The additional annual yield computation due to irrigation subtracts the rainfed yield from the irrigated fresh-weight yield for the same cultivar and fertility level. Because AquaCrop simulates yields as dry matter, I convert dry yields into fresh weight employing conversion factors indicating each crop's dry matter content. This conversion uses dry matter values of 90% for teff, 87.5% for beans, maize, wheat, 22.5% for potato, 6% for tomato [146], and 12.5% for onion [147]. I present these results for the improved cultivar 100% fertility level scenario on a district-level basis. I also show the productivity and food security implications of small-scale irrigation on a country-level.

3.3. Results and Discussion

3.3.1. Yield Increase and Water for Irrigation Requirements

Figure 3.4 suggests that the highest yield increases due to irrigation for the 100% fertility scenario occur in Central and Western woredas (i.e., districts) of Ethiopia, Southern and Southwestern districts of Rwanda, and Eastern and Northwestern districts of Uganda (except for

tomato, which seems to thrive in the Western half). I must note that current yield estimates from the MapSPAM model [171] and reported official yields in Rwanda [169] and Uganda [170] are consistent with our simulated yields for the 25% fertility scenario. For instance, averages on a country level for 100% fertility levels show that maize in Ethiopia increases from 7.8 to 23.2 metric tons per hectare (t/ha) for improved cultivars and from 4.8 to 10.7 t/ha for traditional cultivars. In Rwanda, irrigation increases maize yields from 17.6 to 31.6 t/ha for improved cultivars and 10.4 to 13.5 t/ha for traditional cultivars. In Uganda, maize yields rise from 14.1 to 25.3 t/ha for improved cultivars and 7.9 to 10.5 t/ha for traditional cultivars. FAO data [120] indicates that the highest current yields are 6 t/ha for beans in Northern Africa, 12 t/ha for maize, 48 t/ha for potato, 62 t/ha for onions in Northern America, 8 t/ha for wheat and 310 t/ha for tomato in Western Europe.

I note that a hectare of cultivated land produces different yields, as shown by the different scale of the color scheme for different crops. The standard deviations across districts for common crops are higher for Ethiopia, Uganda, and last Rwanda. This finding is probably intuitive as a country's size influences climate variability. The decreasing order for the percent median yield increase due to irrigation for the reference case is tomato, onion, maize, teff, and wheat, in Ethiopia; tomato, onion, maize, potato, and beans, in Rwanda; and tomato, potato, onion, maize, and beans, in Uganda.

Figure 3.5 shows that the volume of water required for irrigation per additional metric ton of crop is highest for Southeastern Ethiopia, Eastern and Northern Rwanda, and Northeastern Uganda (except for beans, which require more irrigation water in southern parts). It should not be surprising that water requirements are higher for crops with lower yields, such as beans,

wheat, or teff. The specific water footprint to produce an additional metric ton is not as crucial as finding consumption patterns. Perhaps most interesting is that districts in Central Ethiopia, Southwestern Rwanda, and Northwestern Uganda have reasonably high yields and moderate water footprint per additional ton. These yield increases and water for irrigation estimates suggest that those regions may be the most attractive for irrigation.

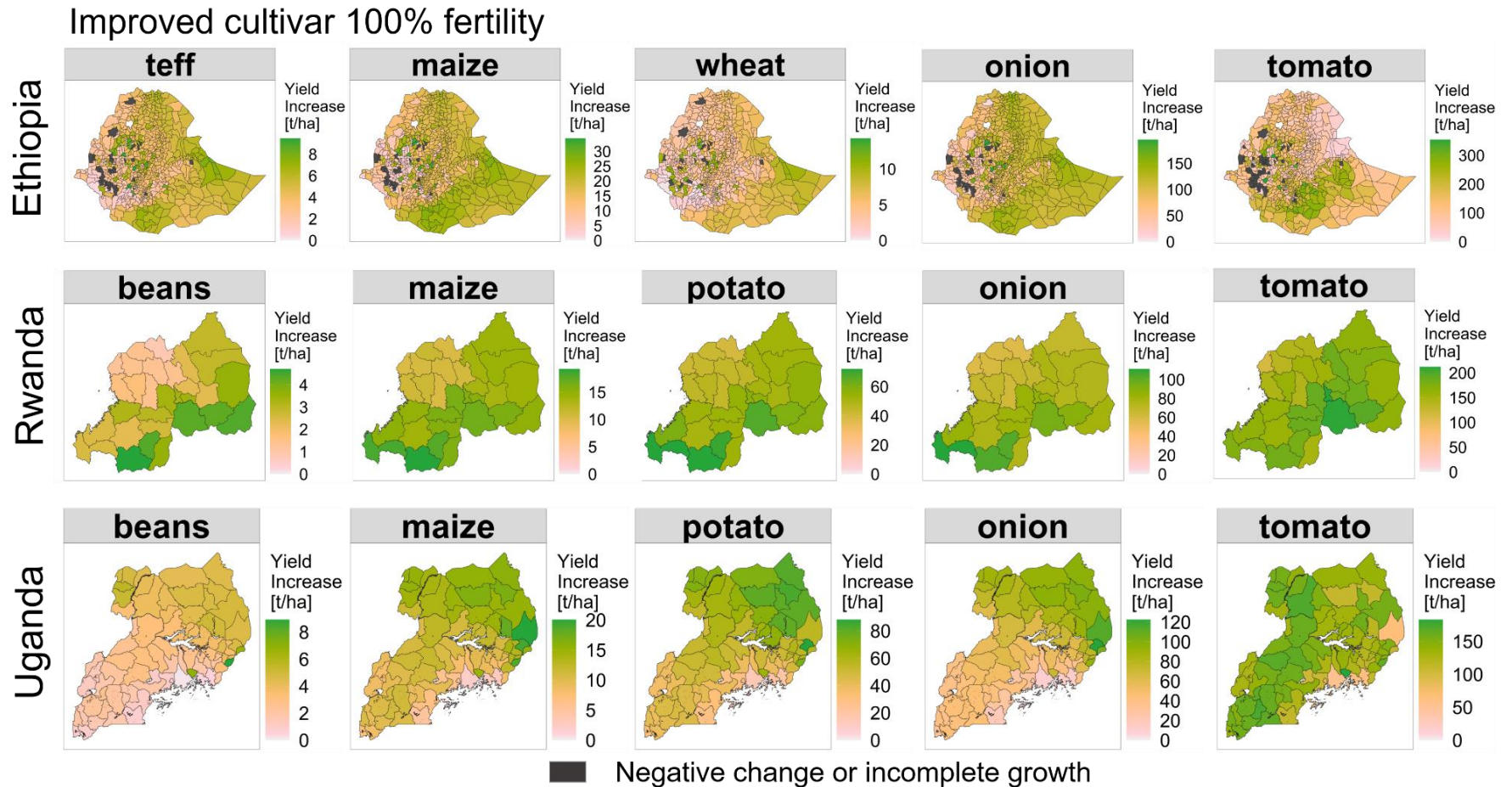


Figure 3.4. Annual average yields over ten years (2010-2019) of simulated crop growth for improved cultivars with 100% fertility. The maps measure the yield increase from rainfed to irrigated crops for the same cultivar and fertility level in metric tons of fresh weight per hectare of land cultivated. Note that the scale of the color scheme is different for different crops. The geographical scale of each country's map is different for better appreciation.

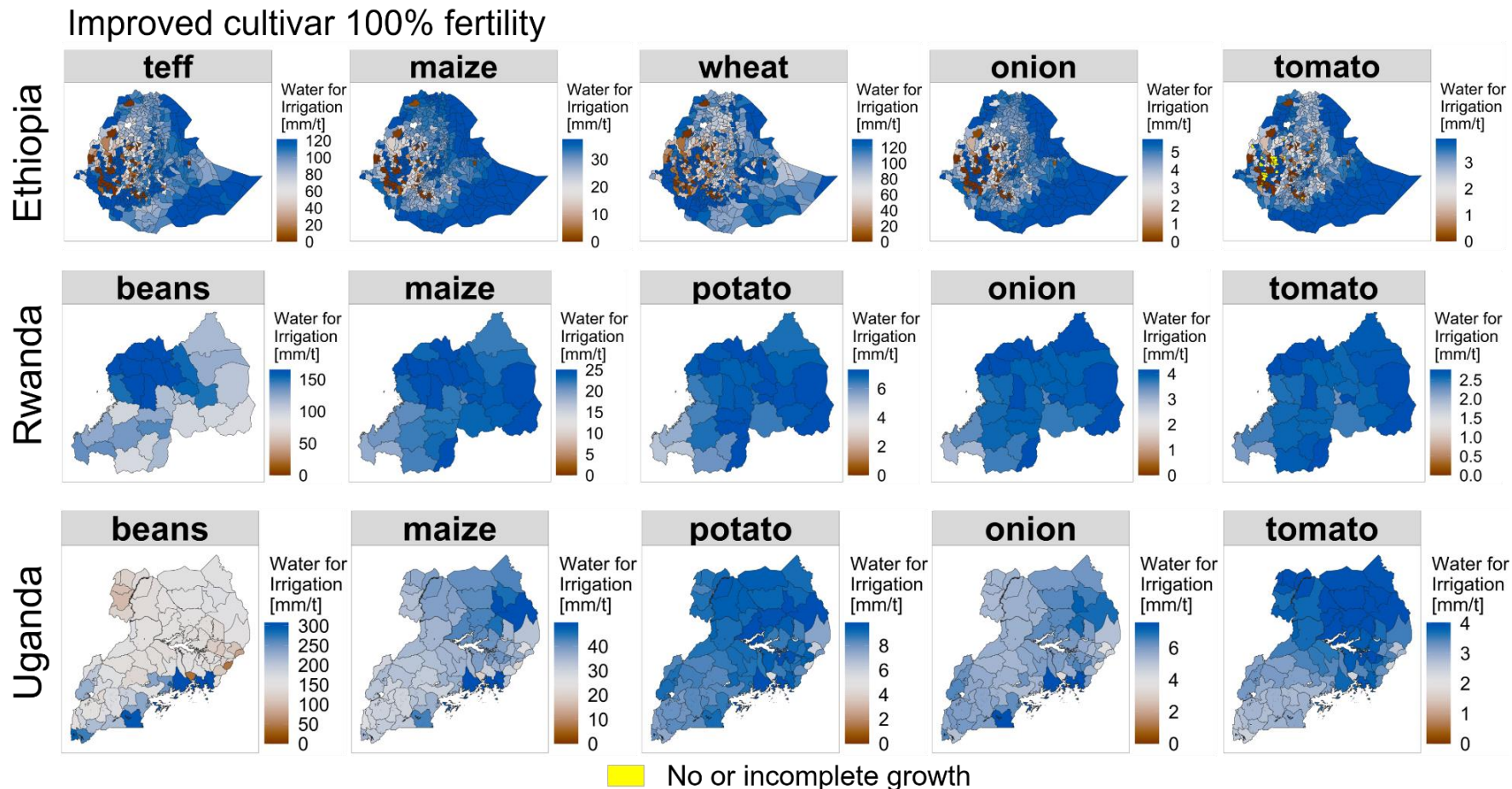


Figure 3.5. Annual average water for irrigation per additional ton over ten years (2010-2019) of simulated crop growth for improved cultivars with 100% fertility level. The maps measure the volume of water from rainfed to irrigated crops grown with the same cultivar and fertility level in millimeters per metric ton of fresh weight. Note that the scale of the color scheme is different for different crops. The geographical scale of each country's map is different for better appreciation.

3.3.2. Electricity Requirements

Figure 3.6 shows that the electricity for irrigation per metric ton is highest for Eastern and Southeastern Ethiopia, Eastern and Northern Rwanda, and Eastern and Northern Uganda (except for beans that are more power-thirsty in Southern Uganda). This finding is consistent with the results shown in Figure 3.5 for water consumption and evidence of a directly proportional relationship between electricity and water use. Unsurprisingly, electricity demand per ton is higher for crops with lower yields such as beans, teff, and wheat. Meanwhile, horticulture crops have the lowest electricity use per ton. I should note that the scale of the color scheme is different for the different crops. For instance, the maximum attainable yields for beans in Rwanda and tomato in Ethiopia are around 4 and 300 t/ha, respectively.

Table 3.2 shows that, on average, electricity demand per metric ton of production is higher in Ethiopia, followed by Uganda and last Rwanda. Ethiopia has, by far, the biggest range of electricity demand values of the three countries. In contrast to Ethiopia, Rwanda and Uganda are cases where the average electricity demand for common crops is lower. These differences are a direct consequence of the volume of water required for irrigation and the depth to the groundwater table. Although multiple factors influence plant growth, water supply is possibly the single most crucial factor. The amount of water required to grow plants can significantly vary depending upon geographical, geological, and agrometeorological aspects such as climatic zone (e.g., rainfall and temperature variability), crop type, type and depth of soils, and even atmospheric carbon dioxide [148]. For instance, crops with deeper roots can hold and absorb more water if soil texture and depth are adequate for water drainage and transport purposes [149]. Because evapotranspiration depends on it, the temperature can also influence water

relations [148]. These factors can vary considerably depending on the district's climate and agroecological zone. For instance, Ethiopia's north-south alignment and spread out along different climate zones usually leads to higher rainfall variability. Because crop-water relations are more or less constant for a specific crop [168], the volume of water for irrigation (e.g., to make up for insufficient rainfall) and, thus, the electricity demand for irrigation increase with decreased precipitation. For instance, Rwanda, the smallest country in this study and with seemingly the more homogeneous meteorological conditions, has the smallest range of electricity requirements per ton.

The other factor that significantly affects electricity demand is the water table's depth. Ethiopia has the largest distances to water tables of the three countries. Along with poor soil's water drainage characteristics and higher rainfall variability, these higher distances can explain the higher electricity demands for irrigation in Ethiopia than in Rwanda or Uganda. Indeed, the highest electricity requirements correlate with higher depths to groundwater.

Table 3.2. Annual average (2010-2019) range of electricity demand for irrigation across districts or woredas measured in kilowatt-hours per additional metric ton of fresh weight.

Ranges of electricity demand for irrigation on a district level [kWh/ton]			
	<i>Ethiopia</i>	<i>Rwanda</i>	<i>Uganda</i>
Teff	2.5 to 5,100 (780)	-	-
Wheat	2.1 to 2,800 (650)	-	-
Beans	-	430 to 1,300 (660)	190 to 5,400 (820)
Potato	-	23 to 36 (32)	25 to 52 (40)
Maize	2.1 to 4,900 (360)	87 to 125 (110)	89 to 280 (170)
Onion	1.4 to 230 (37)	14 to 23 (18)	15 to 41 (27)
Tomato	1.4 to 220 (22)	10 to 16 (12)	11 to 22 (16)

1 – The number in parenthesis denotes the average over feasible districts

Improved cultivar 100% fertility

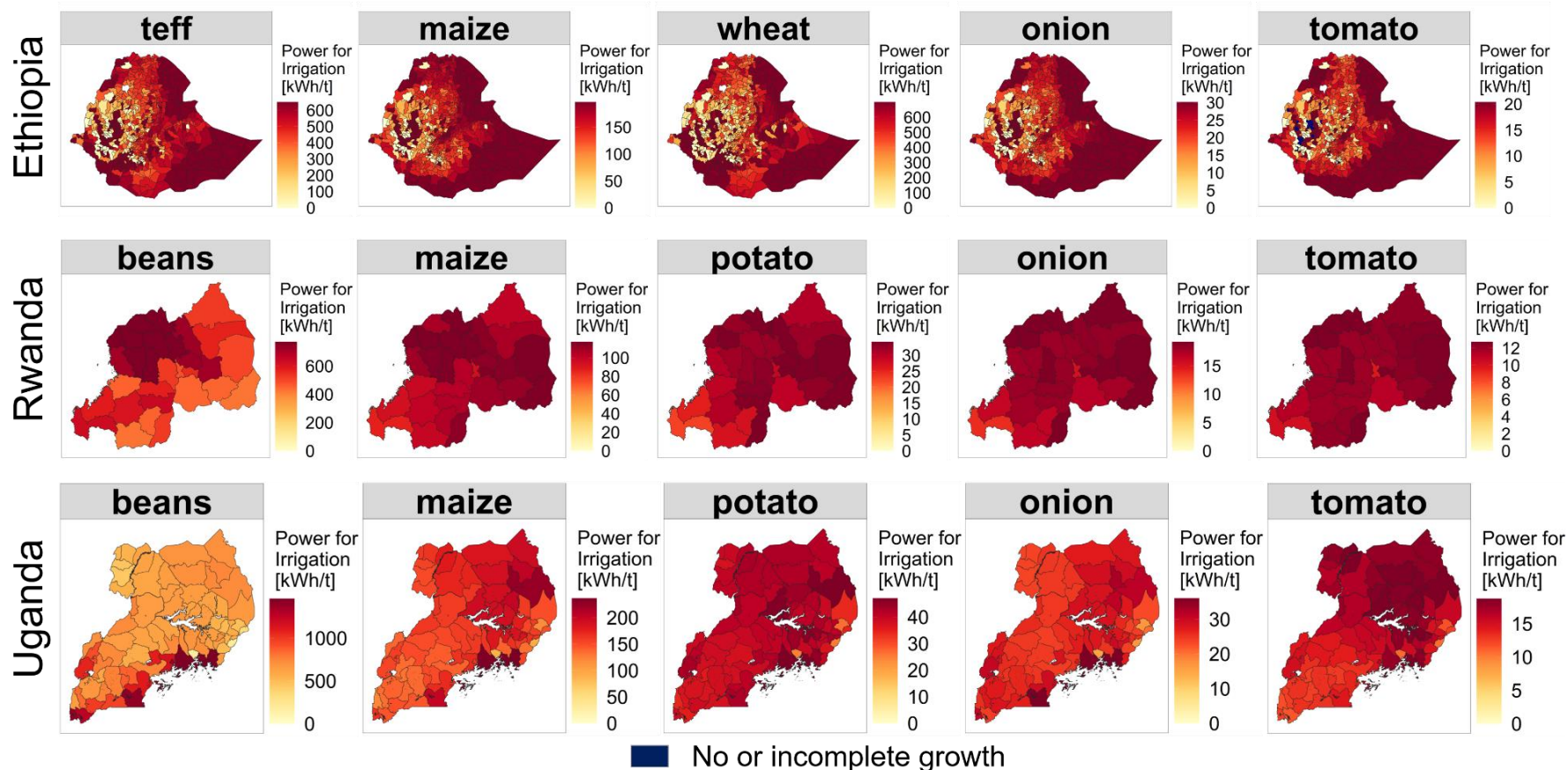


Figure 3.6. Annual average electricity for irrigation per additional ton over ten years (2010-2019) of simulated crop growth for improved cultivars with 100% fertility levels. The maps measure this effect by comparing rainfed and irrigated crops grown with the same cultivar and fertility level in kilowatt-hours per metric ton of fresh weight. Note that the scale of the color scheme is different for different crops. The geographical scale of each country's map is different for better appreciation.

3.3.3. Implications on Productivity and Food Security

Based on my model, Figure 3.7 suggests that irrigation can lead to more than doubling the production of staples and horticulture crops per hectare (in the best case), also achieving more constant and predictable yields. Therefore, production increases can help to ensure physical access to sufficient, safe, and nutritious food. It is in this sense that irrigation can help to tackle one layer of the food security challenge. These results are of particular importance for Rwanda and Uganda because of their high population density [150] and shortage of available land for agriculture (e.g., Rwanda is the second-most densely populated country in Africa).

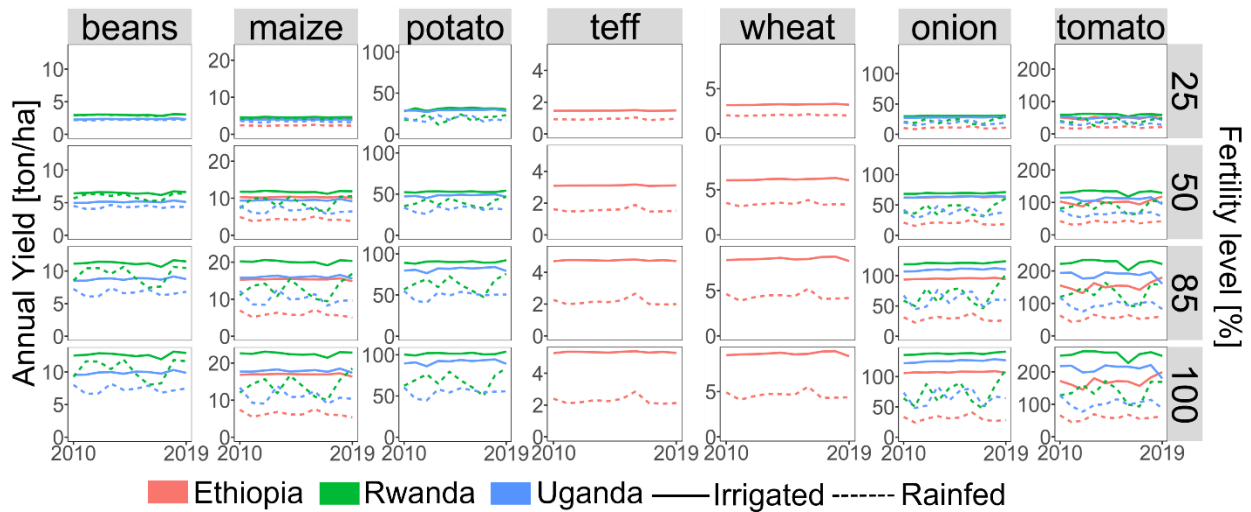


Figure 3.7. Effects of small-scale irrigation on annual yields for crops grown with four fertility levels in Ethiopia, Rwanda, and Uganda.

3.4. Limitations of the study

In considering the results of this work, it is essential to acknowledge its limitations. Our simulations rely on modeling assumptions that may or may not be representative of actual

characteristics. For instance, I find that the low permeability of soils in nearly 200 districts (i.e., woredas) in Central Ethiopia is unsuitable for high fertility scenarios, causing low yields and diminishing returns. This assertion is consistent with Tittonell and Giller's [151] findings that the quality of soils in Africa is highly variable and, in some cases, unresponsive to fertilizers. This uncertainty is critical as low permeability could hinder the transport of nutrients and water to the plant and, ultimately, crop development and irrigation requirements.

Similarly, I model traditional crops' phenology to resemble seeds currently used in East Africa based on studies in other parts of the Global South. However, there seems to be some variability in the use of different seed varieties. For instance, 88% of Rwandan agricultural plots use traditional seeds with only 25% maize plots, 2% of bean and potato plots, and 42% vegetable plots using improved seeds [133]. In Uganda, 77% of cultivated fields use traditional seeds, with improved seeds present in 18% of maize plots, 3% of beans plots, and 1.5 to 9% of potato plots [135]. Gathering specific characteristics of current traditional seeds and potential improved ones could enhance our estimates' accuracy and geolocation. Another important limitation relates to interpreting the water availability balance, given the opposing influence of modeling parameters. AquaCrop's deficit irrigation mode simulations provide high water productivity yields with less water applied to crops. Meanwhile, the assumption that 100% of each simulated hectare of planted land has irrigation is somewhat optimistic and likely offsets the water savings from the deficit irrigation assumption.

Other unmodeled factors could have further implications. For instance, if small-scale irrigation systems rely more on human resources (e.g., flooded irrigation) than on processes facilitated by electrical pumps, water use is likely to increase. Likewise, electricity for irrigation provided

through non-renewable sources like diesel could increase air pollutants' emissions and influence human health. Lastly, I should note not underestimating the unquantified benefits of ensuring food security and reducing poverty in a community.

3.5. Conclusions

My study evaluates the implications of small-scale irrigation systems on crop productivity, electricity for pumping irrigation, and water resource availability in East Africa. I use AquaCrop to simulate yields and water demand for irrigation under different scenarios and combine it with irrigation and hydrology models to estimate the increase in crop productivity, the electricity requirements for irrigation, and the water balance. This study shows that small-scale pressurized irrigation can significantly increase yields in regions with enough water to irrigate horticulture and staple crops sustainably. Meanwhile, the electricity demand for irrigation per additional ton is highest in districts of Ethiopia, followed by Uganda and Rwanda. It is worth noting that the electricity demand for irrigation depends significantly on the amount of water required for irrigation and the groundwater table's depth. However, higher electricity demands for irrigation are not necessarily a reasonable indicator of opportunities with potential for co-investment in electricity and irrigation. Instead, the answer lies somewhere with an adequate balance between both elements such that investors and farmers can find good economic viability and safeguard sustainable food production, especially with regards to water. In Chapter 4, I study the techno-economic feasibility of the system proposed here.

Irrigation also can make yields more predictable year-round, thus ensuring an adequate provision of food in countries with challenging conditions, such as Rwanda with its land constraints or Ethiopia with its regional hydrological and pedological (i.e., soil) limitations. However, water

uses beyond irrigation could increase competition for a finite resource and be detrimental to agriculture productivity. Competing water uses might include potable water supply for human use, produce washing, and even power generation. It is possible that under a future changing climate, our irrigation potential estimates may not be applicable anymore, thus requiring further study.

Another finding consistent with Tiftonell and Giller [151] shows that climatic zone, fertility, and soil characteristics are the most critical biophysical drivers of yield gaps across countries/districts. The climatic zone determines the volume of water and the electricity demand for irrigation. It includes the minimum and maximum temperatures and rainfall, solar radiation, and the length of growing seasons. The cultivar type, on the other hand, is not as important as the factors already mentioned. An exception to this point is potatoes since they seem to respond better to cultivar than fertility and irrigation. This feature is likely due to potatoes not being as sensitive to fertility as maize or onion. In short, these four factors are complementary for increasing crop yields with combined effects proportionally greater than individual effects on crop yields.

This Chapter's primary purpose is to provide quantitative-based insights about the locations where small-scale irrigation systems are technically feasible with an adequate balance between electricity demand for irrigation and yield gains. Admittedly, this Chapter does not intend to predict future yields or irrigation potential, nor tries to forecast the impact of irrigation on individual years with extreme patterns (e.g., rainy, dry, or hot). Any analysis aiming to answer those questions is out of this study's scope and would likely require extensive calibration of relevant parameters, such as climate data or crop physiology. In the next Chapter, I extend the

coverage to evaluate the economic ramifications of irrigation such that investors and farmers can look for opportunities to foster agricultural modernization and boost economic growth [26].

4. Techno-economic analysis of small-scale pressurized irrigation in Ethiopia, Rwanda, and Uganda

Abstract

Pressurized irrigation technologies have the potential to improve agricultural productivity and rural livelihoods, especially for smallholders. While pressurized irrigation often fails because of difficulties with technology adoption and governance issues, scholars have found that economic returns for small-scale projects may be higher than for large-scale projects. This study evaluates the techno-economic potential of small-scale pressurized irrigation in Ethiopia, Rwanda, and Uganda for three staple crops (maize, teff, and wheat, in Ethiopia; maize, potato, and beans in Rwanda and Uganda) and two horticulture crops (tomato and onion). This evaluation uses a combination of econometric tools applied to a previously developed district-level biophysical irrigation model based on agronomic and hydrology aspects. My results show that the Levelized Cost of irrigation (LCOI) is lower than 2016 crop prices with water available for sustainable irrigation in 17-35% of woredas in central and western Ethiopia, 19-71% of Rwanda's western and southern districts, and 15-48% of Uganda's southern and northwestern districts. My model also shows that the projected country-level annual electricity use for irrigation for districts with LCOI lower than 2016 crop prices and positive water availability amounts to 17%, 65%, and 17% of the total electricity generated in Ethiopia, Rwanda, and Uganda. A sensitivity analysis shows that electricity prices can significantly impact the LCOI of staple crops, especially for those grown with low-yield cultivars and 50% or lower fertility levels. These results suggest that integrating a district-level small-scale pressurized irrigation model could help inform decision-making and planning in places where infrastructure might not yet be fully developed or adequate.

4.1. Introduction

East Africa relies mainly on rainfed agriculture, with less than 4% of its cultivated area equipped for irrigation, mostly with non-pressurized technologies, compared to 20% globally and 37% in Asia [98]. With the predominance of smallholder agriculture in East Africa [152], accounting for over 75% of agricultural outputs in countries like Ethiopia and Uganda [153], small-scale pressurized irrigation technologies have the potential to play a decisive role in improving rural livelihoods [97], [105].

In contrast to large-scale commercial projects (mostly in developed nations), adoption of pressurized methods by smallholders (in developing countries) often fails because of difficulties integrating skills and technology, weak governance institutions, and poor access to markets [97], [100], [101], [104]. Interestingly, scholarly studies in Africa found that small-scale irrigation projects' economic returns are higher than for large-scale systems [116], [154]. However, irrigation projects may be economically viable for cash or high-value crops and not for staple crops [116].

Traditional smallholder irrigation technologies include surface methods such as water harvesting, spate irrigation, river flood plain irrigation, hill irrigation, and, the most common, surface irrigation. These technologies are often low-cost and straightforward, but they can also be labor inefficient and lead to excessive water use. Meanwhile, modern technologies include drip and sprinkle irrigation, combined with systems of pipes for water distribution. Additionally, water sources may vary from rainwater harvesting, small dam storage, river streams, and groundwater [104], [105]. In the latter case, it may be necessary to dig a well to collect water for irrigation.

Finding a successful irrigation technology depends on geophysical conditions such as agroclimatic region, topography, and water availability. It also relies on finding the appropriate cooperation mechanisms between governments, NGOs/private sector, and farmers. Experiences in Sub-Saharan Africa (SSA) show that the most successful smallholder projects happened when farmers had some control over technologies (simple) and water supplies (secure) and when stakeholders showed active levels of commitment or engagement during planning and implementation [105], [155]. As noted by Kay [105], perhaps “the most successful technologies are those that improve existing farming systems rather than those that introduce radically new ideas.”

Most efforts to evaluate small-scale irrigation systems' profitability or economic feasibility include engineering economic methods such as Cost-Benefit Analysis (CBA). For instance, Lorenzo et al. [156] use net present costs (NPC) and internal rate of return (IRR) to quantify economic savings from replacing diesel-based irrigation with photovoltaic (PV) systems in Western Africa. Campana et al. [157] find that the payback period (PBP) for irrigation systems of various crops in China is shorter for PVs than for wind-powered systems. You et al. [117] find that IRR is higher for small-scale than large-scale irrigation systems in most African countries. Zou et al. [158] show that four water-saving irrigation technologies are cost-effective for climate change mitigation and adaptation in China and could be profitable to increase grain yields compared to traditional irrigation. Moreover, other studies use tools such as water productivity to evaluate diverse irrigation technologies in Italy [159] or the willingness to pay (WTP) for smallholder irrigation systems in Ghana [160]. In this study, I combine various statistical methods from the literature [157], [158], [161] to perform a techno-economic analysis of the smallholder irrigation system described in Chapter 3 for Ethiopia, Rwanda, and Uganda.

4.2. Materials and Methods

The integrated assessment approach described in Chapter 3 provided estimates of yields, electricity demand for irrigation, and water availability from 2010 to 2019. These estimates were based on AquaCrop simulations and simplified crop relations for two cultivar varieties per crop of beans, maize, onion, potato, teff, tomato, and wheat under four fertility scenarios. They also included a pressurized smallholder (i.e., less than 10 hectares) irrigation system sourced from and equipped with groundwater pumping.

My techno-economic analysis starts by evaluating the irrigation system's costs normalized by the additional metric ton of yield due to irrigation for each crop. This metric is appropriate because it normalizes the costs of a projected intervention (i.e., irrigation) by the outcome from that intervention (i.e., yield change). The normalized metric is analogous to standard metrics used in the literature, such as the Levelized cost of energy (LCOE), the cost-effectiveness ratio (CER) of additional grain yields [158], or the Levelized cost of drinking water supply [162]. I will refer to this metric as the Levelized cost of irrigation (LCOI) from this point forward. I then use LCOI combined with our water availability (i.e., recharge minus irrigation) estimates to evaluate the irrigation potential on a district level basis. Finally, I perform a sensitivity analysis for different electricity prices. This analysis uses the improved cultivar with 100% fertility level scenario as the maximum attainable reference case because proposed policies in the three countries include substantial fertilizer and improved seed use increases.

4.2.1. Levelized Cost of Irrigation (LCOI)

I evaluate a district's LCOI by normalizing the irrigation system's annualized costs with the additional metric ton produced due to irrigation at a given fertility level for crop j , as in Eq. 4.1.

$$LCOI_j = \left(\left(\frac{(1.5 * DTW * C_{bd}) * r}{1 - (1 + r)^{-n_1}} \right) + \left(\frac{(I + OM + E_{irr_j} * C_E) * r}{1 - (1 + r)^{-n_2}} \right) \right) * \frac{1}{Y_{irr_j} - Y_{plu_j}} \quad Eq. 4.1$$

Where the first term approximates the borehole drilling depth as 50% more than the average depth to the groundwater table DTW [137], borehole drilling costs C_{bd} of 250 US\$ m⁻¹ [163], and borehole drilling (for water extraction) lifetime n_1 of 20 years [164]. In the second fraction, I is the capital investment costs for a pressurized irrigation system and equals 5,700 US\$ ha⁻¹ [165]; OM is the operation and maintenance costs, approximated as 5% of I [117] and equals 285 US\$ ha⁻¹. In the same term, E_{irr_j} represents the electricity for pumping requirements for crop j , with electricity costs C_E for pumping to extract and deliver water of 0.5 US\$ kWh⁻¹ [166], assuming electricity sourced from mini-grid solar photovoltaic (PV). The irrigation system lifetime for water delivery, n_2 , equals five years since delivery systems reportedly last 2-5 years before needing any major repairs or equipment replacements [117]. For the discount rate r , I use values of 11% for Ethiopia, 15% for Rwanda, and 17% for Uganda [167]. These rates are applicable in our study because they consider capital costs of large and small-scale PV projects and reflect country-specific factors such as perceived risks by investors or the relative supply and demand of finance. Meanwhile, the last term refers to the difference between the rainfed yield (Y_{plu}) and the irrigated fresh-weight yield (Y_{irr}) for the same fertility level.

I then compare *LCOI* with market crop prices calculated as the ratio of gross production value (GPV) to the harvested area with FAOSTAT data [120]. By FAO definition, GPV measures crop production in monetary terms at the farm gate level without subtracting intermediate uses within the agricultural sector (seed and feed). Then, preferred options are for *LCOI* values that are smaller than market prices. Table 4.1 shows the calculated market prices used in this Chapter.

Table 4.1. Calculated 2000-2016 range of crop prices from FAOSTAT.

	Crop prices, US\$ per metric ton		
	<i>Ethiopia</i>	<i>Rwanda</i>	<i>Uganda</i>
Beans	-	200 to 620 (420)	200 to 620 (420)
Maize	70 to 350 (170)	125 to 410 (300)	125 to 410 (300)
Onion	195 to 450 (320)	280 to 760 (540)	280 to 730 (540)
Potato	-	95 to 680 (280)	95 to 300 (200)
Teff	200 to 800 (490)	-	-
Tomato	110 to 320 (210)	200 to 650 (410)	210 to 650 (410)
Wheat	120 to 530 (300)	-	-

1 – The number in parenthesis indicates the mean value

4.2.2. Irrigation Potential and Implications by District

To estimate the irrigation potential, I combine *LCOI* (Eq. 4.1) and *WaterAvail* (Eq. 3.3) on a district level basis. This calculation relies on the averaged outputs from Chapter 3’s crop growth module (i.e., yields and irrigation water) and irrigation module (i.e., electricity demand for irrigation) over the simulated ten years to find an annual district-level point estimate per crop, fertility level, and watering mode. Averaging these outputs smooths out climate variability across years and enables us to compare different scenarios (e.g., improved vs. traditional crop cultivars) across countries. These averaged values then serve as inputs for the analysis of irrigation potential.

I estimate the irrigation potential as the proportion of districts exhibiting both $LCOI \leq$ specified-crop-price [120] and $WaterAvail \geq 0$ mm/ha w.r.t. the total number of districts per country. I find this proportion for a given country's cultivar and fertility level by dividing all districts with potential across the five crops by the total number of districts multiplied by five. For instance, if the sum of all districts with potential across the five crops grown with improved cultivars and 100% fertility in Rwanda is 98, the irrigation potential would be 65% because the total number of districts multiplied by five is 150. (i.e., 30 districts x 5).

4.2.3. Sensitivity Analysis

Because this study's emphasis is on the effects of irrigation on productivity and energy consumption for irrigation, I perform a sensitivity analysis using 0.1, 0.5, and 1.0 US\$/kWh as the electricity price.

4.3. Results and Discussion

4.3.1. Levelized Cost of Irrigation (LCOI)

Comparing a given crop's LCOI and market price can provide some idea of the economic viability of irrigating a crop. With the introduction of that "economic viability" concept in mind, Figure 4.1 shows that horticulture crops grown with improved cultivars for all fertility levels have the highest proportion of districts with LCOI lower than the crop market prices represented by the vertical dashed lines. For staple crops, LCOI is lower than crop market prices for beans with at least 85% fertility and maize, teff, and wheat with at least 50% fertility, as evidenced by points to the left of the vertical dashed lines. LCOI for potato is lower than market prices for any fertility level when grown with improved seeds and fertility levels above 25% in Uganda and

above 50% in Rwanda when grown with traditional seeds. Additionally, the cultivar choice and at higher fertility rates seem to be less critical in Ethiopia. Therefore, it would make sense (i.e., $LCOI < \text{market prices}$) to grow potato and horticulture crops for the reference case of improved cultivars grown with 25% fertility.

Unsurprisingly, LCOI depends strongly on soil fertility and crop prices. For instance, the proportion of districts with LCOI for maize lower than the highest crop market price since 2000 increases from 0 to 68% in Ethiopia, 0 to 100% in Rwanda, and 0 to 79% in Uganda, when increasing fertility from 25% to 100%. The same comparison for maize but with regard to the lowest crop price since 2000 does not yield increases while going from low- to high-fertility levels and shows that no districts or woredas have LCOI lower than the market crop price. More information about crop market prices from 2000 onwards is available in the SI.

It is worth noting that common crops' prices (i.e., maize, onion, tomato) are substantially lower in Ethiopia than in Rwanda and Uganda, likely due to a higher supply. It is possible that higher yields from irrigation could drive down crop prices as domestic production increases.

Simultaneously, adding post-harvest activities along the crop's value chain (e.g., processing maize for flour production) can help accommodate increased production, likely boosting the irrigation systems' profitability. Domestic production increases will likely depress crop prices and reduce returns on irrigation systems' investments until market prices for various crops reach a balance point, leading to an “efficient” irrigation allocation.



Figure 4.1. Levelized Cost of Irrigation (LCOI) over ten years (2010-2019) for 690 districts in Ethiopia, 30 in Rwanda, and 80 in Uganda. The vertical axis shows the four fertility levels (FERT) at 25%, 50%, 85, and 100%. The horizontal axis shows the annualized costs of the irrigation system per additional yield due to irrigation in US\$ per metric ton. Black vertical dashed lines represent (from left to right) the minimum, mean, and maximum annual crop prices for each country in US\$ per ton (FAOSTAT, 2019) from 2000 to 2016. The first three panels of each row (from left to right) represent staple crops, and the remaining two panels are horticulture crops. Note that the values on the x-axis are different for staple and horticulture crops.

4.3.2. Irrigation Potential by District

In Figure 4.2, darker gradient colors on the upper-right corner of the XY coordinate legend indicate high LCOI and readily available water. In contrast, lighter gradient colors toward the XY coordinate's bottom-left side indicate low LCOI and negative water availability. While the irrigation potential depends upon crop market prices at a specific time, desirable district colors are generally in the purple area, where LCOI is relatively low and water availability is greater or equal to zero. Yellow- and green-colored districts have LCOI around 1,000 US\$/t, which is usually above market prices for most crops. Moreover, I use the improved 100% fertility case as the best-case scenario because proposed policies in countries like Rwanda and Uganda include substantial fertilizer and seed improvements.

Figure 4.2 suggests that the highest irrigation potential for the best-case scenario (i.e., $LCOI \leq 1,000$ US\$/t and $WaterAvail \geq 0$ mm/ha) occur for purple-colored areas. These areas are more pronounced for horticulture crops in Ethiopia's Central-Western districts, most of Rwanda's Western half, and Uganda's Southeastern and Northwestern. The names of the regions where this irrigation potential occur are Amhara, Addis Ababa, Benishangul-Gumuz, and parts of Oromiya and Southern Nations, in Ethiopia; West, South, and parts of North, in Rwanda; Central, East Central, Elgon, West Nile, and parts of Teso, Acholi, South Western, and Western, in Uganda. With limited capital, decision-makers may deem it wise to prioritize the high irrigation potential areas first.

For the 2016 irrigation potential (i.e., $LCOI \leq 2016\text{-crop-price}$ and $WaterAvail \geq 0$), the range of districts with potential across cultivars and fertility levels is 17-35% in Ethiopia, 19-71% in Rwanda, and 15-48% in Uganda. The analysis also shows that fertility levels should be at least

50% to have considerable irrigation potential. Similarly, there is irrigation potential for horticulture crops in at least 60% of all countries' districts for the reference case of improved cultivars and 100% fertility. In contrast to the relatively high proportion of districts with potential in Rwanda and Uganda for potato (87% and 61%, respectively), and Rwanda for maize (97%), crops with the lowest proportion of districts are beans in Rwanda (0%) and Uganda (4%), and wheat in Ethiopia (6%).

The previous exercise suggests that Rwanda has the highest irrigation potential. However, it would be misguided to conclude that irrigation is more attractive in Rwanda than in Uganda or Ethiopia. Such recommendation would require a more comprehensive analysis with additional complexity, especially regarding local crop prices (dependent on regional supply and demand), labor wages, or even the growth of priority crops.

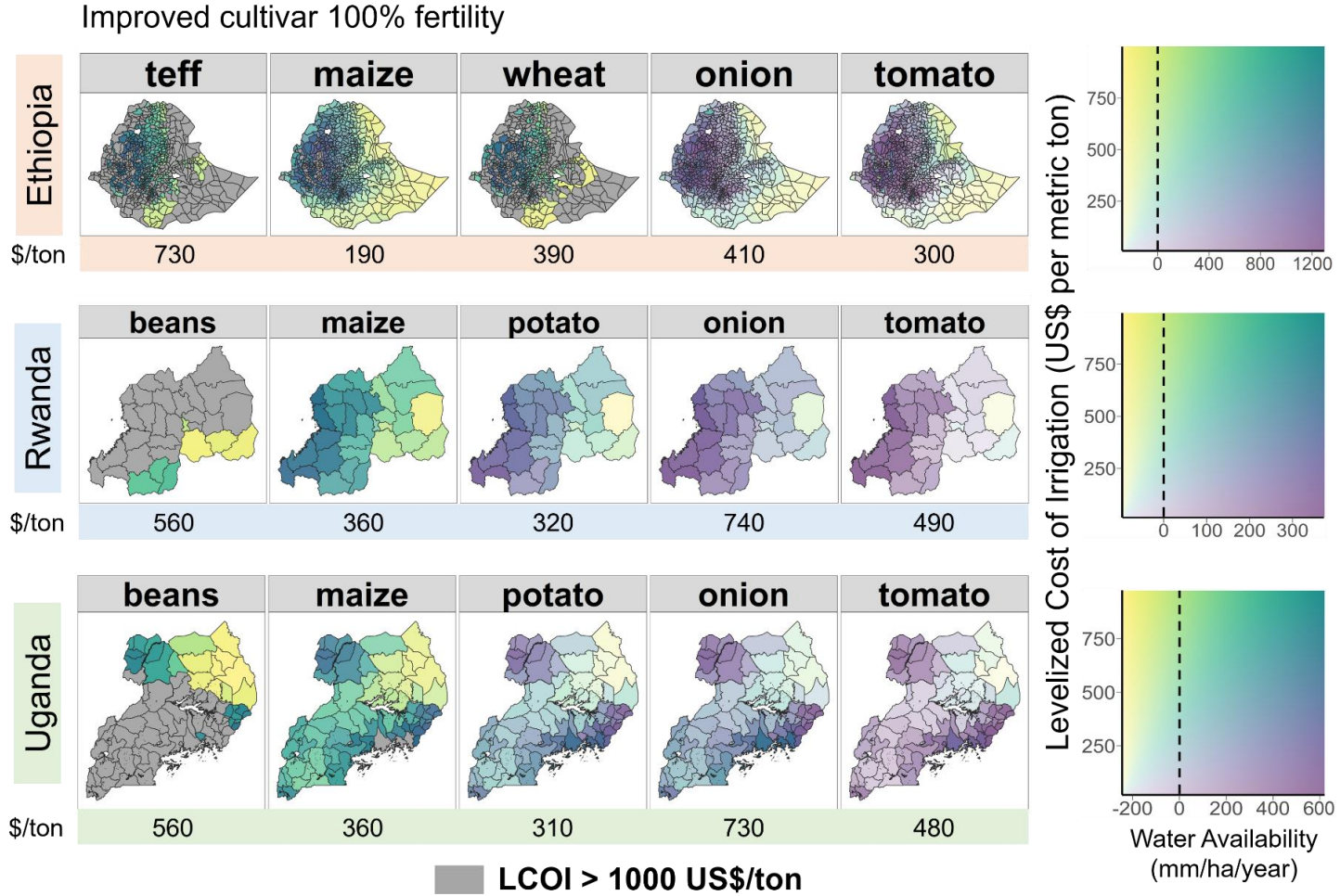


Figure 4.2. Map of irrigation potential for improved cultivars grown with 100% fertility. On the right-hand side, the three plots serve as bivariate legends. The x-axis shows water availability (in mm/ha/yr) while the y-axis displays the Levelized cost of irrigation, LCOI (in US\$ per metric ton). Note that districts with LCOI costs above 1,000 US\$/ton are shown in gray. The labels under each country's maps display the market price per crop (US\$ per metric ton) derived from FAO [120]. Note that the geographical scale of each country's map is different for better appreciation.

4.3.3. Electricity Consumption Potential

I estimated the projected annual electricity consumption for irrigation per country by multiplying our electricity estimates per district by the planted area per district per crop. I extracted the planted areas for each of the simulated crops from MapSPAM [171], an entropy-based model that estimates crop production patterns at high resolution. Reported estimates matching the description of the crops simulated in this study are beans, maize, potato, and wheat. I approximated the planted area for teff, onion, and tomato using reported data for "other cereals" and "vegetables," respectively. Then, filtering districts with both $LCOI \leq 2016\text{-crop-price}$ and $WaterAvail \geq 0$, I aggregated electricity for irrigation use on a country-level. My projections show that annual electricity for irrigation can rise to 1.6 TWh in Ethiopia, 490 GWh in Rwanda, and 670 GWh in Uganda, representing 17%, 65%, and 17% of the latest reported electricity consumption, respectively [169], [172], [173].

4.3.4. Sensitivity Analysis

Table 4.2 shows that LCOI in Ethiopia is more sensitive to changes in electricity prices, followed by Uganda and Rwanda, in that order. The table also indicates that LCOI for tomato grown with traditional seeds in Ethiopia has the highest electricity price change of all crops across countries, followed by maize grown with improved seeds. This change occurred for the increased LCOI due to increases in electricity price from 0.5 to 1.0 US\$/kWh. Similarly, tomatoes grown with traditional seeds had the largest LCOI reduction of all crop cultivars.

Table 4.2. Sensitivity analysis for electricity prices measured as LCOI percent change with respect to the base case with an electricity price of 0.5 US\$ per kilowatt-hours.

LCOI sensitivity for electricity prices with respect to base case [% change]

	<i>Ethiopia</i>	<i>Rwanda</i>	<i>Uganda</i>
Teff	-21 (-18), +27 (+22)	-	-
Wheat	-20 (-25), +25 (+31)	-	-
Beans	-	-17 (-17), +22 (+21)	-20 (-19), +25 (+24)
Potato	-	-18 (-15), +23 (+19)	-21 (-21), +27 (+26)
Maize	-25 (-22), +32 (+27)	-17 (-13), +21 (+17)	-19 (-14), +24 (+17)
Onion	-23 (-19), +29 (+24)	-16 (-14), +20 (+17)	-17 (-19), +21 (+24)
Tomato	-21 (-27), +27 (+34)	-21 (-18), +27 (+23)	-22 (-24), +27 (+30)

1 – Values in parenthesis denotes traditional cultivar.

2 – Negative values are for low prices. Positive values are for high prices.

Moreover, for horticulture crops grown with fertility levels greater than or equal to 50%, electricity price changes do not affect the proportion of districts with LCOI lower than the highest crop market prices (since 2000). Only for staples grown with fertility levels smaller than or equal to 85% are there considerable effects due to electricity price changes. For instance, the proportion of districts with LCOI lower than highest crop prices (since 2000) for improved maize with 85% fertility in Uganda can go from 14 to 79% (from high to low electricity price). The same comparison but for improved maize grown with 50% fertility in Ethiopia yields an increase from 13 to 30% of woredas with LCOI smaller than market prices. Similar increases (for districts with LCOI lower than highest crop prices since 2000) for staples grown with improved seeds and 50% fertility occur for teff (8 to 13%) and wheat (7 to 14%) in Ethiopia, maize (0 to 7%) in Rwanda, and maize (1 to 9%) and potato (86 to 95%) in Uganda. Meanwhile, electricity price changes do not affect the proportion of districts with LCOI smaller than high crop prices for potato grown with any fertility level in Rwanda (equal to 100%) or beans in Rwanda and Uganda (from 0 to 5%). Although crop price is the most critical factor for irrigation's economic viability, the electricity price can significantly impact the economic viability (or LCOI) for most crops, especially for staples.

4.4. Limitations of the study

It is worth mentioning the limitations of this work. First, the irrigation system's cost-effectiveness may depend significantly on the pump's energy source because of the often highly volatile prices of diesel, gasoline, and even photovoltaic systems in SSA. Other factors not considered that may influence output price volatility are extreme weather and market conditions in neighboring countries. For instance, a short supply of maize in Uganda and Kenya may lead to an increased output price (US\$ per ton) in Rwanda. Another aspect not considered is that increasing the production of certain crops with irrigation could depress domestic prices. Similarly, the cost-effectiveness and feasibility of irrigation could change depending on the availability and costs of nutrients (i.e., fertilizers) and labor (i.e., wages) in each country.

I should also note that the term gross production value (GPV) is not the same as the gross value added (GVA) commonly used to measure economic productivity. GPV does not consider all uses alongside crop value chains. Instead, it accounts for intermediate uses and inputs (e.g., sowing, irrigation, harvesting) at farm gate level or up until harvest. This analysis assumes that intermediate uses within the agricultural sector do not change over time. This assumption is important because adding more intermediate services along the value chain—such as post-harvest processing, transportation, or packaging for wholesale or retail market purposes—will likely increase the output price and, in turn, the revenue per hectare.

4.5. Conclusions

This Chapter assessed the techno-economic feasibility of the small-scale pressurized irrigation system depicted in Chapter 3. My study shows that irrigating onion, tomato, and potato is more

economically viable (based on the balance between LCOI, water availability, and crop price) than irrigating beans, maize, teff, and wheat, especially for crops grown with improved seeds with at least 50% fertility levels. These results fall in line with Sheahan and Barret's [107] findings, which point out the economic benefits of combining irrigation, improved seeds, and fertilizers. On the other hand, the least economically viable crops are teff and beans grown with traditional seeds. In this sense, irrigation's economic viability hinges significantly on crop price and LCOI, which in turn depends considerably on water availability, fertility level, and to a lesser extent, cultivar variety.

I find that the districts with the highest irrigation potential occur for horticulture crops grown with improved cultivars in most of Ethiopia's central and western parts (regions of Tigray, Amhara, Benishangul-Gumuz, Gambela, Addis Abeba, and most of Oromia), most of Rwanda's Western and Southern provinces, and parts Uganda's south and northwest (Central region, the western part of Northern region, and southern parts of Western and Eastern regions). Based on the 2016 irrigation potential for the two horticulture crops and three staples, irrigation in Rwanda would be the most attractive, then Uganda and Ethiopia. The same pattern is valid when aggregating the electricity consumption for irrigation for districts with both $LCOI \leq 2016\text{-crop-price}$ and $WaterAvail \geq 0$. In this case, Rwanda's irrigation electricity load can make up to 65% of its total power consumption [169]. Meanwhile, the sensitivity analysis shows that electricity price can significantly impact the economic viability (or LCOI) of staples grown with traditional cultivars and moderate or poor fertility levels.

Future complementary work could focus on the financial and energy impacts of post-harvesting activities on selected crops' value chains. The criteria to choose the appropriate value chains

might contemplate the potential to generate higher added value crops (e.g., through exporting) such as avocado, banana, or coffee. This Chapter intended to provide techno-economic insights at the district-level for small-scale pressurized irrigation systems with the specific aim to help decision-making and planning in places where infrastructure might not yet be fully developed or adequate.

5. Conclusions

We take for granted the things we need the most. Food, energy, and water are arguably the most vital resources humans need. Continued increases in population and challenges exacerbated by climate change are affecting the supply of such resources. The inherent geographical and climate characteristics of a location determine the specific challenges of that part of the world.

Understanding the interlinkages of vital systems such as the food-energy-water (FEW) nexus will become essential while tackling the challenges lying ahead. One of these challenges, for instance, is the energy and water resources competition between the agriculture and power production sectors. Another challenge relates to agriculture's energy consumption, from harvesting to post-harvesting and retail activities. This thesis aims to provide insights into the FEW nexus through case studies in the United States and East Africa. Specifically, I investigate and quantify the impacts of agriculture and food production systems on energy consumption and water resources.

Chapter 2 investigated the impacts of projected climate change scenarios on heating and cooling energy for the broiler chicken industry. This study found that climate change may reduce energy demand for heating and increases in energy demand and water withdrawals for cooling in broiler barns. My results show that water demand for cooling could increase significantly, which creates an additional vulnerability should water resource constraints in the region increase due to climate change [43]. Similarly, the increase in electricity demand for cooling during summer could have implications for the power system, which will likely face other climate-induced constraints, including increased demand from other sectors, water flow restrictions, and capacity deratings for existing power plants [84].

These results' policy and industrial impacts may differ depending upon individual production facilities' characteristics and operation and respective climate zone. For instance, most broiler barns reviewed in the literature use propane for heating and fan ventilation for cooling. With a warming climate, it is possible that some barns, especially in the South, may not be able to cool with ventilation alone, and they may resort to additional cooling devices such as evaporative cooling pads or even air conditioning if the electricity price is low enough. Thus, the change in electricity or gas (e.g., propane) tariffs could influence barns' actual operation and, ultimately, the climate change effects. Efforts to improve energy efficiency and animal-welfare could affect standard industry practices, especially in broiler house sizes and bird density. Other changes that could benefit growers are to increase barn insulation to reduce energy consumption or reduce the number of batches grown in winter when propane consumption is highest (from 6 to 10 times higher than in summer, per my model). Future work could focus on evaluating the energy implications of such production practice modifications or evaluating the impact of clean heating and cooling sources on greenhouse gas emissions. To summarize, this chapter does not intend to forecast the course of energy consumption in individual broiler houses under climate change but to highlight that climate will affect broiler production operations by changing the resource requirement for temperature control in broiler houses.

The second case study in East Africa, described in Chapters 3 and 4, investigates the effects and implications of small-scale pressurized irrigation in a non-industrialized setting. Specifically, I evaluate yield increase trends, water and electricity for irrigation requirements, and the economic viability of small-scale pressurized irrigation through an integrated modeling approach. In that order and consistent with Tittonell and Giller's [151] findings, this study finds that climatic zone (which determines the water available for irrigation), soil fertility, and soil characteristics are the

most important biophysical drivers of agricultural yields at the district/country level. The climatic zone and the hydrogeology (i.e., the study of groundwater) determine the volume of water and electricity demand for irrigation through differences in temperatures, rainfall, growing seasons, and depth to groundwater. While other factors such as the cultivar variety may not seem significant, they can provide an added boost in yields when the main factors just mentioned are not available or too expensive. In turn, irrigation's economic viability depends upon the crop type and its market price. In general, more affordable crops to irrigate (measured through the Levelized cost of irrigation) are (in decreasing order) tomato, onion, potato, maize, wheat, teff, and beans, especially those grown with improved seeds with at least 50% fertility levels. Not surprisingly, the Levelized cost of irrigation (LCOI) is higher for crops grown with traditional seeds and low fertility levels. These results are consistent with Sheahan and Barret's [107] intuitive finding that combining irrigation with fertilizers and improved seeds is critical for obtaining adequate economic returns. These observations are relevant for decision-making and planning because the microclimate and geolocation at the resolutions in my study aim to provide insights into small-scale pressurized irrigation's techno-economic capacity.

Future work could focus on studying the effects of other uses of water and electricity beyond irrigation (e.g., post-harvest processing, storage) and alongside agricultural value chain processes in order to increase the infrastructure's economic returns on investments. Additionally, incorporating and adopting previously unused electrical technologies will most likely provide additional benefits and disposable income as the learning curve decreases over time. Ultimately, as successful case studies by Nordhaus et al. [26] point out, economic growth occurs as part of an overall process of development and modernization, including the adoption of universal electrification, significant energy consumption, industrialization, and agricultural enhancements.

Other work that may be interesting for further study includes evaluating the impact of projected climate change scenarios on irrigation's techno-economic potential. Similarly, there are plans to scope the techno-economic feasibility of non-fossil nitrogen fertilizer production using excess energy from shared (with irrigation) renewable technology infrastructure.

This thesis contributes to expanding the understanding of interdependent food-energy-water nexus systems through two case studies. These case studies shed light on the energy and water consumption impacts of enhancing agricultural production systems in the United States and East Africa. While I provide insights into some of the challenges faced in industrialized and non-industrialized countries, much work remains to be done. There are numerous opportunities to integrate a more comprehensive agricultural decision tool that uses climate data as input to evaluate energy or water impacts. Future work could include developing simplified models that are less computationally intensive or require fewer parameters to generalize well. I hope that parts (or all) of the models described in this thesis will develop into one comprehensive agriculture-energy tool that helps inform decision-makers and planners with unbiased and comprehensive insights.

References

- [1] United Nations, Department of Economic and Social Affairs, Population Division. “World Population Prospects 2019: Highlights ST/ESA/SER.A/423,” United Nations, New York, 2019.
- [2] United Nations, Department of Economic and Social Affairs, Population Division. “World Urbanization Prospects 2018: Highlights (ST/ESA/SER.A/421),” United Nations, New York, 2019.
- [3] Food and Agriculture Organization of the United Nations. “The future of food and agriculture – Alternative pathways to 2050,” Rome, Italy: FAO, 224 pp, 2018.
- [4] U.S. Energy Information Administration. “International Energy Outlook 2020 with projections to 2050,” Washington, DC, 2020.
- [5] WWAP (UNESCO World Water Assessment Programme). “The United Nations World Water Development Report 2019: Leaving No One Behind,” Paris, UNESCO, 2019.
- [6] S. Siebert, J. Burke, J. M. Faures, K. Frenken, J. Hoogeveen, P. Doll, F. T. Portmann. “Groundwater use for irrigation: A global inventory,” *Hydrol. Earth Syst. Sci.*, vol. 7, pp. 3977–4021, 2010.
- [7] WWAP (United Nations World Water Assessment Programme). “The United Nations World Water Development Report 2014: Water and Energy,” Paris, UNESCO, 2014.
- [8] Food and Agriculture Organization of the United Nations. “Energy Smart Food for People and Agriculture, Issue paper,” 25 p., Rome, Italy: FAO, 2011.
- [9] Food and Agriculture Organization of the United Nations. “The State of Food and Agriculture 2019: Moving forward on food loss and waste reduction,” Rome, Italy: FAO, 2019.
- [10] A.M. Hamiche, A.B. Stambouli, S. Flazi. “A review of the water-energy nexus,” *Renewable and Sustainable Energy Reviews*, vol. 65, pp. 319—331, 2016.
- [11] M.C. Rulli, D. Bellomi, A. Cazzoli, G. De Carolis, P. D’Odorico. “The water-land-food nexus of first-generation biofuels,” *Scientific Reports*, vol. 6, 22521, pp. 1—10, 2016.
- [12] International Food Policy Research Institute. “Global nutrition report 2016: From promise to impact: Ending malnutrition by 2030,” Washington, DC: International Food Policy Research Institute, 2016.

- [13] FAO, IFAD, UNICEF, WFP & WHO. “The State of Food Security and Nutrition in the World 2019. Safeguarding against economic slowdowns and downturns,” Rome, FAO, 2019. [Online]. Available: <http://www.fao.org/3/ca5162en/ca5162en.pdf>
- [14] M. Bazilian, H. Rogner, M. Howells, S. Hermann, D. Arent, D. Gielen, et al. “Considering the energy, water and food nexus: Towards an integrated modelling approach,” *Energy Policy*, vol. 39, pp. 7896—7906, 2011.
- [15] M. Howells, S. Hermann, M. Welsch, M. Bazilian, R. Segerstrom, T. Alfstad, et al. “Integrated analysis of climate change, land-use, energy and water strategies,” *Nature Climate Change*, vol. 3, pp. 621—626, 2013.
- [16] P. D’Odorico, K.F. Davis, L. Rosa, J.A. Carr, D. Chiarelli, J. Dell’Angelo, et al. “The Global Food-Energy-Water Nexus,” *Reviews of Geophysics*, vol. 56, pp. 456—531, 2017.
- [17] B.R. Scanlon, B.L. Ruddell, P.M. Reed, R.I. Hook, C. Zheng, V.C. Tidwell, S. Siebert. “The food-energy-water nexus: Transforming science for society,” *Water Resources Research*, vol. 53, pp. 3550—3556, 2017.
- [18] J.P. Newell, B. Goldstein, A. Foster. “A 40-year review of food-energy-water nexus literature and its application to the urban scale,” *Environmental Research Letters*, vol. 14, 073003, pp. 1—18, 2019.
- [19] T. R. Albrecht, A. Crootof, C.A. Scott. “The Water-Energy-Food Nexus: A systematic review of methods for nexus assessment,” *Environmental Research Letters*, vol. 13, 043002, pp. 1—26, 2018.
- [20] J. Zhang, P.E. Campana, T. Yao, Y. Zhang, A. Lundblad, F. Melton, J. Yan. “The water-food-energy nexus optimization approach to combat agricultural drought: a case study in the United States,” *Applied Energy*, vol. 227, pp. 449—464, 2019.
- [21] M.Y. Leung Pah Hang, E. Martinez-Hernandez, M. Leach, A. Yang. “Designing integrated local production systems: A study on the food-energy-water nexus,” *Journal of Cleaner Production*, vol. 135, pp. 1065—1084, 2016.
- [22] R. Lawford, J. Bogardi, S. Marx, S. Jain, C.P. Wostl, K. Knuppe, et al. “Basin perspective on the Water-Energy-Food Security Nexus,” *Environmental Sustainability*, vol. 5, pp. 607—616, 2013.

- [23] I. Ozturk. “Sustainability in the food-energy-water nexus: Evidence from BRICS (Brazil, the Russian Federation, India, China, and South Africa) countries,” *Energy*, vol. 93, pp. 999—1010, 2015.
- [24] G. Rasul, B. Sharma. “The nexus approach to water-energy-food security: an option for adaptation to climate change,” *Climate Policy*, vol. 16, no. 6, pp. 682—702, 2016.
- [25] L. Rosa, K.F. Davis, M.C. Rulli, P. D’Odorico. “Environmental consequences of oil production from oil sands,” *Earth’s Future*, vol. 5, pp. 158—170, 2017.
- [26] T. Nordhaus, K. De Kirby, T. Beek, E. Brush, A. Trembath. “The Road More Traveled: Case Studies in Universal Electrification,” The Breakthrough Institute, 2019. [Online]. Available: <https://thebreakthrough.org/articles/the-road-more-traveled>. [Accessed Jan 2021].
- [27] M.P. Blimpo, M. Cosgrove-Davies. “Electricity Access in Sub-Saharan Africa: Uptake, Reliability, and Complementary Factors for Economic Impact,” Africa Development Forum series, Washington, DC: World Bank, 2019.
- [28] J.L. Izar-Tenorio, P. Jaramillo, W. M. Griffin, M. Small. “Impacts of projected climate change scenarios on heating and cooling demand for industrial broiler chicken farming in the Eastern U.S.,” *Journal of Cleaner Production*, vol. 255, 120306, pp. 1—8.
- [29] United States Department of Agriculture, Foreign Agricultural Service. “Livestock and Poultry,” 2021. [Online Dataset]. Available: https://apps.fas.usda.gov/psdonline/downloads/psd_livestock_csv.zip. [Accessed Jan 2021].
- [30] R. Prinn, H. Jacoby, A. Sokolov, et al. “Integrated global system model for climate policy assessment: Feedbacks and sensitivity studies,” *Climatic Change*, vol. 41, pp. 469, 1999.
- [31] H. Duan, G. Zhang, S. Wang, Y. Fan. “Robust climate change research: a review on multi-model analysis,” *Environmental Research Letters*, vol. 14, 033001, 2019.
- [32] M. Isaac, D.P. van Vuuren. “Modeling global residential sector energy demand for heating and air conditioning in the context of climate change,” *Energy Policy*, vol. 37, no. 2, pp. 507-521, 2009.
- [33] T. Kjellstrom. “Impact of Climate Conditions on Occupational Health and Related Economic Losses: A New Feature of Global and Urban Health in the Context of Climate Change,” *Asia Pacific Journal of Public Health*, vol. 28, no. 25, pp. 28S-37S, 2016.

- [34] T.K. Mideksa, S. Kallbekken. “The impact of climate change on the electricity market: A review,” *Energy Policy*, vol. 38, no. 7, pp. 3579-3585, 2010.
- [35] I. Yildiz. “Review of climate change issues: A forcing function perspective in agricultural and energy innovation,” *International Journal of Energy Research*, vol. 43, no. 6, 2019.
- [36] J.Z. Zhi, J.M. Helman. “Implications of climate changes to building energy and design,” *Sustainable Cities and Society*, vol. 44, pp. 511—519, 2019.
- [37] N., Alexandratos, J. Bruinsma. “World agriculture towards 2030/2050: the 2012 revision,” ESA Working paper No. 12–03. FAO, Rome, 2012.
- [38] Food and Agriculture Organization of the United Nations. “Livestock Primary World Totals,” FAOSTAT, 2018. [Online Dataset]. Available: <http://www.fao.org/faostat/en/#data/QL>. [Accessed: May 2018].
- [39] United States Department of Agriculture, Foreign Agricultural Service. “Livestock and Poultry: World Markets and Trade,” 2018. [Online]. Available: https://apps.fas.usda.gov/psdonline/circulars/livestock_poultry.pdf. [Accessed: May 2018].
- [40] United States Department of Agriculture, Economic Research Service. “Livestock and Meat Domestic Data,” Economic Research Service, 2018. [Online]. Available: <https://www.ers.usda.gov/data-products/livestock-meat-domestic-data/>. [Accessed: May 2018].
- [41] National Chicken Council. “Broiler Chicken Key Industry Facts,” 2012. [Online]. Available: <http://www.nationalchickencouncil.org/about-the-industry/statistics/broiler-chicken-industry-key-facts/>. [Accessed: May 2017].
- [42] United States Department of Agriculture, National Agricultural Statistics Service. “Poultry Production and Value. Economics, Statistics and Market Information System,” 2017. [Online]. Available: <http://usda.mannlib.cornell.edu/MannUsda/viewDocumentInfo.do?documentID=1130>. [Accessed: May 2018].
- [43] D.J. Wuebbles, D.W. Fahey, K.A. Hibbard, et al. “Climate Science Special Report: Fourth National Climate Assessment,” Volume I, U.S. Global Change Research Program, Washington, DC, USA, 470 pp, 2017.

- [44] Y. Liang, G.T. Tabler, S.E. Watkins, H. Xin, I.L. Berry. “Energy use analysis of open-curtain vs. totally enclosed broiler houses in northwest Arkansas,” *Applied Engineering in Agriculture*, vol. 25, pp. 577–584, 2009.
- [45] United States Department of Agriculture, Economic Research Service. “Technology, Organization, and Financial Performance in U.S. Broiler Production,” 2014. [Online]. Available:
https://www.ers.usda.gov/webdocs/publications/43869/48159_eib126.pdf?v=41809.
[Accessed: May 2019].
- [46] United States Department of Agriculture, Animal and Plant Health Inspection Service. “Foreign Animal Disease Preparedness and Response Plan (FAD PReP)/National Animal Health Emergency Management System (NAHEMS) Guidelines,” Poultry Industry Manual, 2013. [Online]. Available:
https://www.aphis.usda.gov/animal_health/emergency_management/downloads/documents_manuals/poultry_ind_manual.pdf. [Accessed: May 2019].
- [47] B. Fairchild. “Environmental Factors to Control when Brooding Chicks,” The University of Georgia, College of Agricultural and Environmental Sciences, Cooperative Extension, Bulletin 1287, 2012. [Online]. Available:
https://secure.caes.uga.edu/extension/publications/files/pdf/B%201287_5.PDF.
[Accessed: May 2018].
- [48] G. Tabler. “Brooding Chicks and Poults: Environmental Critical Control Points,” The University of Arkansas, Division of Agriculture, Cooperative Extension Service, *Avian Advice*, vol. 5, no. 1, pp. 1–5, 2003.
- [49] H. Xin, I.L. Berry, G.T. Tabler, A. Costello. “Heat and Moisture Production of Poultry and Their Housing Systems: Broilers,” *Transactions of the ASAE*, Vol. 44, no. 6, pp. 1851–1857, 2001.
- [50] J. Hamilton, M. Negnevitsky, X. Wang. “Thermal analysis of a single-storey livestock barn,” *Advances in Mechanical Engineering*, vol. 8, no. 4, pp. 1–9, 2016.
- [51] N.K. Sakomura, F.A. Longo, E.O. Oviedo-Rondon, C. Boa-Viagem, A. Ferraudo, et al. “Modeling Energy Utilization and Growth Parameter Description for Broiler Chickens,” *Poultry Science*, vol. 84, pp. 1363—1369, 2005.

- [52] Department for Environment, Food and Rural Affairs UK. “Heat Stress in Poultry: Solving the Problem,” Defra Publications, 2005. [Online]. Available: <https://www.gov.uk/government/publications/heat-stress-in-poultry-solving-the-problem>. [Accessed: Dec 2017].
- [53] A.G. Soldatos, K.G. Arvanitis, P.I. Daskalov, G.D. Pasgianos, N.A. Sigrimis. “Nonlinear Robust Temperature-Humidity Control in Livestock Buildings,” *Computer and Electronics in Agriculture*, vol. 49, pp. 357—376, 2005.
- [54] G. Schauburger, M. Piringer, E. Petz. “Steady-state balance model to calculate the indoor climate of livestock buildings, demonstrated for finishing pigs,” *International Journal of Biometeorology*, Vol. 43, pp. 154–162, 2000.
- [55] J.H. Park, T.M. Peters, R. Altmaier, R.A. Sawvel, T.R. Anthony. “Simulation of air quality and cost to ventilate swine farrowing facilities in winter,” *Computer and Electronics in Agriculture*, vol. 98, pp. 136—145, 2013.
- [56] I. Weindl, H. Lotze-Campen, A. Popp, et al. “Livestock in a changing climate: production system transitions as an adaptation strategy for agriculture,” *Environmental Research Letters*, vol. 10, pp. 1–12, 2015.
- [57] O.F. Godber, R. Wall. “Livestock and food security: vulnerability to population growth and climate change,” *Global Biology Change*, vol. 20, pp. 3092-3102, 2014.
- [58] M.M. Rojas-Downing, A.P. Nejadhashemi, T. Harrigan, S.A. Woznicki. “Climate change and livestock: Impacts, adaptation, and mitigation,” *Climate Risk Management*, vol. 16, pp. 145–163, 2017.
- [59] A.N. Hristov, A.T. Degaetano, C.A. Rotz, et al. “Climate change effects on livestock in the Northeast US and strategies for adaptation,” *Climatic Change*, vol. 146, pp. 33-45, 2018.
- [60] I. Iglesias, S. Quiroga, M. Moneo, L. Garrote. “From climate change impacts to the development of adaptation strategies: Challenges for agriculture in Europe,” *Climatic Change*, vol. 112, pp. 143-168, 2012.
- [61] T. Hasegawa, S. Fujimori, Y. Shin, K. Takahashi, T. Masui, A. Tanaka. “Climate Change Impact and Adaptation Assessment on Food Consumption Utilizing a New Scenario Framework,” *Environmental Science & Technology*, vol. 48, no. 1, pp. 438-445, 2014.

- [62] F. Humpenöder, A. Popp, M. Stevanovic, C. Müller, B.L. Bodirsky, et al. “Land-Use and Carbon Cycle Responses to Moderate Climate Change: Implications for Land-Based Mitigation,” *Environmental Science & Technology*, vol. 49, no. 11, pp. 6731-6739, 2015.
- [63] G.L. Hahn, T.L. Mader, J.A. Harrington, J. A. Nienaber, K.L. Frank. “Living with climatic variability and potential global change: climatological analyses of impacts on livestock performance,” In Proceeding of the 15th Conference on Biometeorology and Aerobiology and the 16th International Congress of Biometeorology, pp. 45–48. American Meteorological Society, Boston, MA, USA, 2002.
- [64] T.L. Mader, K.L. Frank, J.A. Harrington, et al. “Potential climate change effects on warm-season livestock production in the Great Plains,” *Climatic Change*, vol. 97, pp. 529-541, 2009.
- [65] N. Key, S. Sneeringer, D. Marquardt. “Climate Change, Heat Stress, and U.S. Dairy Production,” U.S. Department of Agriculture, Economic Research Service, ERR-175, 2014. [Online]. Available: https://www.ers.usda.gov/webdocs/publications/45279/49164_err175.pdf?v=41913
- [66] N.R. St. Pierre, B. Cobanov, G. Schnitkey. “Economic Losses from Heat Stress by US Livestock Industries,” *Journal of Dairy Science*, vol. 86, pp. E52-E77, 2003.
- [67] M. Rajaniemi, J. Ahokas. “A case study of energy consumption measurement system in broiler production,” *Agronomy Research Biosystem Engineering Special Issue 1*, pp. 195–204, 2012.
- [68] G.D. Butcher, R. Miles. “Heat Stress Management in Broilers,” University of Florida, IFAS, Florida A & M University Cooperative Extension Service, Publication VM65, 2015. [Online]. Available: <http://edis.ifas.ufl.edu/vm019>. [Accessed: Dec 2017].
- [69] L.J. Lara, M.H. Rostagno. “Impact of Heat Stress on Poultry Production,” *Animals*, vol. 3, pp. 356-369, 2013.
- [70] WCRP-CMIP5. “World Climate Research Programme – Coupled Model Intercomparison Project Phase 5. Special Issue of the CLIVAR Exchanges,” Newsletter 56, vol. 15, no. 2, 2011. [Online]. Available: <http://www.clivar.org/sites/default/files/documents/Exchanges56.pdf>. [Accessed: May 2018].

- [71] The University of Kentucky. “Poultry Production Manual, Part of the: Poultry House Evaluation Service (PHES),” College of Agriculture, Food and Environment, 2013. [Online]. Available: http://www2.ca.uky.edu/poultryprofitability/production_manual.html. [Accessed: Dec 2018].
- [72] The University of Arkansas. “Energy Conservation – Poultry Farm Energy Use Evaluation Program,” Division of Agriculture, Cooperative Extension Service, 2015. [Online]. Available: <https://www.uaex.edu/environment-nature/energy/conservation.aspx>. [Accessed: May 2018].
- [73] Cobb-Vantress. “Broiler Management Guide,” 2012. [Online]. Available: <http://www.cobb-vantress.com/docs/default-source/management-guides/broiler-management-guide.pdf>. [Accessed: Dec 2017].
- [74] R. McKibbin, A. Wilkins, A. “Modelling of a Poultry Shed,” In: ANZ mathematics in-industry study group proceedings, pp. 47—59, 2004.
- [75] Commission Internationale du Genie Rural. “Report of Working Group on Climatization of Animal Houses,” CIGR, 1984. [Online]. Available: <http://www.cigr.org/documents/CIGR-Workinggroupreport1984.pdf>. [Accessed: Dec-2017].
- [76] J.C. Geankoplis. “Capítulo 4. Principios de transferencia de calor en estado estacionario,” In: Procesos de Transporte y Operaciones Unitarias, 3ra Edición, CECSA, 1008 p. México, 1998.
- [77] D.P. van Vuuren, J.A. Edmonds, M. Kainuma, et al. “The representative concentration pathways: an overview”, *Climatic Change*, vol. 109, pp. 5-31, 2011.
- [78] J.T. Abatzoglou, “Development of gridded surface meteorological data for ecological applications and modeling,” *International Journal of Climatology*, vol. 33, pp. 121-131, 2011.
- [79] T.J. Bohn, B. Livneh, J.W. Oyler, S.W. Running, B. Nijssen, D.P. Lettenmaier. “Global evaluation of MTCLIM and related algorithms for forcing of ecological and hydrological models,” *Agricultural and Forest Meteorology*, vol. 176, pp. 38-49, 2013.

- [80] J. Derner, D. Briske, M. Reeves, T. Brown-Brandl, et al. "Vulnerability of grazing and confined livestock in the Northern Great Plains to projected mid- and late-twenty-first century climate," *Climatic Change*, vol. 146, pp. 19-32, 2018.
- [81] E. Hawkins, R. Sutton. "The potential to narrow uncertainty in projections of regional precipitation change," *Climate Dynamics*, vol. 37, no. 1, pp. 407-418, 2011.
- [82] M. Czarick, Y. Liang, B. Fairchild. "Poultry Housing Tips: Increasing Evaporative Cooling Pad Set Temperatures," The University of Georgia, College of Agricultural and Environmental Sciences, Cooperative Extension, Vol. 26, No. 5, 2014. [Online]. Available: <https://www.poultryventilation.com/sites/default/files/vol26n5.pdf>. [Accessed: Dec 2017].
- [83] M. Czarick, B. Fairchild. "Cooperative Extension Poultry Housing Tips: It is Difficult to Keep Birds Cool with Air Speed Alone," The University of Georgia, College of Agricultural and Environmental Sciences, Cooperative Extension, Vol. 23, No. 4, 2011. [Online]. <https://www.poultryventilation.com/sites/default/files/tips/2011/vol23n4.pdf>. [Accessed: Dec 2017].
- [84] M.T. Craig, S. Cohen, J. Macknick, C. Draxl, et al. "A review of the potential impacts of climate change on bulk power system planning and operations in the United States," *Renewable and Sustainable Energy Reviews*, 98, 255–267, 2018.
- [85] M. de Vries, M. de Boer. "Comparing environmental impacts for livestock products: A review of life cycle assessments," *Livestock Science*, vol. 128, no. 1-3, pp. 1-11, 2010.
- [86] I. Leinonen, A.G. Williams, J. Wiseman, J. Guy, I. Kyriazakis. "Predicting the environmental impacts of chicken systems in the United Kingdom through a life cycle assessment: Broiler production systems," *Poultry Science*, vol. 91, pp. 8-25, 2012.
- [87] Pelletier, N. "Environmental performance in the US broiler poultry sector: Life cycle energy use and greenhouse gas, ozone depleting, acidifying and eutrophying emissions," *Agricultural Systems*, vol. 98, pp. 67-73, 2008.
- [88] S. Pedersen, H. Jørgensen, P.K. Theil. "Influence of diurnal variation in animal activity and digestion on animal heat production," *Agric Eng Int, CIGR Journal*, special issue 2015, 18th World Congress of CIGR, pp. 18-29, 2015.
- [89] Food and Agriculture Organization of the United Nations. "Rural structures in the tropics: Design and development," Rome, Italy: FAO, 2011.

- [90] K.E. Anderson, T.A. Carter. “Hot Weather Management of Poultry,” North Carolina State University, Cooperative Extension Service, 2007. [Online]. Available: https://www.ces.ncsu.edu/depts/poulsci/tech_manuals/hot_weather_management.html. [Accessed: Dec 2017].
- [91] Czarick, M. “Cooperative Extension Tunnel Fan Selection,” The University of Georgia, Cooperative Extension, Workshop Section 7, 2011. [Online]. Available: <https://www.poultryventilation.com/sites/default/files/workshops/section%207.pdf>. [Accessed: Dec 2017].
- [92] J. Donald, J. Campbell, G. Simpson, K. Macklin. “Evaluating Costs of Tunnel Ventilation Fans,” Auburn University, Alabama Cooperative Extension System, Newsletter no. 51, 2008. [Online]. Available: <http://www.aces.edu/poultryventilation/documents/Nwsltr-51CostsofTunnelFans080114.pdf>. [Accessed: Mar 2018].
- [93] J.D. Palmer. “Evaporative Cooling Design Guidelines Manual for New Mexico Schools and Commercial Buildings,” NRG Engineering Report, 2002. [Online]. Available: <http://www.emnrd.state.nm.us/ECMD/Multimedia/documents/EvapCoolingDesignManual.pdf>. [Accessed: Dec 2017].
- [94] G. Tabler. “Applied Broiler Research Farm Report: Propane and Electricity Usage One Year After Renovations,” The University of Arkansas, Cooperative Extension Service, *Avian Advice*, vol. 9, no. 3, pp. 4–8, 2007.
- [95] Energy Information Administration. “2015 Residential Energy Consumption Survey: Energy Consumption and Expenditures Tables,” EIA, 2018. [Online Dataset]. Available: <https://www.eia.gov/consumption/residential/data/2015/c&e/pdf/ce5.1a.pdf>. [Accessed: Feb 2019].
- [96] Energy Information Administration. “Annual Energy Outlook 2019,” EIA, 2019. [Online Dataset]. Available: <https://www.eia.gov/outlooks/aeo/>. [Accessed: Oct-2019].
- [97] C. Schaffnit-Chatterjee. “Agricultural Value Chains in Sub-Saharan Africa,” Frankfurt: Deutsche Bank Research, 2014.
- [98] S. Svendsen, M. Ewing, S. Msangi. “Measuring irrigation performance in Africa,” IFPRI Discussion Paper 894, International Food Policy Research Institute, Washington, D.C., 2009.

- [99] World Bank. “World Development Indicators. Fertilizer consumption (kilograms per hectare of arable land),” 2017. [Online Dataset]. Available: <https://data.worldbank.org/indicator/AG.CON.FERT.ZS>. [Accessed: Jan-2021].
- [100] R. Stirzaker, J. Pittock, J. “The case for a new irrigation research agenda for sub-Saharan Africa,” In: J. Pittock, R.Q. Grafton, & C. White (Eds.). *Water, food and agricultural sustainability in Southern Africa*, Prahan: Tilde University Press, pp. 91–107, 2014.
- [101] S.N. Mwamakamba, L.M. Sibanda, J. Pittock, R. Stirzaker, H. Bjornlund et al. “Irrigating Africa: policy barriers and opportunities for enhanced productivity of smallholder farmers,” *International Journal of Water Resources Development*, vol. 33, no. 5, pp. 824—838, 2017.
- [102] S. G. Banerjee, K. Malik, A. Tipping, J. Besnard, J. Nash. “Double Dividend: Power and Agriculture Nexus in Sub-Saharan Africa,” World Bank Group Report, 2017.
- [103] J. Daly, D. Hamrick, G. Gereffi, A. Guinn. “Maize Value Chains in East Africa,” International Growth Centre, F-38202-RWA-1, 2016.
- [104] G.A. Cornish. “Pressurised irrigation technologies for smallholders in developing countries – a review,” *Irrigation and Drainage Systems*, vol. 12, pp. 185—201, 1998.
- [105] M. Kay. “Smallholder irrigation technology: prospects for sub-Saharan Africa,” International Program for Technology and Research in Irrigation and Drainage (IPTRID), Rome, 2001.
- [106] M. Giordano, C. de Fraiture, E. Weight, J. van der Bliet. “Water for wealth and food security: supporting farmer-driven investments in agricultural water management,” Synthesis report of the AgWater Solutions Project. Colombo, Sri Lanka: International Water Management Institute (IWMI), 50p, 2012.
- [107] M. Sheahan, C.B. Barrett. “Ten striking facts about agricultural inputs use in Sub-Saharan Africa,” *Food Policy*, vol. 67, pp. 12—25, 2017.
- [108] D.B. Lobell, M.B. Burke, M.B. “On the use of statistical models to predict crop yield responses to climate change,” *Agricultural and Forest Meteorology*, vol. 150, pp. 1443—1452, 2010.
- [109] D.B. Lobell. “Errors in climate datasets and their effects on statistical crop models,” *Agricultural and Forest Meteorology*, vol. 170, pp. 58—66, 2013.

- [110] W. Schlenker, D.B. Lobell. “Robust negative impacts of climate change on African agriculture,” *Environmental Research Letters*, vol. 5, 8 pp, 2010.
- [111] H. El Sharif, J. Wang, A.P. Georgakakos. “Modeling Regional Crop Yield and Irrigation Demand Using SMAP Type of Soil Moisture Data,” *Journal of Hydrometeorology*, vol. 16, pp. 904—916, 2016.
- [112] A. Castañeda-Vera, P.A. Leffelaar, J. Alvaro-Fuentes, C. Cantero-Martinez, M.I. Minguez. “Selecting crop models for decision making in wheat insurance,” *European Journal of Agronomy*, vol. 68, pp. 97—116, 2015.
- [113] C. Folberth, T. Gaiser, K.C. Abbaspour, R. Schulin, H. Yang. “Regionalization of Large-Scale Crop Growth Models for Sub-Saharan Africa: Model Setup, Evaluation, and Estimation of Maize Yields,” *Agriculture, Ecosystems and Environment*, vol. 151, pp. 21—33, 2012.
- [114] C. Folberth, H. Yang, T. Gaiser, K.C. Abbaspour, R. Schulin. “Modeling Maize Yield Responses to Improvement in Nutrient, Water and Cultivar Inputs in Sub-Saharan Africa,” *Agricultural Systems*, vol. 119, pp. 22—34, 2013.
- [115] E. Blanc. “Statistical Emulators of Irrigated Crop Yields and Irrigation Water Requirements,” *Agricultural and Forestry Meteorology*, vol. 284, pp. 1—28, 2020.
- [116] M. Rosegrant, C. Ringler, I. De Jong. “Irrigation: Tapping Potential,” In: V. Foster, C. Briceño-Garmendia (Eds.). *Africa’s Infrastructure: A Time for Transformation*. Africa Development Forum. World Bank. pp. 287–298, 2009.
- [117] L. You, C. Ringler, U. Wood-Sichra, R. Robertson, S. Wood, T. Zhu, et al. “What is the irrigation potential for Africa? A combined biophysical and socio-economic approach,” *Food Policy*, vol. 36, pp. 770—782, 2011.
- [118] S. Gheewala, T. Silalertruksa, P. Nilsalab, R. Mungkung, S. Perret, N. Chaiyawannakarn, “Water Footprint and Impact of Water Consumption for Food, Feed, Fuel Crops Production in Thailand,” *Water*, vol. 6, pp. 1698—1718, 2014.
- [119] M.M. Mekonnen, A.Y. Hoekstra. “The green, blue and grey water footprint of crops and derived crop products,” *Hydrology and Earth System Sciences*, vol. 15, pp. 1577—1600, 2011.

- [120] Food and Agriculture Organization of the United Nations. “Data,” FAOSTAT 2019. [Online Dataset]. Available: <http://www.fao.org/faostat/en/#data>. [Accessed: March 2021].
- [121] P. Steduto, T.C. Hsiao, D. Raes, E. Fereres. “AquaCrop – The FAO Crop Model to Simulate Yield Response to Water: I. Concepts and Underlying Principles,” *Agronomy Journal*, vol. 101, no. 3, pp. 426–437, 2009.
- [122] P. Stackhouse. “POWER Data Methodology,” NASA 2019. [Online]. Available: <http://power.larc.nasa.gov>
- [123] FAO/IIASA/ISRIC/ISSCAS/JRC. “Harmonized World Soil Database (version 1.2),” FAO, Rome, Italy and IIASA, Laxenburg, Austria, 2012.
- [124] K.E. Saxton, W.J. Rawls, J.S. Romberger, R.I. Papendick. “Estimating Generalized Soil-Water Characteristics from Texture,” *Soil Science Society of America Journal*, vol. 50, pp. 1031—1036, 1986.
- [125] E. Vanuytrecht, D. Raes, P. Steduto, T.C. Hsiao, E. Fereres, L.K. Heng, M. Garcia-Vila, P. Mejias-Moreno. “AquaCrop: FAO’S Crop Water Productivity and Yield Response Model,” *Environmental Modelling and Software*, pp. 1—10, 2014.
- [126] D. Raes, P. Steduto, T.C. Hsiao, E. Fereres. “Chapter 1, FAO crop-water productivity model to simulate yield response to water. AquaCrop Version 6.0 – 6.1. Reference Manual,” Rome, Italy: Food and Agriculture Organization of the United Nations, 2018. [Online]. Available: <http://www.fao.org/3/a-br246e.pdf>
- [127] Y.K. Agbemabiese, A.G. Shaibu, V.D. Gbedzi. “Validation of AquaCrop for Different Irrigation Regimes of Onion (*Allium Cepa*) in Bontanga Irrigation Scheme,” *International Journal of Irrigation and Agricultural Development*, vol. 1, no. 1, pp. 1—12, 2017.
- [128] G.N. Karuku, B.A. Mbindah. “Validation of AquaCrop model for simulation of rainfed bulb onion (*Allium Cepa* L.) yields in West Ugenya Sub-County, Kenya,” *Tropical and Subtropical Agroecosystems*, vol. 23, no. 6, pp. 1—11, 2020.
- [129] H. Van Gaelen, A. Tsegay, N. Delbecque, N. Shrestha, M. Garcia, H. Fajardo, et al. “A semi-quantitative approach for modelling crop response to soil fertility: Evaluation of the AquaCrop procedure,” *Journal of Agricultural Science*, vol. 153, pp. 1218-1233, 2015.

- [130] D. Raes. “AquaCrop training handbook I. Understanding AquaCrop,” Food and Agriculture Organization of the United Nations, Rome, Italy, 2017. [Online]. Available: <http://www.fao.org/3/a-i6051e.pdf>
- [131] United States Department of Agriculture, Foreign Agricultural Service. “Ethiopia 2008 Crop Assessment Report,” Commodity Intelligence Report, Foreign Agricultural Service, 2008. [Online]. Available: https://ipad.fas.usda.gov/highlights/2008/11/eth_25nov2008/
- [132] Central Statistical Agency of The Federal Democratic Republic of Ethiopia. “Agricultural Sample Survey 2018/19 (2011 E.C.), Volume I, Report on Area and Production of Major Crops,” Statistical Bulletin 589, Addis Ababa, June 2019. [Online]. Available: <http://www.csa.gov.et/survey-report/category/373-eth-agss-2018?download=958:report-on-area-and-production-of-major-crops-2011-meher-season-1>. [Accessed: May 2020].
- [133] National Institute of Statistics of Rwanda. “Seasonal Agricultural Survey (SAS) Annual Report 2019,” December 2019. [Online]. Available: <https://www.statistics.gov.rw/publication/seasonal-agricultural-survey-2019-annual-report>
- [134] Ministry of Agriculture and Animal Resources. “Strategic Plan for the Transformation of Agriculture in Rwanda – Phase II (PSTA II),” 2009. [Online]. Available: http://rwanda.countrystat.org/fileadmin/user_upload/countrystat_fenix/congo/docs/PSTA_II-php.pdf
- [135] Uganda Bureau of Statistics. “Uganda Annual Agricultural Survey 2018,” Kampala, Uganda; UBOS, 2020. [Online]. Available: https://www.ubos.org/wp-content/uploads/publications/01_20202019_Statistical_Abstract_-Final.pdf
- [136] H.R. Duke. “Chapter 12: Pumping Systems,” In: Design and Operation of Farm Irrigation Systems, 2nd Edition, American Society of Agricultural and Biological Engineers, pp. 392—435, 2007.
- [137] G. Fipps. “Calculating Horsepower Requirements and Sizing Irrigation Supply Pipelines,” Texas Agricultural Extension Service B-6011, 2017. [Online]. Available: <http://riograndewater.org/media/1064/b-6011-calculating-horsepower-requirements-and-sizing-irrigation-supply-pipelines.pdf>

- [138] S. Siebert, J. Burke, J.M. Faures, K. Frenken, J. Hoogeveen, P. Döll, F.T. Portmann. “Groundwater use for irrigation – a global inventory,” *Hydrology and Earth System Sciences*, vol. 14, pp. 1863–1880, 2010.
- [139] A.M. MacDonald, H.C. Bonsor, B.É.Ó. Dochartaigh, R.G. Taylor. “Quantitative maps of groundwater resources in Africa,” *Environmental Research Letters*, vol. 7, no. 2, 2012.
- [140] E. Rodríguez-Huerta, M. Rosas-Casals, L.M. Hernández-Terrones. “A water balance model to estimate climate change impact on groundwater recharge in Yucatan Peninsula, Mexico,” *Hydrological Sciences Journal*, vol. 65, no. 3, pp. 470-486, 2020.
- [141] W.M. Alley. “On the Treatment of Evapotranspiration, Soil Moisture Accounting, and Aquifer Recharge in Monthly Water Balance Models,” *Water Resources Research*, vol. 20, no. 8, pp. 1137—1149, 1984.
- [142] SHER Ingénieurs-Conseils s.a. “Consultancy Services for Development of Rwanda National Water Resources Master Plan, Tender Number 021/RNRA/2011-2012,” Master Plan Report: Main Volume. Rwanda Natural Resources Authority, 2014. [Online]. Available:
https://environment.gov.rw/uploads/media/Rwanda_Water_Resources_Master_Plan_01.pdf
- [143] Food and Agriculture Organization of the United Nations. “AQUASTAT Country Profile –Ethiopia,” Food and Agriculture Organization of the United Nations (FAO). Rome, Italy, 2016. [Online]. Available: <http://www.fao.org/3/i9732en/I9732EN.pdf>
- [144] Food and Agriculture Organization of the United Nations) “AQUASTAT Country Fact Sheet – Rwanda,” Food and Agriculture Organization of the United Nations (FAO). Rome, Italy, 2019. [Online]. Available: https://storage.googleapis.com/fao-aquastat.appspot.com/countries_regions/factsheets/summary_statistics/en/RWA-CF.pdf
- [145] Food and Agriculture Organization of the United Nations. “AQUASTAT Country Profile – Uganda,” Food and Agriculture Organization of the United Nations (FAO). Rome, Italy, 2014. [Online]. Available: <http://www.fao.org/3/i9827en/I9827EN.pdf>.
- [146] D. Raes, P. Steduto, T.C. Hsiao, E. Fereres. “Annexes, AquaCrop Version 6.0 – 6.1. Reference Manual,” Rome, Italy: Food and Agriculture Organization of the United Nations, 2018. [Online]. Available: <http://www.fao.org/3/BR244E/br244e.pdf>

- [147] K. Hendriksen, S.L. Hansen. “Increasing the Dry Matter Production in Bulb Onions (*Allium cepa* L.),” *Acta Horticulturae*, vol. 555, pp. 147-152, 2001.
- [148] H. Lambers, R.S. Oliveira. “Plant Water Relations,” In: *Plant Physiological Ecology*. Springer, Cham, 2019.
- [149] G. Chavarria and H. P. dos Santos. “Plant Water Relations: Absorption, Transport and Control Mechanisms,” In: G. Montanaro & B. Dichio (Eds.). *Advances in Selected Plant Physiology Aspects*, IntechOpen, 2012.
- [150] World Bank. “World Development Indicators. Population density (people per sq. km of land area),” 2018. [Online Dataset]. Available: <https://data.worldbank.org/indicator/EN.POP.DNST>. [Accessed: Feb-2021].
- [151] P. Tittonell, K.E. Giller. “When yield gaps are poverty traps: The paradigm of ecological intensification in African smallholder agriculture,” *Field Crops Research*, vol. 143, pp. 76—90, 2013.
- [152] D. Gollin. “Smallholder agriculture in Africa: An overview and implication for policy,” IIED Working Paper, IIED, London, 2014.
- [153] A. Salami, A.B. Kamara, Z. Brixiova. “Smallholder Agriculture in East Africa: Trends, Constraints and Opportunities,” Working Papers Series N° 105, African Development Bank, Tunis, Tunisia, 2010.
- [154] L. You, C. Ringler, G. Nelson, U. Wood-Sichra, R. Robertson, S. Wood, G. Zhe, T. Zhu, Y. Sun. “Torrents and trickles: irrigation spending needs in Africa,” AICD Background Paper 9, World Bank, Washington, DC, September 2009.
- [155] M. Tesfaw. “Small Scale Irrigation Development,” *Irrigation & Drainage Systems Engineering*, vol. 7, no.1, pp. 1—7, 2018.
- [156] C. Lorenzo, R.H. Almeida, M. Martínez-Núñez, L. Narvarte, L.M. Carrasco. “Economic assessment of large power photovoltaic irrigation systems in the ECOWAS region,” *Energy*, vol. 155, pp. 992—1003, 2018.
- [157] P.E. Campana, H. Li, J. Yan. “Techno-economic feasibility of the irrigation system for the grassland and farmland conservation in China: Photovoltaic vs wind power water pumping,” *Energy Conversion and Management*, vol. 103, pp. 311—320, 2015.

- [158] X. Zou, Y. Li, R. Cremades, Q. Gao, Y. Wan, X. Qin. “Cost-effectiveness analysis of water-saving irrigation technologies based on climate change response: A case study in China,” *Agricultural Water Management*, vol. 129, pp. 9—20, 2013.
- [159] E. Borsato, M. Martello, F. Marinello, L. Bortolini. “Environmental and Economic Sustainability Assessment for Two Different Sprinkler and A Drip Irrigation Systems: A Case Study on Maize Cropping,” *Agriculture*, vol. 9, no. 187, pp. 1—15, 2019.
- [160] N. A. Akrofi, D.B. Sarpong, H.A.S. Somuah, Y. Osei-Owusu. “Paying for privately installed irrigation services in Northern Ghana: The case of the smallholder Bhungroo Irrigation Technology,” *Agricultural Water Management*, vol. 216, pp. 284—293, 2019.
- [161] H. Zhai, E. Rubin. “Techno-Economic Assessment of Polymer Membrane Systems for Postcombustion Carbon Capture at Coal-Fired Power Plants,” *Environmental Science & Technology*, vol. 47, pp. 3006—3014, 2013.
- [162] H. Cooley, R. Phurisamban, R. “The Cost of Alternative Water Supply and Efficiency Options in California,” Pacific Institute, October 2016. [Online}. Available: https://pacinst.org/wp-content/uploads/2016/10/PI_TheCostofAlternativeWaterSupplyEfficiencyOptionsinCA.pdf
- [163] K. Danert, R.C. Carter, D. Adekile, A. MacDonald. “Cost-effective boreholes in sub-Saharan Africa,” In Proceedings of the 33rd WEDC International Conference, Accra, Ghana, 7–11 April 2008. [Online]. Available: <http://nora.nerc.ac.uk/id/eprint/9185/1/CEB%20Danert%20Draft%204%20UNESCO%2022%20April09.pdf>. [Accessed: Dec 2019].
- [164] S. Cha, Y. Cho, S.J. Kim, Y. Lee, S. Choi, P. Asuming, Y. Kim, & Y. Jin. “Cost-benefit analysis of water source improvements through borehole drilling or rehabilitation: an empirical study based on a cluster randomized controlled trial in the Volta Region, Ghana,” *Global Health Action*, vol. 11, no. 1, 2018.
- [165] D. Bricca, E. Bocci, E. Santini. “Technical and economic analysis of solar pumping irrigation system for rural areas in Ethiopia,” 2019 IEEE International Conference on Environment and Electrical Engineering and 2019 IEEE Industrial and Commercial Power Systems Europe, Genova, Italy, 2019, pp. 1-6.

- [166] C. Brunet, O. Savadogo, P. Baptiste, M. Bouchard. “Shedding some light on photovoltaic solar energy in Africa – A literature review,” *Renewable and Sustainable Energy Reviews*, vol. 96, pp. 325—342, 2018.
- [167] J. Ondraczek, N. Komendantova, A. Patt. “WACC the dog: The effect of financing costs on the levelized costs of solar PV power,” *Renewable Energy*, vol. 75, pp. 888—898, 2015.
- [168] P. Steduto, T.C. Hsiao, E. Fereres, D. Raes. “Crop yield response to water. FAO Irrigation and Drainage Paper No. 66,” Food and Agriculture Organization of the United Nations, Rome 2012.
- [169] National Institute of Statistics of Rwanda. “Energy Statistics, 2017,” Dataset, 2018. [Online]. Available: <http://statistics.gov.rw/publication/energy-statistics-2017>
- [170] Uganda Bureau of Statistics. “Uganda Census of Agriculture 2008/2009. Volume IV: Crop Area and Production Report,” Kampala, Uganda, UBOS, December 2010. [Online]. Available: https://www.ubos.org/wp-content/uploads/publications/03_2018UCACrop.pdf
- [171] International Food Policy Research Institute. “Spatially-Disaggregated Crop Production Statistics Data in Africa South of the Sahara for 2017,” Harvard Dataverse, V2, 2020.
- [172] International Energy Agency. “Ethiopia Country Profile,” IEA, Paris, 2018. [Online]. Available: <https://www.iea.org/countries/ethiopia>
- [173] Uganda Bureau of Statistics. “2019 Statistical Abstract,” Kampala, Uganda, UBOS, 2020. [Online]. Available: https://www.ubos.org/wp-content/uploads/publications/06_2020AAS_2018_Report_Final_050620.pdf
- [174] M. Yuan, L. Zhang, F. Gou, Z. Su, J.H.J. Spiertz, W. van der Werf. “Assessment of Crop Growth and Water Productivity for Five C3 Species in Semi-Arid Inner Mongolia,” *Agricultural Water Management*, vol. 122, pp. 28—38, 2013.
- [175] K.T. Zeleke. “AquaCrop Calibration and Validation for Faba Bean (*Vicia faba* L.) under Different Agronomic Management,” *Agronomy*, vol. 9, no. 6, pp. 320, 2019.
- [176] U. Akumaga, A. Tarhule, A.A. Yusuf. “Validation and testing of the FAO AquaCrop model under different levels of nitrogen fertilizer on rainfed maize in Nigeria, West Africa,” *Agricultural and Forest Meteorology*, vol. 232, pp. 225—234, 2017.

- [177] N. Shrestha, D. Raes, E. Vanuytrecch, S.K. Sah. “Cereal yield stabilization in Terai (Nepal) by water and soil fertility management modeling,” *Agricultural Water Management*, vol. 122, pp. 53—62, 2013.
- [178] N. Zinyengere, T. Mhizha, E. Mashonjowa, B. Chipindu, S. Geerts, D. Raes. “Using seasonal climate forecasts to improve maize production decision support in Zimbabwe,” *Agricultural and Forest Meteorology*, vol. 151, pp. 1792—1799, 2011.
- [179] G.N. Karuku, B.A. Mbindah. “Validation of AquaCrop model for simulation of rainfed bulb onion (*Allium Cepa* L.) yields in West Ugenya Sub-County, Kenya,” *Tropical and Subtropical Agroecosystems*, vol. 23, no. 6, pp. 1—11, 2020.
- [180] A. Araya, S.D. Keesstra, L. Stroosnijder. “Simulating yield response to water of Teff (*Eragrostis tef*) with FAO’s AquaCrop model,” *Field Crops Research*, vol. 116, pp. 196—204, 2010.
- [181] R.O. Darko, Y. Shouqi, Y. Haofang, L. Junping, A. Abbey. “Calibration and validation of AquaCrop for deficit and full irrigation of tomato,” *International Journal of Agriculture & Biological Engineering*, vol. 9, no. 3, pp. 104—110, 2016.
- [182] R. Linker, I. Ioslovich, G. Sylaios, F. Plauborg, A. Battilani. “Optimal model-based deficit irrigation scheduling using AquaCrop: A simulation study with cotton, potato and tomato,” *Agricultural Water Management*, vol. 163, pp. 236—243, 2016.
- [183] B. Andarzian, M. Bannayan, P. Steduto, H. Mazraeh, M.E. Barati, et al. “Validation and testing of the AquaCrop model under full and deficit irrigated wheat production in Iran,” *Agricultural Water Management*, vol. 100, pp. 1—8, 2011.
- [184] I.D. Magalhães, G.B. Lyra, J.L. de Souza, I. Teodoro et al. “Performance of the AquaCrop model for bean (*Phaseolus vulgaris* L.) under irrigation condition,” *Australian Journal of Crop Science*, vol. 13, no. 7, pp. 1188—1196, 2019.
- [185] N. Katerji, P. Campi, M. Mastrorilli. “Productivity, evapotranspiration, and water use efficiency of corn and tomato crops simulated by AquaCrop under contrasting water stress conditions in the Mediterranean region,” *Agricultural Water Management*, vol. 130, pp. 14—26, 2013.
- [186] M. Pérez-Ortolá, A. Daccacche, T.M. Hess, J.W. Knox. “Simulating impacts of irrigation heterogeneity on onion (*Allium cepa* L.) yield in a humid climate,” *Irrigation Science*, vol. 33, pp. 1—14, 2014.

- [187] F. Montoya, D. Camargo, J.F. Ortega, J.I. Corcoles, A. Dominguez. “Evaluation of Aquacrop Model for a Potato Crop Under Different Irrigation Conditions,” *Agricultural Water Management*, vol. 164, pp. 267—280, 2016.
- [188] H. Haileselassie, A. Araya, S. Habtu, K.G. Meles, G. Gebru, et al. “Exploring optimal farm resources management strategy for Quncho-teff (*Eragrostis tef* (Zucc.) Trotter) using AquaCrop model,” *Agricultural Water Management*, vol. 178, pp. 148—158, 2016.
- [189] S. Kale Celik, S. Madenoglu, B. Sonmez. “Evaluating AquaCrop Model for Winter Wheat under Various Irrigation Conditions in Turkey,” *Journal of Agricultural Sciences*, vol. 24, no. 2, pp. 205—217, 2018.
- [190] C.W. Thornthwaite, J.R. Mather. “Instructions and Tables for Computing Potential Evapotranspiration and The Water Balance,” *Publications in Climatology*, vol. 10, no. 3, pp. 185–311, 1957.

Appendix A. Supplemental Information for Chapter 2

A.1. Materials and methods

A.1.1. Steady-state thermodynamic model

This model approximates the recommended indoor temperature inside the barn, T_{in} , per day of age of the broiler, d , using a linear relationship. The relationship is modeled after available literature with one-day-old chicks entering the house at a temperature of 32 °C, with a reduction of 0.5 °C per day until the temperature in the house reaches 21 °C [47]-[50].

$$T_{in} = \begin{cases} 32.5 - 0.5d, & 0 < d \leq 23 \\ 21, & d > 23 \end{cases} \quad (Eq. A.1)$$

To perform the thermal heat balances, the model uses equations to approximate the live body weight (as a function of bird age), the daily water intake, the metabolic energy, the latent heat (of vaporization) production, the conductive heat losses, and the temperature change. The model also includes different housing areas per brooding stages, as stated by poultry industry guidelines [46], [73]. The model approximates this brooding spacing by adjusting the space where chickens grow to be: i) half the area of the house for chicks of up to one week of age, ii) three-quarters of the house for chickens between one and two weeks of age, and iii) full house area for broilers older than two weeks of age.

Live body weight (m) or mass of bird per day of age, d , is estimated through a piecewise regression equation from publicly available data reported by the Applied Broiler Research Farm (ABRF) – a 4-house commercial-scale broiler barn owned by the University of Arkansas – for

four flocks grown in 2013. This equation is calibrated to calculate the average market weight (~6.2 lb) at the average harvest age (49 days) reported by USDA-ERS [45]:

$$m(kg) = \begin{cases} 0.079153 + 0.013674d + 3.34 \times 10^{-3}d^2, & \{0 < d \leq 28\} \\ -0.74635 + 0.143509d, & \{28 < d \leq 56\} \end{cases} \quad (Eq. A.1)$$

Daily water intake (DWI) and **metabolic energy (ME)** per bird and day of age are estimated as a function of indoor temperature, T_{in} (in °C), and mass, m (in kg). DWI is adapted through a multi-variate regression from the same available data set by the ABRF. Since metabolism and water intake vary with the level of activity of the bird over the day, a sinusoidal function for relative animal activity is used to convert daily metabolic heat and water intake rates to hourly rates with h as the hour of the day (from 0 to 23 hours) as described by Pedersen et al. [88].

$$DWI = \sum_{d=1}^{49} \sum_{h=1}^{24} (583.5 - 17.1T_{in} + 25.25m) \left(1 - \left(a * \sin \left[\frac{2\pi}{24} * (h + 6 - h_{min}) \right] \right) \right) \quad (Eq. A.2)$$

Metabolic energy, ME, can be approximated as sensible heat produced, SHP, in steady-state conditions [74]. As developed by Sakomura et al. [51] and used by Hamilton et al. [50], ME is calculated with equation 3.

$$ME = \sum_{d=1}^{49} \sum_{h=1}^{24} m^{0.75} (307.87 - 15.63T_{in} + 0.3105T_{in}^2) \left(1 - \left(a * \sin \left[\frac{2\pi}{24} * (h + 6 - h_{min}) \right] \right) \right) \quad (Eq. A.3)$$

With $a = 0.21$ for ME and $a = 0.46$ for DWI as a constant for amplitude with respect to 1; and $h_{min} = 0.38$ for ME and $h_{min} = 0.67$ for DWI for the hour of the day with minimum activity, both selected for broilers [88].

Latent heat production (LHP) is the energy required to evaporate water from the chicken body for internal cooling. This study assumes that 80% of the water returns to the barn, with half of it as liquid excretions and the other half as vapor from respiration [83], [74]. The equation to calculate LHP links the mass of the vapor returned to the barn, \dot{m} , with the enthalpy of vaporization of water, h_{fg} , as a function of indoor temperature [75], [76].

$$LHP = 0.4 * DWI * h_{fg} \quad (Eq. A.4)$$

$$h_{fg} = 2500 - 2.327 * T_{in} \quad (Eq. A.5)$$

Heat losses through the building are calculated with Fourier's Law as described by Geankoplis [76] and FAO [89] for steady-state heat transfer in buildings. **Conductive heat losses (\dot{Q}_b)** are estimated with equation 5 as losses through the walls, roof and floors. **Infiltration heat losses (\dot{Q}_{inf})** are estimated with equation 6 as air infiltrated through leaks in the building structure. U_{th} , or most commonly known as the U-value, is the overall heat transfer coefficient or thermal transmittance of the structure (inversely proportional to the insulation), A is the surface area of the walls/roof or floor, ACH is the number of air changes per hour (as representative of the tightness of the building), m_{air} is the mass of air, $C_{p_{air}}$ is the specific heat capacity of air, and ΔT as the difference between inside, T_{in} , and outside temperature, T_o (in °C).

$$\dot{Q}_b = U_{th} A \Delta T \quad (Eq. A.6)$$

$$\dot{Q}_{inf} = ACH m_{air} C_{p_{air}} \Delta T \quad (Eq. A.7)$$

The overall energy balance is calculated as heat gain or loss as reported by the CGIR Report [75] and Hamilton et al. [50].

$$\dot{Q}_{gain/loss} = ME - LHP - \dot{Q}_b - \dot{Q}_{inf} \quad (Eq. A.8)$$

The **temperature gained or lost** ($\Delta T_{gain/loss}$) with reference to the (indoor) temperature set point, T_{in} , is calculated through the heat transfer equation by Geankoplis [76], with m_{air} as the mass of air, and $C_{p_{air}}$ as the specific heat capacity of air; positive values refer to a net heat gain while negative means net heat loss as compared to the set temperature required.

$$\Delta T_{gain/loss} = \frac{\dot{Q}_{gain/loss}}{m_{air} C_{p_{air}}} \quad (Eq. A.9)$$

To estimate heating and cooling demands, the model adopts energy efficiency relations (airflow rate, power/heat consumption), best practice heuristics, and thermal evaporation conversions (evaporative water). The **airflow rate**, v_{rate} , is estimated using air exchange rates (AER, in units of 1/min) to achieve a house volume of air exchanged. This is approximated as a house air exchange every minute, in summer, and a house air exchange every 8 minutes, in winter [90], [73]. For tunnel ventilation systems, I approximated the airflow capacity as the volume of the house times the seasonal AER. Ventilation time, t_{vent} , is characterized through an adaptation of the method shown by CIGR [75] as the number of times that the temperature gain, ΔT_{gain} , is greater than the temperature tolerance of chickens, ΔT_{tol} . This temperature tolerance ranges from 2 to 5 °C [75] but it is approximated as 3 °C in our study.

$$v_{rate} = V_{house} * AER \quad (Eq. A.10)$$

$$t_{vent} = \frac{\Delta T_{gain/loss}}{\Delta T_{tol}} \quad (Eq. A.11)$$

Energy for ventilation is estimated for two cases. The first, when the net heat gain is positive, is adapted from Czarick [91] and Donald et al. [92] as the product of the airflow rate and the number of minutes fans run divided by the ventilation efficiency rating (VER). The second,

when the net heat gain is negative, is approximated with a best practice heuristic to remove harmful gases in cold weather with ventilation times between 5 and 8 minutes per hour [73], [71]. Analogously, **energy for heating** is calculated as the absolute value of the heat loss, \dot{Q}_{loss} , divided by the energy-to-heating efficiency of the propane furnace.

$$E_{vent} = \frac{v_{rate} * t_{vent}}{VER} \quad (Eq. A.12)$$

$$E_{heat} = \frac{\dot{Q}_{loss}}{\eta_{heat}} \quad (Eq. A.13)$$

When outside air is too hot to chill chickens—i.e., when T_o is higher than T_{in} —additional cooling is required. The most common system currently in use is known as **evaporative cooling pads**, which use water to remove excess heat from incoming air. According to Czarick et al. [82], evaporative cooling pads should be used when the outside temperature reaches between 28 and 32 °C. For the purpose of this model, the former is used and is denoted as T_{pads} . The amount of water required to remove excess heat from air (cooling) is estimated combining evaporative cooling formulas by Geankoplis [76] and Palmer (2002) as shown by equation A.14. $\eta_{ev.pads}$ represents the efficiency of the evaporative cooling pads system.

$$V_{water} = \frac{t_{vent} * m_{air} * C_{p,air} (T_o - (T_{set} + \Delta T_{tol}))}{h_{fg} * \eta_{ev.pads}} \quad (Eq. A.14)$$

The model estimates **energy for evaporative cooling** by multiplying this volume of water by a factor of energy use per volume of water pumped, e_{water} , as described by Martin et al (2011).

$$E_{ev.pads} = V_{water} * e_{water} \quad (Eq. A.15)$$

Finally, the **energy for cooling** is estimated as the sum of the energy for ventilation and the energy for evaporative cooling. Table A.1 summarizes the predetermined values used for the different input variables of the model.

Table A.1. Values assumed for the different parameters required to calculate the thermal heat fluxes in a single-story broiler house.

Parameter	
Number of birds per flock	20,328
Days of age (to harvest time), d	49 days
Volume of the house, V_{house}	4,700 m³
Area, A	
Roof and walls (structural component)	2,500 m²
Floor	1,700 m²
Heat transfer coefficient, U_{th} , of the structure	
Walls and roof (fiberglass)	1.0 W/m²-°C
Floor (Litter)	0.2 W/m²-°C
Temperature tolerance, ΔT_{tol}	3 °C
Air Exchange Rate, AER	
Summer	1/ min
Winter	1/8 min
Ventilation flow rate (summer), v_{rate}	4,800 m³/min
	171,000 ft³/min (CFM)
Ventilation efficiency rating, VER	18 ft³/min-W (CFM/W)
Propane (heating) furnace efficiency ratio, η_{heat}	0.85
Evaporative cooling pad system efficiency, $\eta_{ev.pads}$	0.85
Starting operating temperature of cooling pads, T_{pads}	28 °C
Air density, ρ_{air}	1.21 kg/m³
Specific heat capacity of air, $C_{p,air}$	1,006.1 J/kg-°C
Energy for pumping, e_{water}	0.52 Wh/m³

A.1.2. General Circulation Models (GCM)

Table A.2. Names of the twenty general circulation models (GCMs) used in our study.

Modeling Center (or Group)	Model Name
Beijing Climate Center, China Meteorological Administration	BCC-CSM1.1 BCC-CSM1.1(m)
College of Global Change and Earth System Science, Beijing Normal University	BNU-ESM
Canadian Centre for Climate Modelling and Analysis	CanESM2

National Center for Atmospheric Research	CCSM4
Centre National de Recherches Météorologiques / Centre Européen de Recherche et Formation Avancée en Calcul Scientifique	CNRM-CM5
Commonwealth Scientific and Industrial Research Organization in collaboration with Queensland Climate Change Centre of Excellence	CSIRO-Mk3.6.0
NOAA Geophysical Fluid Dynamics Laboratory	GFDL-ESM2G GFDL-ESM2M
Met Office Hadley Centre (additional HadGEM2-ES realizations contributed by Instituto Nacional de Pesquisas Espaciais)	HadGEM2-CC HadGEM2-ES
Institute for Numerical Mathematics	INM-CM4
Institut Pierre-Simon Laplace	IPSL-CM5A-LR IPSL-CM5A-MR IPSL-CM5B-LR
Japan Agency for Marine-Earth Science and Technology, Atmosphere and Ocean Research Institute (The University of Tokyo), and National Institute for Environmental Studies	MIROC-ESM MIROC-ESM-CHEM
Atmosphere and Ocean Research Institute (The University of Tokyo), National Institute for Environmental Studies, and Japan Agency for Marine-Earth Science and Technology	MIROC5
Meteorological Research Institute	MRI-CGCM3
Norwegian Climate Centre	NorESM1-M

A.2. Additional Results

A.2.1. Analysis of Regression Slopes and Statistical Significance

To confirm the significance of the effect of climate change on energy demand, I first obtained the slopes of each general circulation model (GCM) through linear regression for early (2010 to 2045) and full (2010 to 2095) periods per RCP. I found that the changes observed in the twenty models are indeed statistically significant during both periods and RCPs. The analysis shows that energy for cooling increases more steeply after mid-century for RCP 8.5 and remains relatively more stable under RCP 4.5.

Table A.3 and Table A.4 show the summary of cooling and heating slopes per period per RCP. Similarly, I compared linear regression slopes for cooling and heating energy demands per GCM for the two climate change scenarios, RCP 8.5 and RCP 4.5. Note that there is heterogeneity

among the results of the simulations produced by different GCMs. Table A.5 to Table A.8 show comparison matrices for the period 2010 to 2095 for both RCPs. Table A.9 to Table A.12 show matrices for the period comprised between 2010 and 2045.

Table A.3. Regression slopes for cooling for early (2010 to 2045) and full (2010 to 2095) periods per GCM and RCP climate change scenario

GCM	Cooling Demand Slopes (GJ-yr ⁻¹)			
	RCP 8.5		RCP 4.5	
	2010-2045	2010-2095	2010-2045	2010-2095
1	0.10*** (0.89)	0.15*** (1.0)	0.08*** (0.87)	0.05*** (0.79)
2	0.09*** (0.79)	0.13*** (0.87)	0.09*** (0.94)	0.06*** (0.83)
3	0.11*** (0.96)	0.15*** (0.97)	0.05* (0.58)	0.06*** (0.88)
4	0.12*** (1.03)	0.16*** (1.03)	0.11*** (1.13)	0.07*** (0.98)
5	0.11*** (0.98)	0.14*** (0.92)	0.08*** (0.82)	0.06*** (0.8)
6	0.13*** (1.13)	0.13*** (0.83)	0.08*** (0.83)	0.07*** (1.07)
7	0.05* (0.45)	0.13*** (0.86)	0.11*** (1.15)	0.08*** (1.1)
8	0.09** (0.75)	0.13*** (0.86)	0.05 (0.49)	0.03** (0.47)
9	0.08** (0.72)	0.13*** (0.86)	0.12*** (1.31)	0.05*** (0.68)
10	0.13*** (1.11)	0.23*** (1.49)	0.17*** (1.82)	0.11*** (1.6)
11	0.18*** (1.60)	0.22*** (1.46)	0.13*** (1.35)	0.11*** (1.65)
12	0.07** (0.59)	0.10*** (0.63)	0.06*** (0.65)	0.04*** (0.6)
13	0.15*** (1.33)	0.16*** (1.08)	0.08*** (0.88)	0.07*** (0.98)
14	0.12*** (1.05)	0.18*** (1.16)	0.09*** (0.96)	0.07*** (1.01)
15	0.11*** (0.96)	0.14*** (0.89)	0.10*** (1.08)	0.08*** (1.09)
16	0.13*** (1.17)	0.14*** (0.93)	0.11*** (1.19)	0.07*** (0.97)
17	0.17*** (1.46)	0.19*** (1.28)	0.13*** (1.43)	0.10*** (1.45)
18	0.16*** (1.40)	0.20*** (1.30)	0.11*** (1.17)	0.09*** (1.32)
19	0.08*** (0.71)	0.09*** (0.63)	0.04** (0.45)	0.05*** (0.67)
20	0.11*** (0.92)	0.14** (0.94)	0.08*** (0.9)	0.07*** (1.06)
AVG	0.11	0.15	0.09	0.07
Std Dev	0.034	0.036	0.032	0.02

1- Number in parenthesis denotes ratio to mean.
2- Statistical significance codes: 0 '***' 0.001 '**' 0.01 '*' 0.05 '.' 0.1 ' ' 1

Table A.4. Regression slopes for heating demand for early (2010-2045) and late (2010-2095) periods per GCM and RCP climate change scenario

GCM	Heating Demand Slopes (GJ-yr ⁻¹)			
	RCP 8.5		RCP 4.5	
	2010-2045	2010-2095	2010-2045	2010-2095
1	-1.18*** (0.91)	-1.30*** (0.88)	-0.49 (0.38)	-0.48*** (0.69)
2	-0.67* (0.52)	-1.18*** (0.80)	-0.91** (0.71)	-0.44*** (0.64)
3	-1.56*** (1.21)	-1.75*** (1.18)	-0.71 (0.55)	-0.49*** (0.72)
4	-1.15*** (0.89)	-1.47*** (0.99)	-1.62*** (1.26)	-0.84*** (1.22)
5	-1.11*** (0.86)	-1.40*** (0.95)	-0.85** (0.66)	-0.48*** (0.7)
6	-1.68*** (1.3)	-1.51*** (1.02)	-1.26*** (0.98)	-0.81*** (1.17)
7	-0.89* (0.69)	-1.33*** (0.9)	-1.34*** (1.04)	-0.73*** (1.06)
8	-1.00** (0.77)	-1.18*** (0.8)	-0.54 (0.42)	-0.26** (0.38)
9	-1.01** (0.79)	-1.28*** (0.87)	-1.14** (0.88)	-0.45*** (0.65)
10	-1.40*** (1.08)	-1.83*** (1.24)	-1.9*** (1.47)	-0.98*** (1.42)
11	-1.18*** (0.92)	-1.72*** (1.17)	-1.7*** (1.32)	-1.16*** (1.69)
12	-0.58* (0.45)	-1.07*** (0.72)	-0.54* (0.42)	-0.46*** (0.66)
13	-1.79*** (1.39)	-1.66*** (1.12)	-0.72** (0.56)	-0.57*** (0.82)
14	-1.39*** (1.08)	-1.67*** (1.13)	-0.89* (0.69)	-0.54*** (0.78)
15	-1.02** (0.79)	-1.39*** (0.94)	-1.23** (0.95)	-1.03*** (1.5)
16	-2.01*** (1.56)	-1.60*** (1.09)	-1.29*** (1.0)	-0.89*** (1.3)
17	-1.88*** (1.46)	-1.79*** (1.21)	-1.45*** (1.12)	-0.93*** (1.35)
18	-2.03*** (1.57)	-1.83*** (1.24)	-1.70*** (1.32)	-0.98*** (1.43)
19	-1.16*** (0.9)	-1.07*** (0.72)	-0.36 (0.28)	-0.53*** (0.77)
20	-1.12*** (0.86)	-1.52*** (1.03)	-1.0** (0.78)	-0.71*** (1.04)
AVG	-1.29	-1.48	-1.08	-0.69
Std	0.42	0.25	0.45	0.25
Dev				

1- Number in parenthesis denotes ratio to mean.
2- Statistical significance codes: 0 '*' 0.001 '**' 0.01 '*' 0.05 '.' 0.1 ' ' 1**

Table A.5. Comparison matrix for ratios of regression slopes for cooling demand 2010-2095 across GCMs for RCP 8.5 scenario

Cooling → Slopes 2010-2099 (yr ⁻¹) ↓	GCM	0.15	0.13	0.15	0.16	0.14	0.13	0.13	0.13	0.13	0.23	0.22	0.10	0.16	0.18	0.14	0.14	0.19	0.20	0.09	0.14
		1	2	3	4	5	6	7	8	9	10	11	12	13	14	15	16	17	18	19	20
0.15	1	1	0.9	1.0	1.0	0.9	0.8	0.9	0.9	0.9	1.5	1.5	0.6	1.1	1.2	0.9	0.9	1.3	1.3	0.6	0.9
0.13	2	1.2	1	1.1	1.2	1.1	1.0	1.0	1.0	1.0	1.7	1.7	0.7	1.2	1.3	1.0	1.1	1.5	1.5	0.7	1.1
0.15	3	1.0	0.9	1	1.1	0.9	0.9	0.9	0.9	0.9	1.5	1.5	0.6	1.1	1.2	0.9	1.0	1.3	1.3	0.6	1.0
0.16	4	1.0	0.8	0.9	1	0.9	0.8	0.8	0.8	0.8	1.4	1.4	0.6	1.0	1.1	0.9	0.9	1.2	1.3	0.6	0.9
0.14	5	1.1	0.9	1.1	1.1	1	0.9	0.9	0.9	0.9	1.6	1.6	0.7	1.2	1.3	1.0	1.0	1.4	1.4	0.7	1.0
0.13	6	1.2	1.0	1.2	1.2	1.1	1	1.0	1.0	1.0	1.8	1.8	0.8	1.3	1.4	1.1	1.1	1.5	1.6	0.8	1.1
0.13	7	1.2	1.0	1.1	1.2	1.1	1.0	1	1.0	1.0	1.7	1.7	0.7	1.3	1.4	1.0	1.1	1.5	1.5	0.7	1.1
0.13	8	1.2	1.0	1.1	1.2	1.1	1.0	1.0	1	1.0	1.7	1.7	0.7	1.3	1.3	1.0	1.1	1.5	1.5	0.7	1.1
0.13	9	1.2	1.0	1.1	1.2	1.1	1.0	1.0	1.0	1	1.7	1.7	0.7	1.3	1.4	1.0	1.1	1.5	1.5	0.7	1.1
0.23	10	0.7	0.6	0.7	0.7	0.6	0.6	0.6	0.6	0.6	1	1.0	0.4	0.7	0.8	0.6	0.6	0.9	0.9	0.4	0.6
0.22	11	0.7	0.6	0.7	0.7	0.6	0.6	0.6	0.6	0.6	1.0	1	0.4	0.7	0.8	0.6	0.6	0.9	0.9	0.4	0.6
0.10	12	1.6	1.4	1.5	1.6	1.5	1.3	1.4	1.4	1.4	2.4	2.3	1	1.7	1.8	1.4	1.5	2.0	2.0	1.0	1.5
0.16	13	0.9	0.8	0.9	1.0	0.9	0.8	0.8	0.8	0.8	1.4	1.3	0.6	1	1.1	0.8	0.9	1.2	1.2	0.6	0.9
0.18	14	0.9	0.7	0.8	0.9	0.8	0.7	0.7	0.7	0.7	1.3	1.3	0.5	0.9	1	0.8	0.8	1.1	1.1	0.5	0.8
0.14	15	1.1	1.0	1.1	1.2	1.0	0.9	1.0	1.0	1.0	1.7	1.6	0.7	1.2	1.3	1	1.0	1.4	1.5	0.7	1.1
0.14	16	1.1	0.9	1.0	1.1	1.0	0.9	0.9	0.9	0.9	1.6	1.6	0.7	1.2	1.3	1.0	1	1.4	1.4	0.7	1.0
0.19	17	0.8	0.7	0.8	0.8	0.7	0.6	0.7	0.7	0.7	1.2	1.1	0.5	0.8	0.9	0.7	0.7	1	1.0	0.5	0.7
0.20	18	0.8	0.7	0.8	0.8	0.7	0.6	0.7	0.7	0.7	1.1	1.1	0.5	0.8	0.9	0.7	0.7	1.0	1	0.5	0.7
0.09	19	1.6	1.4	1.6	1.7	1.5	1.3	1.4	1.4	1.4	2.4	2.3	1.0	1.7	1.9	1.4	1.5	2.0	2.1	1	1.5
0.14	20	1.1	0.9	1.0	1.1	1.0	0.9	0.9	0.9	0.9	1.6	1.5	0.7	1.1	1.2	0.9	1.0	1.4	1.4	0.7	1

1- Green denotes ratio higher than one. Red denotes lower than one ratio.
2- Cooling Demand 2010-2095 for RCP 8.5

Table A.6. Comparison matrix for ratios of regression slopes for cooling demand 2010-2095 across GCMs for RCP 4.5 scenario

Cooling → Slopes 2010-2099 (yr ⁻¹) ↓	GCM	0.05	0.05	0.05	0.06	0.05	0.07	0.07	0.03	0.04	0.10	0.10	0.04	0.06	0.06	0.07	0.07	0.09	0.08	0.04	0.06
		1	2	3	4	5	6	7	8	9	10	11	12	13	14	15	16	17	18	19	20
0.05	1	1	1.0	1.1	1.2	1.1	1.5	1.5	0.5	0.8	2.1	2.1	0.8	1.3	1.3	1.5	1.4	1.9	1.7	0.9	1.4
0.05	2	1.0	1	1.0	1.2	1.1	1.4	1.4	0.5	0.8	2.0	2.1	0.7	1.3	1.2	1.5	1.4	1.8	1.7	0.8	1.3
0.05	3	0.9	1.0	1	1.1	1.0	1.3	1.4	0.5	0.8	1.9	2.0	0.7	1.2	1.2	1.4	1.3	1.7	1.6	0.8	1.3
0.06	4	0.8	0.8	0.9	1	0.9	1.2	1.2	0.4	0.7	1.7	1.7	0.6	1.1	1.0	1.3	1.2	1.5	1.4	0.7	1.1
0.05	5	0.9	0.9	1.0	1.1	1	1.3	1.4	0.5	0.8	1.9	1.9	0.7	1.2	1.2	1.4	1.3	1.7	1.6	0.8	1.3
0.07	6	0.7	0.7	0.7	0.9	0.8	1	1.0	0.4	0.6	1.4	1.5	0.5	0.9	0.9	1.1	1.0	1.3	1.2	0.6	1.0
0.07	7	0.7	0.7	0.7	0.8	0.7	1.0	1	0.4	0.6	1.4	1.4	0.5	0.9	0.9	1.0	1.0	1.3	1.2	0.6	0.9
0.03	8	1.8	1.9	2.0	2.3	2.0	2.7	2.7	1	1.5	3.8	3.9	1.4	2.4	2.3	2.8	2.6	3.4	3.2	1.6	2.5
0.04	9	1.2	1.2	1.3	1.5	1.3	1.7	1.8	0.6	1	2.5	2.5	0.9	1.6	1.5	1.8	1.7	2.2	2.1	1.0	1.7
0.10	10	0.5	0.5	0.5	0.6	0.5	0.7	0.7	0.3	0.4	1	1.0	0.4	0.6	0.6	0.7	0.7	0.9	0.8	0.4	0.7
0.10	11	0.5	0.5	0.5	0.6	0.5	0.7	0.7	0.3	0.4	1.0	1	0.4	0.6	0.6	0.7	0.7	0.9	0.8	0.4	0.6
0.04	12	1.3	1.4	1.4	1.6	1.4	1.9	2.0	0.7	1.1	2.7	2.8	1	1.7	1.7	2.0	1.9	2.4	2.3	1.1	1.8
0.06	13	0.8	0.8	0.8	0.9	0.8	1.1	1.1	0.4	0.6	1.6	1.6	0.6	1	1.0	1.2	1.1	1.4	1.3	0.7	1.1
0.06	14	0.8	0.8	0.8	1.0	0.9	1.1	1.2	0.4	0.7	1.6	1.7	0.6	1.0	1	1.2	1.1	1.5	1.4	0.7	1.1
0.07	15	0.6	0.7	0.7	0.8	0.7	0.9	1.0	0.4	0.5	1.3	1.4	0.5	0.8	0.8	1	0.9	1.2	1.1	0.6	0.9
0.07	16	0.7	0.7	0.8	0.9	0.8	1.0	1.0	0.4	0.6	1.5	1.5	0.5	0.9	0.9	1.1	1	1.3	1.2	0.6	1.0
0.09	17	0.5	0.6	0.6	0.7	0.6	0.8	0.8	0.3	0.5	1.1	1.1	0.4	0.7	0.7	0.8	0.8	1	0.9	0.5	0.7
0.08	18	0.6	0.6	0.6	0.7	0.6	0.8	0.9	0.3	0.5	1.2	1.2	0.4	0.8	0.7	0.9	0.8	1.1	1	0.5	0.8
0.04	19	1.2	1.2	1.3	1.4	1.3	1.7	1.7	0.6	1.0	2.4	2.5	0.9	1.5	1.5	1.8	1.7	2.2	2.0	1	1.6
0.06	20	0.7	0.7	0.8	0.9	0.8	1.0	1.1	0.4	0.6	1.5	1.5	0.5	0.9	0.9	1.1	1.0	1.3	1.3	0.6	1

1- Green denotes ratio higher than one. Red denotes lower than one ratio.

2- Cooling Demand 2010-2095 for RCP 4.5

Table A.7. Comparison matrix for ratios of regression slopes for heating demand 2010-2095 across GCMs for RCP 8.5 scenario

Heating → Slopes 2010-2099 (yr ⁻¹) ↓	GCM	-1.3	-1.2	-1.8	-1.5	-1.4	-1.5	-1.3	-1.2	-1.3	-1.8	-1.7	-1.1	-1.7	-1.7	-1.4	-1.6	-1.8	-1.8	-1.1	-1.5
		1	2	3	4	5	6	7	8	9	10	11	12	13	14	15	16	17	18	19	20
-1.3	1	1	0.9	1.3	1.1	1.1	1.2	1.0	0.9	1.0	1.4	1.3	0.8	1.3	1.3	1.1	1.2	1.4	1.4	0.8	1.2
-1.2	2	1.1	1	1.5	1.2	1.2	1.3	1.1	1.0	1.1	1.6	1.5	0.9	1.4	1.4	1.2	1.4	1.5	1.6	0.9	1.3
-1.8	3	0.7	0.7	1	0.8	0.8	0.9	0.8	0.7	0.7	1.0	1.0	0.6	0.9	1.0	0.8	0.9	1.0	1.0	0.6	0.9
-1.5	4	0.9	0.8	1.2	1	1.0	1.0	0.9	0.8	0.9	1.2	1.2	0.7	1.1	1.1	0.9	1.1	1.2	1.2	0.7	1.0
-1.4	5	0.9	0.8	1.2	1.0	1	1.1	0.9	0.8	0.9	1.3	1.2	0.8	1.2	1.2	1.0	1.1	1.3	1.3	0.8	1.1
-1.5	6	0.9	0.8	1.2	1.0	0.9	1	0.9	0.8	0.8	1.2	1.1	0.7	1.1	1.1	0.9	1.1	1.2	1.2	0.7	1.0
-1.3	7	1.0	0.9	1.3	1.1	1.1	1.1	1	0.9	1.0	1.4	1.3	0.8	1.2	1.3	1.0	1.2	1.3	1.4	0.8	1.1
-1.2	8	1.1	1.0	1.5	1.2	1.2	1.3	1.1	1	1.1	1.5	1.5	0.9	1.4	1.4	1.2	1.4	1.5	1.6	0.9	1.3
-1.3	9	1.0	0.9	1.4	1.1	1.1	1.2	1.0	0.9	1	1.4	1.3	0.8	1.3	1.3	1.1	1.3	1.4	1.4	0.8	1.2
-1.8	10	0.7	0.6	1.0	0.8	0.8	0.8	0.7	0.6	0.7	1	0.9	0.6	0.9	0.9	0.8	0.9	1.0	1.0	0.6	0.8
-1.7	11	0.8	0.7	1.0	0.9	0.8	0.9	0.8	0.7	0.7	1.1	1	0.6	1.0	1.0	0.8	0.9	1.0	1.1	0.6	0.9
-1.1	12	1.2	1.1	1.6	1.4	1.3	1.4	1.2	1.1	1.2	1.7	1.6	1	1.6	1.6	1.3	1.5	1.7	1.7	1.0	1.4
-1.7	13	0.8	0.7	1.1	0.9	0.8	0.9	0.8	0.7	0.8	1.1	1.0	0.6	1	1.0	0.8	1.0	1.1	1.1	0.6	0.9
-1.7	14	0.8	0.7	1.0	0.9	0.8	0.9	0.8	0.7	0.8	1.1	1.0	0.6	1.0	1	0.8	1.0	1.1	1.1	0.6	0.9
-1.4	15	0.9	0.8	1.3	1.1	1.0	1.1	1.0	0.8	0.9	1.3	1.2	0.8	1.2	1.2	1	1.2	1.3	1.3	0.8	1.1
-1.6	16	0.8	0.7	1.1	0.9	0.9	0.9	0.8	0.7	0.8	1.1	1.1	0.7	1.0	1.0	0.9	1	1.1	1.1	0.7	0.9
-1.8	17	0.7	0.7	1.0	0.8	0.8	0.8	0.7	0.7	0.7	1.0	1.0	0.6	0.9	0.9	0.8	0.9	1	1.0	0.6	0.8
-1.8	18	0.7	0.6	1.0	0.8	0.8	0.8	0.7	0.6	0.7	1.0	0.9	0.6	0.9	0.9	0.8	0.9	1.0	1	0.6	0.8
-1.1	19	1.2	1.1	1.6	1.4	1.3	1.4	1.2	1.1	1.2	1.7	1.6	1.0	1.6	1.6	1.3	1.5	1.7	1.7	1	1.4
-1.5	20	0.9	0.8	1.2	1.0	0.9	1.0	0.9	0.8	0.8	1.2	1.1	0.7	1.1	1.1	0.9	1.1	1.2	1.2	0.7	1

1- Green denotes ratio higher than one. Red denotes lower than one ratio.
2- Heating Demand 2010-2095 for RCP 8.5

Table A.8. Comparison matrix for ratios of regression slopes for heating demand 2010-2095 across GCMs for RCP 4.5 scenario

Heating → Slopes 2010-2099 (yr ⁻¹) ↓	GCM	-0.8	-0.8	-0.9	-1.5	-0.7	-1.3	-1.3	-0.5	-0.8	-1.7	-1.7	-0.8	-0.9	-0.9	-1.5	-1.3	-1.6	-1.6	-0.9	-1.3
		1	2	3	4	5	6	7	8	9	10	11	12	13	14	15	16	17	18	19	20
-0.8	1	1	1.0	1.1	1.8	0.8	1.6	1.6	0.6	1.0	2.0	2.1	0.9	1.2	1.1	1.8	1.6	2.0	1.9	1.1	1.5
-0.8	2	1.0	1	1.1	1.7	0.8	1.6	1.5	0.5	0.9	2.0	2.1	0.9	1.1	1.1	1.7	1.6	1.9	1.9	1.1	1.5
-0.9	3	0.9	1.0	1	1.7	0.8	1.5	1.5	0.5	0.9	1.9	2.0	0.9	1.1	1.1	1.7	1.5	1.8	1.8	1.0	1.4
-1.5	4	0.6	0.6	0.6	1	0.5	0.9	0.9	0.3	0.5	1.1	1.2	0.5	0.6	0.6	1.0	0.9	1.1	1.1	0.6	0.9
-0.7	5	1.2	1.2	1.3	2.1	1	1.9	1.9	0.7	1.2	2.4	2.5	1.1	1.4	1.4	2.1	1.9	2.4	2.3	1.3	1.9
-1.3	6	0.6	0.6	0.7	1.1	0.5	1	1.0	0.4	0.6	1.3	1.3	0.6	0.7	0.7	1.1	1.0	1.2	1.2	0.7	1.0
-1.3	7	0.6	0.6	0.7	1.1	0.5	1.0	1	0.4	0.6	1.3	1.3	0.6	0.7	0.7	1.1	1.0	1.2	1.2	0.7	1.0
-0.5	8	1.8	1.8	1.9	3.2	1.5	2.9	2.8	1	1.7	3.6	3.8	1.7	2.1	2.0	3.2	2.9	3.5	3.5	2.0	2.8
-0.8	9	1.0	1.1	1.1	1.8	0.9	1.6	1.6	0.6	1	2.1	2.2	1.0	1.2	1.2	1.8	1.7	2.0	2.0	1.1	1.6
-1.7	10	0.5	0.5	0.5	0.9	0.4	0.8	0.8	0.3	0.5	1	1.0	0.5	0.6	0.6	0.9	0.8	1.0	1.0	0.5	0.8
-1.7	11	0.5	0.5	0.5	0.8	0.4	0.8	0.7	0.3	0.5	1.0	1	0.4	0.5	0.5	0.8	0.8	0.9	0.9	0.5	0.7
-0.8	12	1.1	1.1	1.2	1.9	0.9	1.7	1.7	0.6	1.0	2.2	2.3	1	1.2	1.2	1.9	1.7	2.1	2.1	1.2	1.7
-0.9	13	0.9	0.9	0.9	1.6	0.7	1.4	1.4	0.5	0.8	1.8	1.8	0.8	1	1.0	1.5	1.4	1.7	1.7	1.0	1.3
-0.9	14	0.9	0.9	0.9	1.6	0.7	1.4	1.4	0.5	0.9	1.8	1.9	0.8	1.0	1	1.6	1.4	1.7	1.7	1.0	1.4
-1.5	15	0.6	0.6	0.6	1.0	0.5	0.9	0.9	0.3	0.5	1.1	1.2	0.5	0.6	0.6	1	0.9	1.1	1.1	0.6	0.9
-1.3	16	0.6	0.6	0.7	1.1	0.5	1.0	1.0	0.3	0.6	1.3	1.3	0.6	0.7	0.7	1.1	1	1.2	1.2	0.7	1.0
-1.6	17	0.5	0.5	0.5	0.9	0.4	0.8	0.8	0.3	0.5	1.0	1.1	0.5	0.6	0.6	0.9	0.8	1	1.0	0.6	0.8
-1.6	18	0.5	0.5	0.6	0.9	0.4	0.8	0.8	0.3	0.5	1.0	1.1	0.5	0.6	0.6	0.9	0.8	1.0	1	0.6	0.8
-0.9	19	0.9	0.9	1.0	1.6	0.8	1.4	1.4	0.5	0.9	1.8	1.9	0.8	1.0	1.0	1.6	1.5	1.8	1.8	1	1.4
-1.3	20	0.6	0.7	0.7	1.2	0.5	1.0	1.0	0.4	0.6	1.3	1.4	0.6	0.7	0.7	1.2	1.0	1.3	1.3	0.7	1

1- Green denotes ratio higher than one. Red denotes lower than one ratio.
2- Heating Demand for RCP 4.5

Table A.9. Comparison matrix for ratios of regression slopes for cooling demand 2010-2045 across GCMs for RCP 8.5 scenario

Cooling → Slopes 2010-2050 (yr ⁻¹) ↓	GCM	0.10	0.09	0.11	0.12	0.11	0.13	0.05	0.09	0.08	0.13	0.18	0.07	0.15	0.12	0.11	0.13	0.17	0.16	0.08	0.11
		1	2	3	4	5	6	7	8	9	10	11	12	13	14	15	16	17	18	19	20
0.10	1	1	0.9	1.1	1.2	1.1	1.3	0.5	0.8	0.8	1.2	1.8	0.7	1.5	1.2	1.1	1.3	1.6	1.6	0.8	1.0
0.09	2	1.1	1	1.2	1.3	1.2	1.4	0.6	1.0	0.9	1.4	2.0	0.7	1.7	1.3	1.2	1.5	1.8	1.8	0.9	1.2
0.11	3	0.9	0.8	1	1.1	1.0	1.2	0.5	0.8	0.8	1.2	1.7	0.6	1.4	1.1	1.0	1.2	1.5	1.5	0.7	1.0
0.12	4	0.9	0.8	0.9	1	1.0	1.1	0.4	0.7	0.7	1.1	1.5	0.6	1.3	1.0	0.9	1.1	1.4	1.4	0.7	0.9
0.11	5	0.9	0.8	1.0	1.0	1	1.1	0.5	0.8	0.7	1.1	1.6	0.6	1.4	1.1	1.0	1.2	1.5	1.4	0.7	0.9
0.13	6	0.8	0.7	0.8	0.9	0.9	1	0.4	0.7	0.6	1.0	1.4	0.5	1.2	0.9	0.9	1.0	1.3	1.2	0.6	0.8
0.05	7	2.0	1.7	2.1	2.3	2.2	2.5	1	1.7	1.6	2.5	3.5	1.3	2.9	2.3	2.1	2.6	3.2	3.1	1.6	2.0
0.09	8	1.2	1.1	1.3	1.4	1.3	1.5	0.6	1	1.0	1.5	2.1	0.8	1.8	1.4	1.3	1.6	1.9	1.9	0.9	1.2
0.08	9	1.2	1.1	1.3	1.4	1.4	1.6	0.6	1.0	1	1.5	2.2	0.8	1.9	1.5	1.3	1.6	2.0	1.9	1.0	1.3
0.13	10	0.8	0.7	0.9	0.9	0.9	1.0	0.4	0.7	0.6	1	1.4	0.5	1.2	0.9	0.9	1.1	1.3	1.3	0.6	0.8
0.18	11	0.6	0.5	0.6	0.6	0.6	0.7	0.3	0.5	0.5	0.7	1	0.4	0.8	0.7	0.6	0.7	0.9	0.9	0.4	0.6
0.07	12	1.5	1.3	1.6	1.7	1.7	1.9	0.8	1.3	1.2	1.9	2.7	1	2.2	1.8	1.6	2.0	2.5	2.4	1.2	1.5
0.15	13	0.7	0.6	0.7	0.8	0.7	0.8	0.3	0.6	0.5	0.8	1.2	0.4	1	0.8	0.7	0.9	1.1	1.0	0.5	0.7
0.12	14	0.8	0.8	0.9	1.0	0.9	1.1	0.4	0.7	0.7	1.1	1.5	0.6	1.3	1	0.9	1.1	1.4	1.3	0.7	0.9
0.11	15	0.9	0.8	1.0	1.1	1.0	1.2	0.5	0.8	0.7	1.2	1.7	0.6	1.4	1.1	1	1.2	1.5	1.4	0.7	1.0
0.13	16	0.8	0.7	0.8	0.9	0.8	1.0	0.4	0.6	0.6	0.9	1.4	0.5	1.1	0.9	0.8	1	1.2	1.2	0.6	0.8
0.17	17	0.6	0.5	0.7	0.7	0.7	0.8	0.3	0.5	0.5	0.8	1.1	0.4	0.9	0.7	0.7	0.8	1	1.0	0.5	0.6
0.16	18	0.6	0.6	0.7	0.7	0.7	0.8	0.3	0.5	0.5	0.8	1.1	0.4	1.0	0.8	0.7	0.8	1.0	1	0.5	0.7
0.08	19	1.3	1.1	1.4	1.5	1.4	1.6	0.6	1.1	1.0	1.6	2.3	0.8	1.9	1.5	1.4	1.7	2.1	2.0	1	1.3
0.11	20	1.0	0.9	1.0	1.1	1.1	1.2	0.5	0.8	0.8	1.2	1.7	0.6	1.5	1.1	1.1	1.3	1.6	1.5	0.8	1

1- Green denotes ratio higher than one. Red denotes lower than one ratio.
2- Cooling Demand 2010-2045 for RCP 8.5

Table A.10. Comparison matrix for ratios of regression slopes for cooling demand 2010-2045 across GCMs for RCP 4.5 scenario

Cooling → Slopes 2010-2050 (yr ⁻¹) ↓	GCM	0.08	0.09	0.05	0.11	0.08	0.08	0.11	0.05	0.12	0.17	0.13	0.06	0.08	0.09	0.10	0.11	0.13	0.11	0.04	0.08
		1	2	3	4	5	6	7	8	9	10	11	12	13	14	15	16	17	18	19	20
0.08	1	1	1.1	0.7	1.3	0.9	1.0	1.3	0.6	1.5	2.1	1.6	0.7	1.0	1.1	1.2	1.4	1.6	1.3	0.5	1.0
0.09	2	0.9	1	0.6	1.2	0.9	0.9	1.2	0.5	1.4	1.9	1.4	0.7	0.9	1.0	1.1	1.3	1.5	1.2	0.5	0.9
0.05	3	1.5	1.6	1	1.9	1.4	1.4	2.0	0.8	2.2	3.1	2.3	1.1	1.5	1.6	1.8	2.0	2.4	2.0	0.8	1.5
0.11	4	0.8	0.8	0.5	1	0.7	0.7	1.0	0.4	1.2	1.6	1.2	0.6	0.8	0.8	0.9	1.0	1.3	1.0	0.4	0.8
0.08	5	1.1	1.2	0.7	1.4	1	1.0	1.4	0.6	1.6	2.2	1.7	0.8	1.1	1.2	1.3	1.5	1.7	1.4	0.5	1.1
0.08	6	1.0	1.1	0.7	1.4	1.0	1	1.4	0.6	1.6	2.2	1.6	0.8	1.1	1.1	1.3	1.4	1.7	1.4	0.5	1.1
0.11	7	0.8	0.8	0.5	1.0	0.7	0.7	1	0.4	1.1	1.6	1.2	0.6	0.8	0.8	0.9	1.0	1.2	1.0	0.4	0.8
0.05	8	1.8	1.9	1.2	2.3	1.7	1.7	2.3	1	2.6	3.7	2.7	1.3	1.8	1.9	2.2	2.4	2.9	2.4	0.9	1.8
0.12	9	0.7	0.7	0.4	0.9	0.6	0.6	0.9	0.4	1	1.4	1.0	0.5	0.7	0.7	0.8	0.9	1.1	0.9	0.3	0.7
0.17	10	0.5	0.5	0.3	0.6	0.4	0.5	0.6	0.3	0.7	1	0.7	0.4	0.5	0.5	0.6	0.7	0.8	0.6	0.2	0.5
0.13	11	0.6	0.7	0.4	0.8	0.6	0.6	0.8	0.4	1.0	1.3	1	0.5	0.6	0.7	0.8	0.9	1.1	0.9	0.3	0.7
0.06	12	1.3	1.5	0.9	1.8	1.3	1.3	1.8	0.8	2.0	2.8	2.1	1	1.4	1.5	1.7	1.8	2.2	1.8	0.7	1.4
0.08	13	1.0	1.1	0.7	1.3	0.9	0.9	1.3	0.6	1.5	2.1	1.5	0.7	1	1.1	1.2	1.4	1.6	1.3	0.5	1.0
0.09	14	0.9	1.0	0.6	1.2	0.9	0.9	1.2	0.5	1.4	1.9	1.4	0.7	0.9	1	1.1	1.2	1.5	1.2	0.5	0.9
0.10	15	0.8	0.9	0.5	1.1	0.8	0.8	1.1	0.5	1.2	1.7	1.3	0.6	0.8	0.9	1	1.1	1.3	1.1	0.4	0.8
0.11	16	0.7	0.8	0.5	1.0	0.7	0.7	1.0	0.4	1.1	1.5	1.1	0.5	0.7	0.8	0.9	1	1.2	1.0	0.4	0.8
0.13	17	0.6	0.7	0.4	0.8	0.6	0.6	0.8	0.3	0.9	1.3	0.9	0.5	0.6	0.7	0.8	0.8	1	0.8	0.3	0.6
0.11	18	0.7	0.8	0.5	1.0	0.7	0.7	1.0	0.4	1.1	1.5	1.2	0.5	0.7	0.8	0.9	1.0	1.2	1	0.4	0.8
0.04	19	2.0	2.1	1.3	2.5	1.8	1.9	2.6	1.1	2.9	4.1	3.0	1.4	2.0	2.2	2.4	2.7	3.2	2.6	1	2.0
0.08	20	1.0	1.1	0.7	1.3	0.9	0.9	1.3	0.6	1.5	2.0	1.5	0.7	1.0	1.1	1.2	1.3	1.6	1.3	0.5	1

1- Green denotes ratio higher than one. Red denotes lower than one ratio.
2- Cooling Demand 2010-2045 for RCP 4.5

Table A.11. Comparison matrix for ratios of regression slopes for heating demand 2010-2045 across GCMs for RCP 8.5 scenario

Heating → Slopes 2010-2050 (yr ⁻¹) ↓	GCM	-1.2	-0.7	-1.6	-1.2	-1.1	-1.7	-0.9	-1.0	-1.0	-1.4	-1.2	-0.6	-1.8	-1.4	-1.0	-2.0	-1.9	-2.0	-1.2	-1.1
		1	2	3	4	5	6	7	8	9	10	11	12	13	14	15	16	17	18	19	20
-1.2	1	1	0.6	1.3	1.0	0.9	1.4	0.8	0.8	0.9	1.2	1.0	0.5	1.5	1.2	0.9	1.7	1.6	1.7	1.0	0.9
-0.7	2	1.8	1	2.3	1.7	1.7	2.5	1.3	1.5	1.5	2.1	1.8	0.9	2.7	2.1	1.5	3.0	2.8	3.0	1.7	1.7
-1.6	3	0.8	0.4	1	0.7	0.7	1.1	0.6	0.6	0.7	0.9	0.8	0.4	1.2	0.9	0.7	1.3	1.2	1.3	0.7	0.7
-1.2	4	1.0	0.6	1.3	1	1.0	1.5	0.8	0.9	0.9	1.2	1.0	0.5	1.6	1.2	0.9	1.7	1.6	1.8	1.0	1.0
-1.1	5	1.1	0.6	1.4	1.0	1	1.5	0.8	0.9	0.9	1.3	1.1	0.5	1.6	1.3	0.9	1.8	1.7	1.8	1.0	1.0
-1.7	6	0.7	0.4	0.9	0.7	0.7	1	0.5	0.6	0.6	0.8	0.7	0.3	1.1	0.8	0.6	1.2	1.1	1.2	0.7	0.7
-0.9	7	1.3	0.7	1.7	1.3	1.2	1.9	1	1.1	1.1	1.6	1.3	0.7	2.0	1.6	1.1	2.3	2.1	2.3	1.3	1.3
-1.0	8	1.2	0.7	1.6	1.2	1.1	1.7	0.9	1	1.0	1.4	1.2	0.6	1.8	1.4	1.0	2.0	1.9	2.0	1.2	1.1
-1.0	9	1.2	0.7	1.5	1.1	1.1	1.7	0.9	1.0	1	1.4	1.2	0.6	1.8	1.4	1.0	2.0	1.9	2.0	1.1	1.1
-1.4	10	0.8	0.5	1.1	0.8	0.8	1.2	0.6	0.7	0.7	1	0.8	0.4	1.3	1.0	0.7	1.4	1.3	1.4	0.8	0.8
-1.2	11	1.0	0.6	1.3	1.0	0.9	1.4	0.8	0.8	0.9	1.2	1	0.5	1.5	1.2	0.9	1.7	1.6	1.7	1.0	0.9
-0.6	12	2.0	1.1	2.7	2.0	1.9	2.9	1.5	1.7	1.7	2.4	2.0	1	3.1	2.4	1.7	3.4	3.2	3.5	2.0	1.9
-1.8	13	0.7	0.4	0.9	0.6	0.6	0.9	0.5	0.6	0.6	0.8	0.7	0.3	1	0.8	0.6	1.1	1.1	1.1	0.6	0.6
-1.4	14	0.8	0.5	1.1	0.8	0.8	1.2	0.6	0.7	0.7	1.0	0.9	0.4	1.3	1	0.7	1.4	1.4	1.5	0.8	0.8
-1.0	15	1.2	0.7	1.5	1.1	1.1	1.6	0.9	1.0	1.0	1.4	1.2	0.6	1.8	1.4	1	2.0	1.8	2.0	1.1	1.1
-2.0	16	0.6	0.3	0.8	0.6	0.5	0.8	0.4	0.5	0.5	0.7	0.6	0.3	0.9	0.7	0.5	1	0.9	1.0	0.6	0.6
-1.9	17	0.6	0.4	0.8	0.6	0.6	0.9	0.5	0.5	0.5	0.7	0.6	0.3	0.9	0.7	0.5	1.1	1	1.1	0.6	0.6
-2.0	18	0.6	0.3	0.8	0.6	0.5	0.8	0.4	0.5	0.5	0.7	0.6	0.3	0.9	0.7	0.5	1.0	0.9	1	0.6	0.6
-1.2	19	1.0	0.6	1.3	1.0	1.0	1.5	0.8	0.9	0.9	1.2	1.0	0.5	1.5	1.2	0.9	1.7	1.6	1.7	1	1.0
-1.1	20	1.1	0.6	1.4	1.0	1.0	1.5	0.8	0.9	0.9	1.3	1.1	0.5	1.6	1.2	0.9	1.8	1.7	1.8	1.0	1

1- Green denotes ratio higher than one. Red denotes lower than one ratio.
2- Heating Demand 2010-2045 for RCP 8.5

Table A.12. Comparison matrix for ratios of regression slopes for heating demand 2010-2045 across GCMs for RCP 4.5 scenario

Heating → Slopes 2010-2050 (yr ⁻¹) ↓	GCM	-0.5	-0.9	-0.7	-1.6	-0.8	-1.3	-1.3	-0.5	-1.1	-1.9	-1.7	-0.5	-0.7	-0.9	-1.2	-1.3	-1.4	-1.7	-0.4	-1.0
		1	2	3	4	5	6	7	8	9	10	11	12	13	14	15	16	17	18	19	20
-0.5	1	1	1.9	1.4	3.3	1.7	2.6	2.7	1.1	2.3	3.8	3.4	1.1	1.5	1.8	2.5	2.6	2.9	3.4	0.7	2.0
-0.9	2	0.5	1	0.8	1.8	0.9	1.4	1.5	0.6	1.2	2.1	1.9	0.6	0.8	1.0	1.3	1.4	1.6	1.9	0.4	1.1
-0.7	3	0.7	1.3	1	2.3	1.2	1.8	1.9	0.8	1.6	2.7	2.4	0.8	1.0	1.2	1.7	1.8	2.0	2.4	0.5	1.4
-1.6	4	0.3	0.6	0.4	1	0.5	0.8	0.8	0.3	0.7	1.2	1.1	0.3	0.4	0.5	0.8	0.8	0.9	1.0	0.2	0.6
-0.8	5	0.6	1.1	0.8	1.9	1	1.5	1.6	0.6	1.3	2.2	2.0	0.6	0.9	1.0	1.4	1.5	1.7	2.0	0.4	1.2
-1.3	6	0.4	0.7	0.6	1.3	0.7	1	1.1	0.4	0.9	1.5	1.3	0.4	0.6	0.7	1.0	1.0	1.1	1.3	0.3	0.8
-1.3	7	0.4	0.7	0.5	1.2	0.6	0.9	1	0.4	0.8	1.4	1.3	0.4	0.5	0.7	0.9	1.0	1.1	1.3	0.3	0.7
-0.5	8	0.9	1.7	1.3	3.0	1.6	2.3	2.5	1	2.1	3.5	3.1	1.0	1.3	1.6	2.3	2.4	2.7	3.1	0.7	1.8
-1.1	9	0.4	0.8	0.6	1.4	0.7	1.1	1.2	0.5	1	1.7	1.5	0.5	0.6	0.8	1.1	1.1	1.3	1.5	0.3	0.9
-1.9	10	0.3	0.5	0.4	0.9	0.4	0.7	0.7	0.3	0.6	1	0.9	0.3	0.4	0.5	0.6	0.7	0.8	0.9	0.2	0.5
-1.7	11	0.3	0.5	0.4	1.0	0.5	0.7	0.8	0.3	0.7	1.1	1	0.3	0.4	0.5	0.7	0.8	0.9	1.0	0.2	0.6
-0.5	12	0.9	1.7	1.3	3.0	1.6	2.3	2.5	1.0	2.1	3.5	3.1	1	1.3	1.6	2.3	2.4	2.7	3.1	0.7	1.8
-0.7	13	0.7	1.3	1.0	2.3	1.2	1.8	1.9	0.8	1.6	2.6	2.4	0.8	1	1.2	1.7	1.8	2.0	2.4	0.5	1.4
-0.9	14	0.6	1.0	0.8	1.8	1.0	1.4	1.5	0.6	1.3	2.1	1.9	0.6	0.8	1	1.4	1.5	1.6	1.9	0.4	1.1
-1.2	15	0.4	0.7	0.6	1.3	0.7	1.0	1.1	0.4	0.9	1.6	1.4	0.4	0.6	0.7	1	1.1	1.2	1.4	0.3	0.8
-1.3	16	0.4	0.7	0.6	1.3	0.7	1.0	1.0	0.4	0.9	1.5	1.3	0.4	0.6	0.7	0.9	1	1.1	1.3	0.3	0.8
-1.4	17	0.3	0.6	0.5	1.1	0.6	0.9	0.9	0.4	0.8	1.3	1.2	0.4	0.5	0.6	0.8	0.9	1	1.2	0.3	0.7
-1.7	18	0.3	0.5	0.4	1.0	0.5	0.7	0.8	0.3	0.7	1.1	1.0	0.3	0.4	0.5	0.7	0.8	0.9	1	0.2	0.6
-0.4	19	1.4	2.5	2.0	4.5	2.3	3.5	3.7	1.5	3.1	5.2	4.7	1.5	2.0	2.4	3.4	3.6	4.0	4.7	1	2.8
-1.0	20	0.5	0.9	0.7	1.6	0.8	1.3	1.3	0.5	1.1	1.9	1.7	0.5	0.7	0.9	1.2	1.3	1.4	1.7	0.4	1

1- Green denotes ratio higher than one. Red denotes lower than one ratio.
2- Heating Demand 2010-2045 for RCP 4.5

A.2.2. Analysis of Variance (ANOVA)

I used a simple analysis of variance (ANOVA) to compare the effect of the GCM (treatment) on the demand metric (response variable). When the effect of the treatment applies to more than one factor, it is appropriate to extend the ANOVA to account for the combined effect of such treatment on the response variable. The simplest extension is a two-way ANOVA model without interactions, but these interactions could also be checked.

In our study, I aim to measure if the effect of the models and the effect of the year on the demand metric are significant. The results show that there is evidence of a significant effect of the two treatments (GCM and Year) in the demand change of the two metrics by 2045 and 2095 with extremely low p-values. Table A.13 summarizes these p-values for the two RCP scenarios.

Table A.13. ANOVA probability values (p-values) for treatment effects by 2045 and 2095 per RCP

Metric	2010 to 2045		2010 to 2095	
	RCP 8.5	RCP 4.5	RCP 8.5	RCP 4.5
Cooling	5E-77	1E-59	0	2E-195
Heating	2E-45	2E-32	0	6E-141

For the ANOVA model to be consistent, it is important to verify the relevant model assumptions. Thus, I checked for normality of the residuals of the model through histograms of residual plots and QQ-plots. Histograms show that the residuals are a close approximation to the normal distribution for heating but not as much for cooling with big upper tails. This same trend is observed in the normal Q-Q plots, with heating demand being close to normal, but with cooling demand diverging from the linear assumption. Figure A.1 and Figure A.2 show these results. Given these results, I need an additional test to account for possible correlation for the time series data, which I do through an analysis of covariance (ANCOVA).

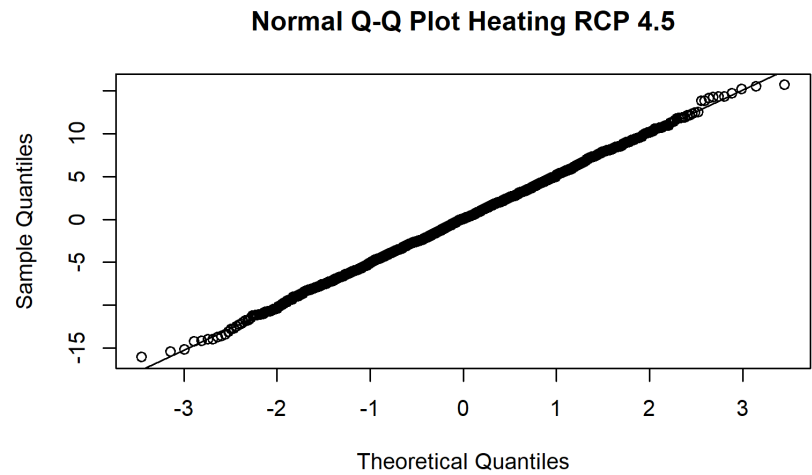
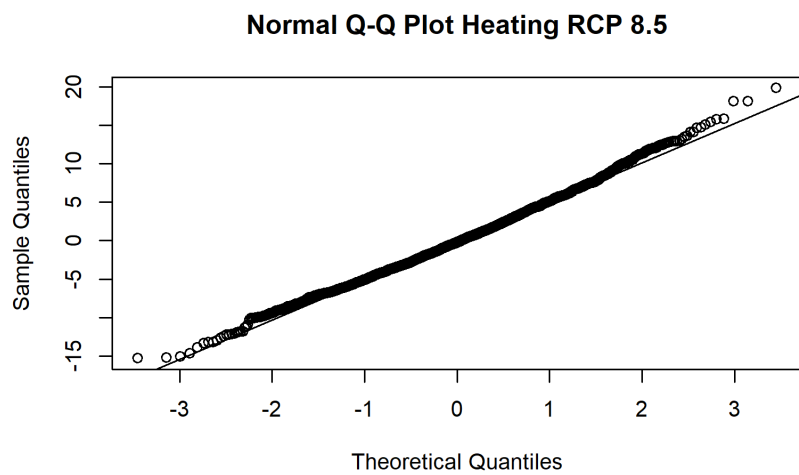
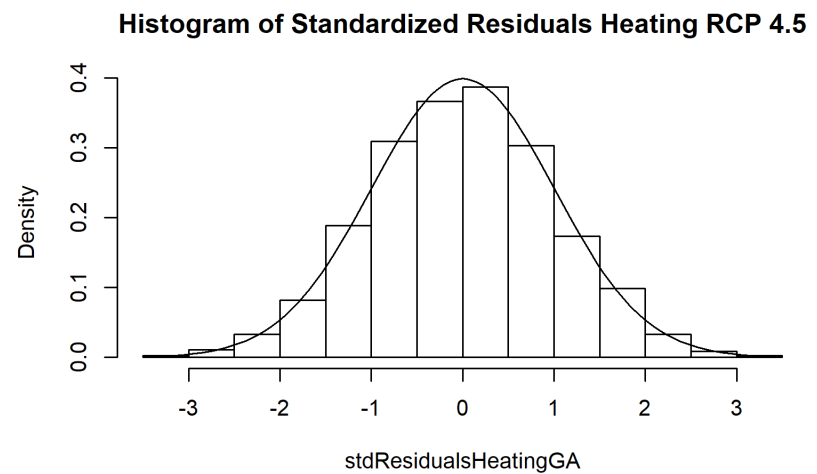
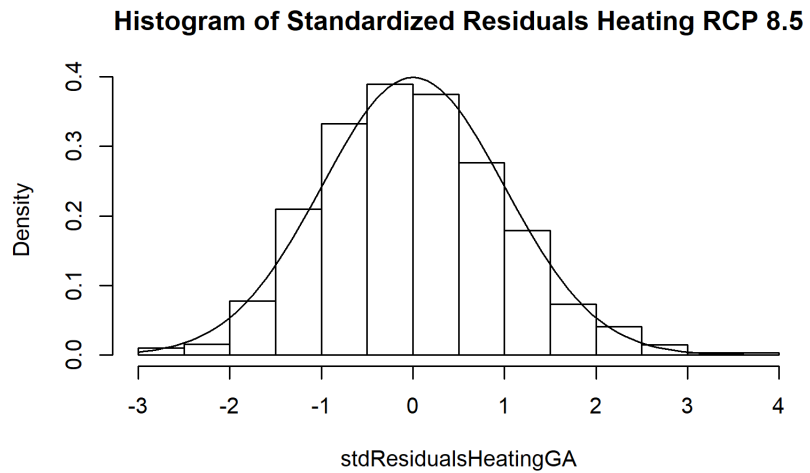
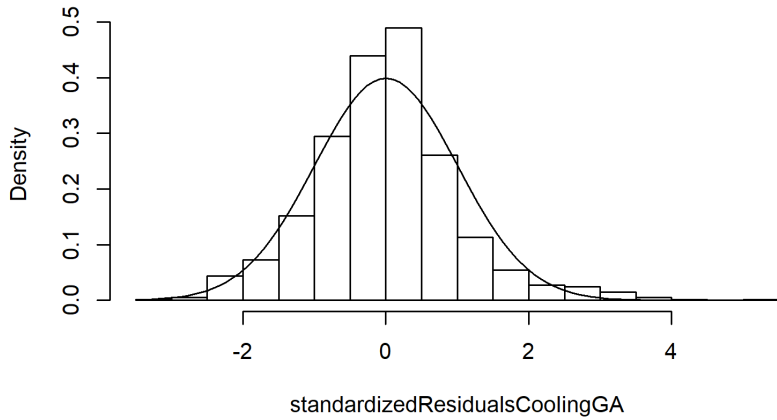
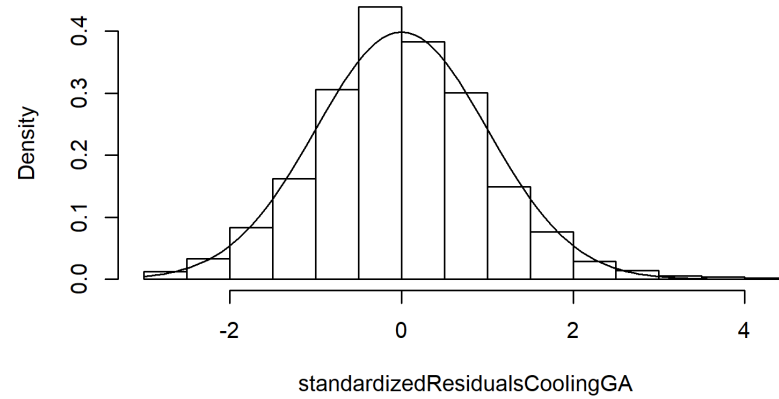


Figure A.1. Histogram of Standardized Residuals and Normal Q-Q Plots for Heating Demand for climate change scenarios RCP 8.5 and RCP 4.5.

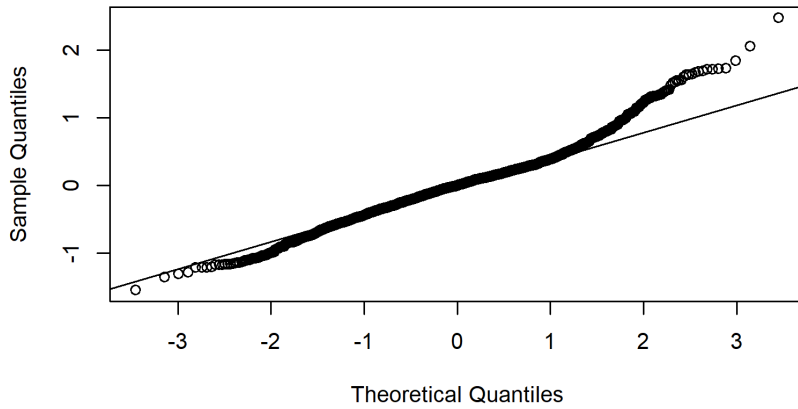
Histogram of Standardized Residuals Cooling RCP 8.5



Histogram of Standardized Residuals Cooling RCP 4.5



Normal Q-Q Plot Cooling RCP 8.5



Normal Q-Q Plot Cooling RCP 4.5

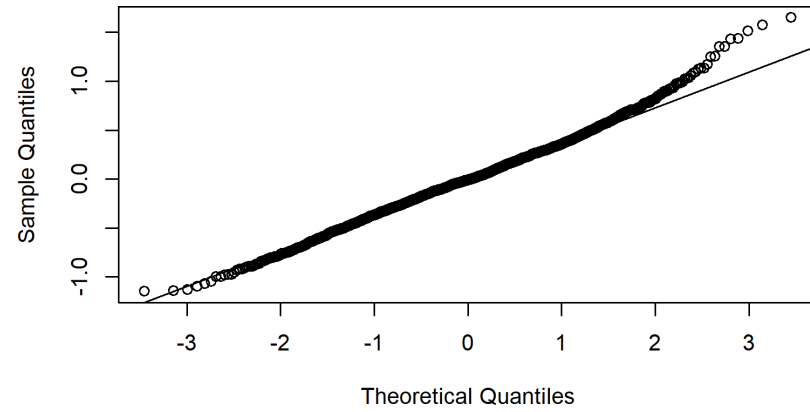


Figure A.2. Histogram of Standardized Residuals and Normal Q-Q Plots for Cooling Demand for climate change scenarios RCP 8.5 and RCP 4.5. Note the big upper tail on both RCPs.

A.2.3. Analysis of Covariance (ANCOVA)

To round off the significance analysis, I performed an additional check for autocorrelated data using an analysis of covariance (ANCOVA) test to compare the difference between slopes of multiple general circulation models (GCM). Here the treatments are the twenty GCMs, the independent variable is the Year, and the dependent variable is the demand metric. To be consistent with our previous analyses, I performed the analysis for two periods: 2010 to 2095 and 2010 to 2045.

The results show that models and years have a significant effect on the demand change of heating and cooling. For the two climate scenarios and the two response variables, p-values of the years are all below 10^{-13} , while p-values of the models are all below 10^{-29} . These results show that there is evidence of a significant effect of the year in the demand change of heating and cooling by 2045 and 2095. Table A.14 shows the percent of the variability in the response variable explained and unexplained by the model.

Table A.14. Percent of the variability of heating and cooling (response variables) explained by the linear model within periods 2010-2045 and 2010-2095 for RCP 8.5 and RCP 4.5

Metric	2010 to 2045				2010 to 2095			
	RCP 8.5		RCP 4.5		RCP 8.5		RCP 4.5	
	Heating	Cooling	Heating	Cooling	Heating	Cooling	Heating	Cooling
Explained	40%	56%	35%	50%	77%	84%	48%	59%
Unexplained	60%	44%	65%	50%	23%	16%	52%	41%

A.2.4. Validation of Results

As a validation exercise, I compared our results with the results of a study at the Poultry House Evaluation Service (PHES) of the University of Kentucky. In such study, researchers evaluated the energy consumption of 20 farms in the state of Kentucky [71]. This study reported a range of propane consumption for heating of 3.8-9.0 gallons per thousand pounds of live weight, with an

average of 5.9 gals/1,000 lbs. In our study, I found an average annual propane consumption of about 5 gals/1,000 lbs. of live weight. For electricity, the PHES reported values for total electricity usage but not for ventilation alone. Considering that about 50% of the total electricity used in a typical broiler house is for ventilation alone [94], I adjusted the PHES values for electricity used in ventilation to 13-29 kWh per thousand pounds of live weight, with an average of 19 kWh/1,000 lbs. In our study, I found average annual electricity for ventilation consumption of about 19 kWh/1,000 lbs.

A.2.5. Energy Demand for Heating and Cooling

Figure A.3 shows the change in annual average HVAC energy consumption per 1,000 chickens produced in 2095 w.r.t. 2018 for 22 poultry-producing states and per RCP scenario. These estimates rely on the annual average energy consumption per broiler house from the thermodynamic simulations reported in Figure 2 in the main paper. I note that energy changes were about one order of magnitude greater for RCP 8.5 than for RCP 4.5. Table A.15 includes the coordinates of the 12x12 km-cells used in our simulation and its corresponding state-level 2017 broiler production, as reported by the U.S. Department of Agriculture (USDA).

In general, the magnitude of energy changes for heating, cooling, and total energy were greater in RCP 8.5 than in RCP 4.5 for most states. This means, for instance, that the state with the smallest change in energy for cooling in RCP 8.5 was higher in magnitude than the state with the largest change in energy for cooling in RCP 4.5. However, this was not the case for heating. The highest reduction in energy for heating by 2095 w.r.t. 2018 in RCP 4.5 occurred in Minnesota with an average decrease of 2 gal per thousand pounds of broiler weight produced. While in the RCP 8.5 simulation, nine states (i.e., AL, AR, DE, GA, KY, MS, NC, SC, TN) had a smaller

reduction in energy for heating (i.e., <2 gal/1,000 lb broiler weight) than Minnesota RCP 4.5. This result indicates that increased temperatures may indeed lead to substantial reductions in energy consumption in northern latitudes, even in case of moderate climate-induced changes.

Propane consumption changes by 2095 w.r.t. 2018 were consistent among RCPs, with highest energy changes occurring in the Northern states of Minnesota, Wisconsin, and Michigan. Under RCP 4.5, the magnitude of these changes stem between 0.6 and 1.1 gal/1,000 lb of broiler weight in Southern states under RCP 4.5; and from 1 to 2 gal/1,000 lb of broiler weight produced in Northern states. Under RCP 8.5, the magnitude of reductions in propane consumption ranged between 1.2 and 2.2 gal/1,000 lb of broiler weight in Southern states, and from 2 to 4 gal/1,000 lb of broiler weight produced in Northern states.

In the other hand, energy for cooling changes in 2095 w.r.t 2018 were not as consistent among RCPs as heating and had smaller variability than heating. Under RCP 4.5, the largest change in energy demand for cooling occurred in Iowa, Illinois, and Missouri, with increases of roughly 2.0 kWh per 1,000 lb of broiler weight produced. Under RCP 8.5, the increase in energy for cooling was substantially larger than under RCP 4.5. The largest changes occurred in Arkansas, Missouri, and Mississippi, with increases of roughly 5.0 kWh per 1,000 lb of broiler weight.

Total energy changes were dominated by reductions in energy for heating, leading to total reductions in HVAC energy demand in all states. In total, the magnitude of energy reductions by late century w.r.t. 2018 under RCP 4.5 were between 50 and 75 kJ/1,000 lb of broiler weight in Southern states, and about 100 to 190 MJ/1,000 lb of broiler weight in Northern states. Under RCP 8.5, the magnitude of these reductions by 2095 w.r.t. 2018 ranged from 100 to 180 kJ/1,000

lb of broiler weight in Southern states, and from 200 to 370 kJ/1,000 lb of broiler weight in Northern states.

By comparison, the average U.S. household used 10.4 MWh of electricity (for all end-uses) per year in 2017. Similarly, the average household with space heating in the US (118 million households) used 36 GJ of energy for space heating in 2015 [95].

Figure A.4 shows that the ratio of total HVAC energy demand in 2095 w.r.t. 2018 is smaller than one in all major broiler-producing states. This means that the total energy demand decreases over time. These results suggest that Northern states (e.g., Minnesota, Wisconsin, Michigan) may see the largest percent reductions in energy for heating by 2095 w.r.t 2018. It also shows that the largest percent increases in energy for cooling will occur in Northern states. However, the results from Figure S3 suggest that Southern states (e.g., Arkansas, Mississippi, and Missouri) will see the largest magnitude of changes in energy for cooling occur in Southern

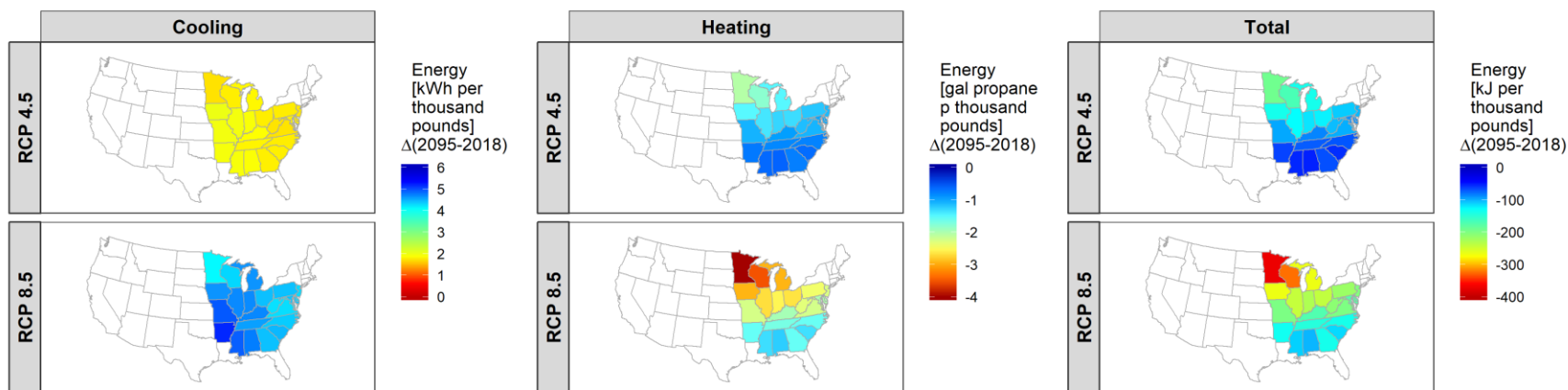


Figure A.3. Magnitude of change in average annual HVAC energy consumption per thousand pounds of broiler weight produced in 2095 with respect to 2018 on selected broiler-producing states. Note the different scales and units on the panels. Left-hand panel measures changes in electricity for cooling in kWh per 1,000 pounds of broiler weight. Middle panel measures changes in gallons of propane for heating per 1,000 pounds of broiler weight. Right-hand side panel measures changes of combined heating and cooling energy per 1,000 pounds of broiler weight. Note that the magnitude of energy changes is roughly twice as high for RCP 8.5 than for RCP 4.5 for most states.

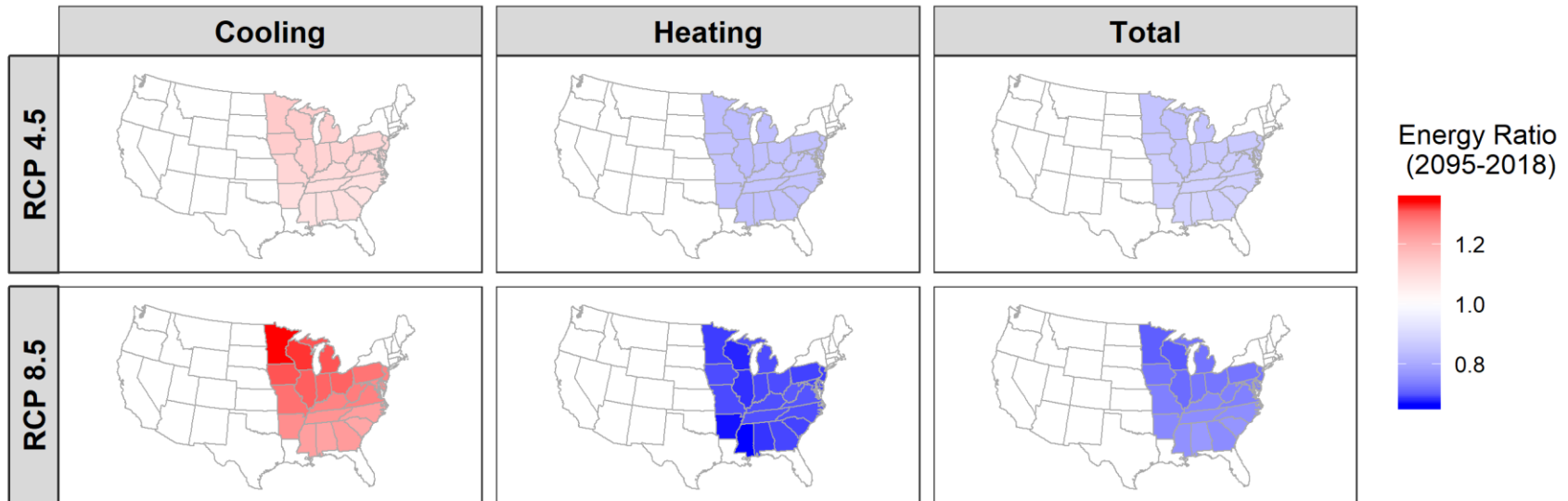


Figure A.4. Ratio of annual average HVAC energy consumption in 2095 with respect to 2018 in 22 major broiler-producing states across GCMs and RCPs. A ratio of one indicates no energy consumption difference between the two years. Note that energy for cooling ratios are all greater than one (increases) and energy for heating ratios are all smaller than one (decreases).

Table A.15. Simulated-cell location's coordinates and associated 2017 state-level broiler chicken production per reported by USDA.

State (Simulated-cell location)	Latitude	Longitude	State-level broiler production 2017 (thousand head)
Alabama (Montgomery)	32.38	-86.26	1,095,400
Arkansas (Little Rock)	34.70	-92.26	1,059,000
Delaware (Georgetown)	38.70	-75.38	259,800
Georgia (Gainesville)	34.30	-83.82	1,363,400
Illinois (Cook County)	41.75	-87.66	52,082
Indiana (Delphi)	40.58	-86.66	52,082
Iowa (Elkhart)	41.78	-93.47	52,082
Kentucky (Hardinburg)	37.77	-86.45	295,800
Maryland (Ruthsburg)	39.06	-75.96	306,700
Michigan (Ira Township)	42.72	-82.66	52,082
Mississippi (Pearl)	32.28	-90.10	59,700
Missouri (Jefferson City)	38.57	-92.19	741,100
Minnesota (Duluth)	46.08	-92.31	291,100
New Jersey (Chesterfield)	40.15	-74.63	52,082
North Carolina (Raleigh)	35.81	-78.63	830,800
Ohio (Riley Township)	41.36	-82.99	99,300
Pennsylvania (Harrisburg)	40.28	-76.87	185,200
South Carolina (Columbia)	34.01	-80.95	243,100
Tennessee (Shelbyville)	35.49	-86.45	171,500
Virginia (Harrisonburg)	38.44	-78.87	277,400
West Virginia (Moorefield)	39.06	-78.96	86,100
Wisconsin (Brown County)	44.28	-88.07	53,800

A.2.6. The effect of insulation and bird density on HVAC demand under climate change

I performed a parametric study modeling 30 years of energy demand for various levels of insulation, energy (electricity and propane) prices, and broiler house sizes. I compared two house sizes: the most common broiler house size in the U.S. with 440-ft length per 42-ft wide [45], and the largest modern size of 700-ft x 66-ft. I assumed 5.5 batches per year [45], chicken density of 1.1 birds per square foot [46], insulation replacements every 10 years with commercial insulation prices, and a 7% discount rate. I assumed a constant average price for electricity and propane over the 30 years but performed a parametric analysis for different average prices based on

values from EIA's Annual Energy Outlook 2019 [96]. This analysis aims to identify the potential value of insulation. However, the effectiveness of adding insulation will depend on the specific characteristics of the production system used in each broiler house.

Figure A.5 shows that the net present costs (NPC) of combined energy and insulation are higher for lower levels of insulation (i.e., lower levels of R), with the highest cost-effectiveness around insulation levels between R-11 and R-19. Interestingly, the energy price combination depicted as 'price 1' (electricity price doubling propane price) yields the lowest NPC for both house sizes. This is an intuitive result due to the much higher demand for heating than for cooling in broiler houses. Then, the regional pricing of fuels, which will depend on future market conditions and are highly uncertain, could substantially influence the energy bills of farmers.

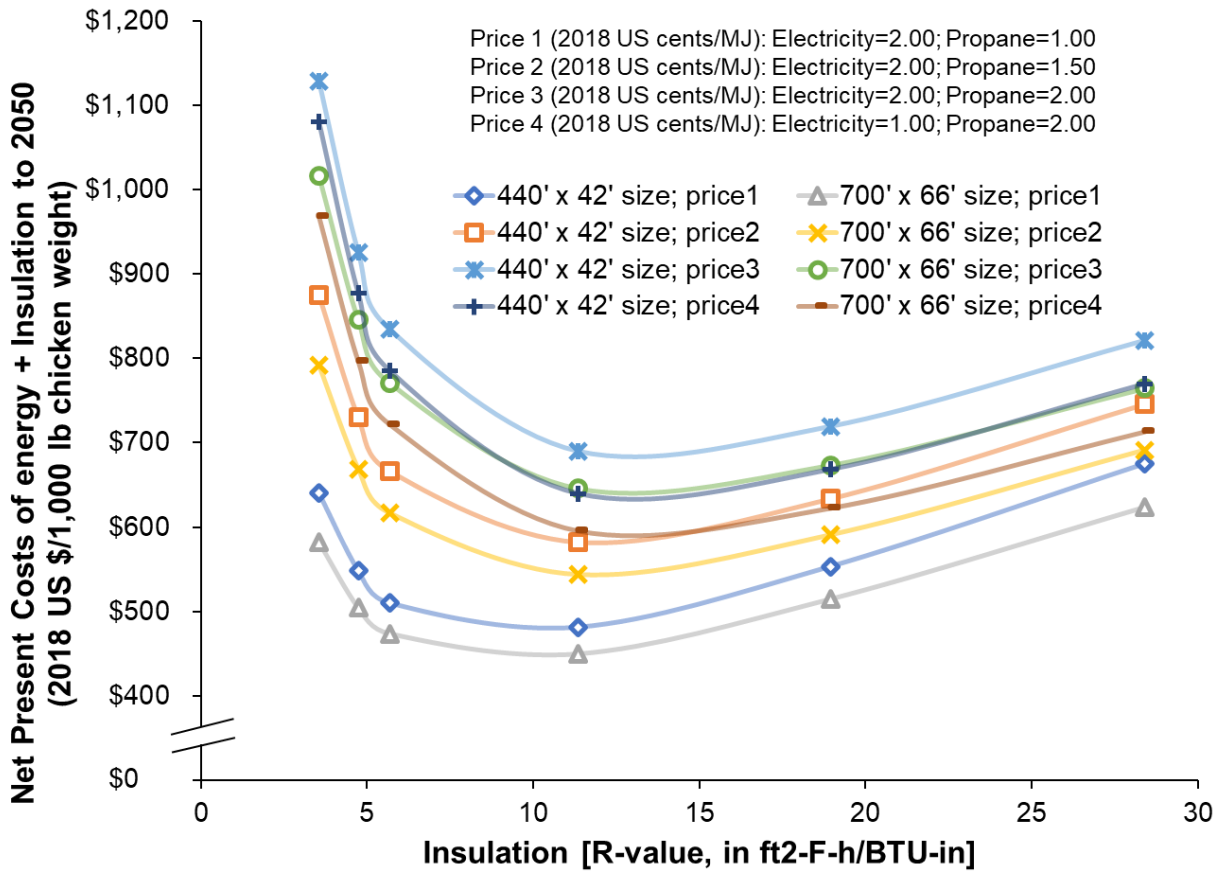


Figure A.5. Estimated net present costs (NPC) of operational energy costs at varying insulation levels from 2018 to 2050 for two broiler house sizes. The horizontal axis depicts the insulation value, R, in English units. Note that the lowest level of insulation depicted, R-4, implies no insulation. The vertical axis shows the net present costs of energy and insulation combined to 2050 in 2018 US\$ per thousand pounds of broiler weight produced. The 440' x 42' house represents the most common house size, housing around 20,000 chickens per batch. The 700' x 66' house represents a modern size with about 50,000 chickens per batch. The energy prices (for electricity and propane) are varied parametrically to represent possible future scenarios. The current pricing in the U.S. is closer to price 2, with the price of electricity around US \$0.020/MJ and the price of propane around US \$0.015/MJ [96].

Appendix B. Supplemental Information for Chapters 3 and 4

B.1. Materials and methods

B.1.1. AquaCrop model

B.1.1.1. Crop Data

The low-yield cultivars (LY) relied on literature values that resembled small-scale farmers' traditional nature in each country. Beans LY used the calibrated default crop file from AquaCrop with a few modifications to the phenology and the maximum canopy cover (CCx) parameters after studies by Yuan et al. [174] and Zeleke [175]. Maize LY relied on data by Akumaga et al. [176] in Nigeria, Shrestha et al. [177] in Nepal, and Zinyengere et al. [178] in Zimbabwe. Onion LY is one of four crop varieties (all traditional cultivars) modeled in calendar mode following the parameters described in Agbemabiese et al. [127], with modifications from Karuku & Mbindah [179]. Potato LY is another crop variety modeled in calendar mode using as a base the default crop file from AquaCrop for Lima, Peru, and modified after the parameters described in Yuan et al. [174]. Teff LY is the last variety with phenology in calendar mode, with modifications of AquaCrop's default crop file after studies by Araya et al. [180] in Ethiopia. Tomato LY is the last variety with phenology parameters modeled in calendar mode after the studies by Darko et al. [181] and Linker et al. [182]. Finally, I modeled wheat LY with crop files modifications after Andarzian et al. [183] in Iran. Table B.1 depicts the nonconservative characteristics used in our model for the low-yield varieties.

Table B.1. Nonconservative characteristics of small-scale, low-yield crop varieties, as used in AquaCrop.

Nonconservative parameters	Beans	Maize	Onion	Potato	Teff	Tomato	Wheat
Phenology (growing degree days from sowing, GDD)							
Emergence	91	77	20*	37*	13*	7*	284
Maximum rooting to depth	1162	694	86*	108*	54*	80*	1178
Senescence	1162	1024	80*	113*	85*	100*	1372
Maturity	1727	1359	100*	125*	96*	131*	2040
Flowering or tuber formation	751	716	47*	72*	57*	91*	1277
Flowering length	301	354	-	-	16*	11*	140
Length build-up Harvest Index	879	643	31*	51*	35*	32*	763
Crop Growth							
Plant Density (plants/m ²)	13.2	5.3	26.6	5.0	1000	6.0	4.5
Maximum rooting depth (m)	1.7	1.0	1.0	1.3	0.6	0.8	1.5
Water productivity for ET ₀ and CO ₂ , WP* (g/m ²)	15	33.7	33.7	18	20	17	15
Canopy Growth Coefficient, CGC (%/GDD)	0.74	1.07	16.6*	13.9*	9.9*	11.0*	0.54
Canopy Decline Coefficient, CDC (%/GDD)	0.60	1.05	8.0*	14.5*	16.2*	8.0*	0.4
Maximum Canopy Cover, CC _x (%)	85	75	70	76	80	55	95
Reference Harvest Index, HI ₀ (%)	40	40	70	75	25	50	40
Fertility Stress							
Potential biomass production (%)	51	40	50	50	50	51	50
Reduction canopy expansion				Strong			
Average CC _x decline (%/day)	0.25	0.30	0.09	0.11	0.43	0.14	0.43
Planting dates							
Rainy-Dry Ethiopia				June 1 – October 15			
Rainy-Dry Rwanda				September 15 – May 1			
Rainy-Dry Uganda				March 15 – November 10			
1 – A star (*) besides a number denotes parameter evaluated in calendar <i>day</i> instead of <i>GDD</i>							

For the characterization of high-yield (HY) cultivars, I sought to build crop files that resembled improved-seed varieties maximizing yields. Beans HY hinged on the characteristics described in Magalhães et al. [184] in Brazil. For maize HY, I used the default AquaCrop file calibrated for Davis, California, and modified heavily with the phenology described in Katerji et al. [185] for Foggia, Italy. For onion HY, I created the crop file using the parameter values described by Pérez-Ortolá et al. [186]. For potato HY, the crop file relied on studies by Montoya et al. [187] in Spain with slight modifications from Yuan et al. [174]. I modeled teff HY in GDD mode

following the characteristics described by Haileselassie et al. [188] in Ethiopia. Similarly, I modified AquaCrop's default tomato with the calibrated features described by Katerji et al. [185] to construct tomato HY. Finally, I adjusted the wheat HY crop file characteristics following the study by Kale Celik [189] in Turkey. Table B.2 shows the nonconservative parameters of improved, high-yield cultivars.

Table B.2. Nonconservative characteristics of improved, high-yield crop varieties, as used in AquaCrop.

Nonconservative parameters	Beans	Maize	Onion	Potato	Teff	Tomato	Wheat
Phenology (growing degree days from sowing, GDD)							
Emergence	100	72	60	332	48	165	123
Maximum rooting to depth	968	1406	347	969	460	1013	780
Senescence	1254	1392	1263	1468	864	1590	1768
Maturity	1548	1660	1450	2324	1032	1935	2605
Flowering or tuber formation	875	840	816	589	565	705	1320
Flowering length	200	162	-	-	280	720	179
Length build-up Harvest Index	515	810	550	1735	387	810	1209
Crop Growth							
Plant Density (plants/m ²)	15.0	5.0	50	5.9	200	3.3	4.3
Maximum rooting depth (m)	1.7	1.0	0.4	0.6	0.6	0.6	1.5
Water productivity for ET ₀ and CO ₂ , WP* (g/m ²)	15	33.7	19	19	31	18	15
Canopy Growth Coefficient, CGC (%/GDD)	1.01	1.31	0.95	1.2	1.17	0.76	0.44
Canopy Decline Coefficient, CDC (%/GDD)	0.68	1.0	0.54	0.27	1.42	0.4	0.35
Maximum Canopy Cover, CC _x (%)	90	90	65	96	81	80	80
Reference Harvest Index, HI ₀ (%)	40	46	80	82	27	60	40
Fertility Stress							
Potential biomass production (%)	51	52	50	53	50	50	51
Reduction canopy expansion				Strong			
Average CC _x decline (%/day)	0.08	0.11	0.06	0.11	0.3	0.07	0.18
Planting dates							
Rainy-Dry Ethiopia				June 1 – October 15			
Rainy-Dry Rwanda				September 15 – May 1			
Rainy-Dry Uganda				March 15 – November 10			
1 – A star (*) besides a number denotes parameter evaluated in calendar <i>day</i> instead of <i>GDD</i>							

B.1.1.2. *Field Management Strategy: Irrigation Deficit*

I set the irrigation deficit strategy such that the root zone depletion does not drop more than 25% of the readily available soil water (RAW). RAW is the range between the amount of water at field capacity (or 0%) and the amount of water at threshold for stomatal closure (or 100%). I chose this level of irrigation in order to maximize water productivity [126], [146] as full irrigation may lead to diminishing returns.

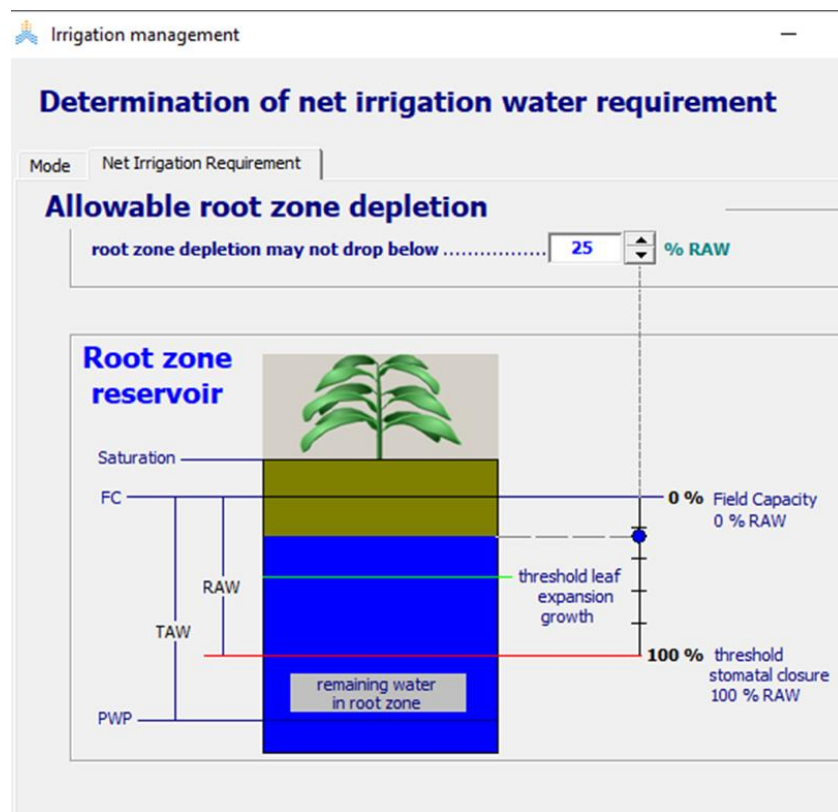


Figure B.1. Deficit irrigation strategy with root zone depletion not dropping more than 25% of the readily available soil water (RAW). Note that % RAW is a range between field capacity and the threshold to stomatal closure. (Screenshot from AquaCrop standalone version 6.0).

B.1.1.3. Simulations with AquaCrop

My model simulated crops in GDD and calendar mode using the centroid coordinate points and elevation above sea level of each of the 690 woredas (districts) in Ethiopia, the 30 districts in Rwanda, and the 80 districts in Uganda. Table B.3 and Table B.4 show the description of the coordinates, the elevation, and the depth to groundwater values used.

Table B.3. Coordinate points, elevation above sea level, and depth to groundwater for Rwanda's districts.

District	Latitude	Longitude	Elevation (m)	Average depth to groundwater (m)
Bugesera	-2.24	30.15	1429	11.1
Burera	-1.47	29.83	2097	11.7
Gakenke	-1.7	29.78	1747	9.8
Gasabo	-1.89	30.14	1748	11.8
Gatsibo	-1.62	30.45	1434	11.6
Gicumbi	-1.62	30.11	2087	12.3
Gisagara	-2.62	29.84	1601	8.4
Huye	-2.52	29.71	1676	8.2
Kamonyi	-2.01	29.9	1717	12.0
Karongi	-2.16	29.43	2068	12.4
Kayonza	-1.85	30.64	1307	11.0
Kicukiro	-2.01	30.14	1408	11.8
Kirehe	-2.23	30.71	1469	10.8
Muhanga	-1.95	29.72	1699	10.0
Musanze	-1.5	29.61	1923	9.3
Ngoma	-2.18	30.46	1397	10.8
Ngororero	-1.88	29.57	2128	12.0
Nyabihu	-1.65	29.51	2382	12.1
Nyagatare	-1.34	30.38	1405	9.4
Nyamagabe	-2.41	29.47	2252	9.8
Nyamasheke	-2.37	29.17	1583	12.1
Nyanza	-2.34	29.79	1583	10.3
Nyarugenge	-1.99	30.03	1686	3.5
Nyaruguru	-2.69	29.52	1920	9.2
Rubavu	-1.65	29.34	1972	12.9
Ruhango	-2.19	29.77	1764	10.4
Rulindo	-1.74	29.99	1924	10.7
Rusizi	-2.57	29.09	1518	11.3

Rutsiro	-1.9	29.4	2166	13.5
Rwamagana	-1.98	30.35	1513	15.4

Table B.4. Coordinate points, elevation above sea level, and depth to groundwater for Uganda's districts

District	Latitude	Longitude	Elevation (m)	Average depth to groundwater (m)
Abim	2.75	33.73	1250	8.1
Adjumani	3.23	31.77	847	7.3
Amolatar	1.62	32.74	1054	14.2
Amuria	2.10	33.69	1124	5.1
Amuru	2.75	31.90	1001	7.0
Apac	1.99	32.62	1042	8.8
Arua	2.87	31.13	773	7.2
Budaka	1.06	33.99	1128	8.3
Bududa	1.05	34.40	1836	5.1
Bugiri	-0.16	33.80	1137	13.9
Bukedea	1.36	34.13	1076	6.3
Bukwo	1.27	34.68	2279	4.2
Buliisa	1.96	31.39	618	11.3
Bundibugyo	0.89	30.25	887	10.2
Bushenyi	-0.42	30.14	1409	10.2
Busia	0.41	34.01	1203	8.8
Butaleja	0.88	33.93	1078	5.9
Dokolo	1.94	33.08	1039	8.3
Gulu	2.83	32.43	1051	6.7
Hoima	1.44	31.07	1092	11.2
Ibanda	-0.08	30.49	1397	7.1
Iganga	0.73	33.45	1117	8.1
Isingiro	-0.85	30.88	1394	8.2
Jinja	0.56	33.21	1127	9.0
Kaabong	3.61	34.03	1435	9.6
Kabale	-1.22	29.98	2053	13.5
Kabarole	0.60	30.29	1490	9.5
Kaberamaido	1.76	33.22	1049	11.2
Kalangala	-0.58	32.38	1133	15.9
Kaliro	1.07	33.48	1054	10.9
Kampala	0.32	32.60	1170	13.9
Kamuli	1.12	33.13	1049	11.6
Kamwenge	0.23	30.49	1565	7.6
Kanungu	-0.81	29.73	1307	7.4

Kapchorwa	1.41	34.53	2031	5.4
Kasese	0.12	30.00	1529	13.5
Katakwi	1.92	34.04	1063	9.1
Kayunga	0.97	32.89	1069	11.7
Kibaale	0.95	31.07	1141	9.2
Kiboga	1.01	31.77	1145	7.2
Kiruhura	-0.22	30.87	1343	9.0
Kisoro	-1.22	29.68	1751	13.9
Kitgum	3.49	32.96	1047	7.1
Koboko	3.53	31.01	1184	4.5
Kotido	3.03	33.98	1249	6.5
Kumi	1.48	33.88	1137	10.0
Kyenjojo	0.57	30.81	1275	6.7
Lira	2.35	33.21	1052	6.7
Luwero	0.83	32.58	1124	8.5
Lyantonde	-0.22	31.19	1313	9.3
Manafwa	0.89	34.34	1407	7.7
Maracha (nyadri)	3.19	31.10	955	5.0
Masaka	-0.36	31.72	1222	13.0
Masindi	1.88	31.87	1114	7.5
Mayuge	-0.09	33.55	1136	14.7
Mbale	1.02	34.20	1207	8.9
Mbarara	-0.57	30.57	1410	9.9
Mityana	0.44	32.06	1252	10.1
Moroto	2.50	34.39	1189	7.3
Moyo	3.53	31.67	678	9.1
Mpigi	0.14	31.94	1196	11.3
Mubende	0.52	31.54	1267	6.9
Mukono	-0.22	33.08	1136	14.5
Nakapiripirit	1.86	34.65	1191	7.5
Nakaseke	1.05	32.17	1080	6.6
Nakasongola	1.35	32.43	1087	7.9
Namutumba	0.87	33.68	1114	9.8
Nebbi	2.48	31.16	981	7.3
Ntungamo	-0.94	30.28	1419	12.0
Oyam	2.37	32.49	1056	7.6
Pader	2.92	33.12	1042	9.0
Pallisa	1.17	33.76	1075	10.5
Rakai	-0.77	31.52	1167	11.7
Rukungiri	-0.71	29.89	1342	9.2
Sironko	1.29	34.35	1485	3.8
Soroti	1.61	33.46	1055	13.1
Ssembabule	-0.03	31.34	1228	9.3

Tororo	0.73	34.08	1144	6.5
Wakiso	0.22	32.45	1226	12.2
Yumbe	3.52	31.29	902	4.7

B.1.2. Irrigation model

I calculate the total dynamic head (*TDH*) as the sum of the pumping lift, friction losses, pump operating pressure, and change in elevation, as described by Duke [136] and Fipps [137].

$$TDH = (\text{pumping lift}) + (\text{friction loss}) + (\text{op. pressure}) + (\text{elevation}) \quad (\text{Eq. B.1})$$

The first term, *pumping lift*, refers to the vertical distance from the water level in the well to the pump outlet during pumping. I assume that the pumping lift is equal to the estimated depth to the groundwater table. The *friction losses* and *operating pressure* terms refer to the pipe specifications and the system's design. Elements considered in the calculation of total dynamic head are the pipe diameter, the type of fittings (e.g., valves, elbows, length), the pipe material, the horizontal distance of the pipe to the column and the pivot, the system flow rate and the operating pressure of the pump. The fourth term, *elevation*, refers to the vertical distance from the pump discharge to the irrigation location. Table B.5 shows the assumptions used to run the irrigation water pumping model.

Table B.5. Parameter values used in the mathematical formulation of the model to estimate electricity demand for pumping. Assumed and calculated values after Fipps (2017).

Parameter	Value
Mainline pipe diameter and material (assumed)	0.1 m plastic (4 in)
Pump column pipe diameter and material (assumed)	0.15 m steel (6 in)
Friction losses in well casing (Fipps, 2017)	0.67 m/30.5-m pipe
Friction losses in horizontal mainline (Fipps, 2017)	2.19 m/30.5-m pipe
Volumetric flow rate (calculated after Fipps (2017))	25 L/s
Distance from pump to pivot (assumed)	1,220 m (40 x 30.5-m sections)
Operating pressure (assumed)	240 kPa

Types of fittings in the system (assumed)	Check valve, gate valve, two standard elbows
Pump efficiency (Fipps, 2017)	75%

B.1.2.1. Groundwater Data

The British Geological Survey (BGS) used high-resolution remotely sensed data to find the depth to groundwater, aquifer storage, and aquifer productivity to build a groundwater map of Africa. Like the geoprocessing I did for soil data, I clipped BGS's depth to groundwater (DTW) data to obtain the mean, minimum, and maximum depths for each district in each country. I used the mean data point of each district as an input for our model.

B.1.3. Hydrology model

The first part of the model assesses groundwater recharge (R) as the monthly mass water balance between precipitation (P), actual evapotranspiration (ET_a), and the change in soil moisture or soil-moisture storage (ΔS).

$$R = P - ET_a - \Delta S \quad (\text{Eq. B.2})$$

I developed a simplified hydrological model following the methods in Rodríguez-Huerta et al. (2020) and Alley et al. (1984). This model assumes a specific soil-moisture storage capacity, STC , with recharge occurring after the soil-moisture (S) reaches STC . I estimate STC or water holding capacity as the product of the available water capacity (AWC) and the root depth of vegetation (RDV) [190].

$$STC = AWC * RDV. \quad (\text{Eq. B.3})$$

The next step is to calculate the available water capacity (AWC) by subtracting the amount of water in the soil at permanent wilting point (PWP) from the amount of water at field capacity (FC) (British Columbia Ministry of Agriculture, 2015). As described in section 2.1.2. of the main manuscript, I calculated the amount of water at FC and PWP using the pedotransfer functions from Saxton et al. [124].

$$AWC = FC - PWP \quad (Eq. B.4)$$

The actual evapotranspiration (ET_a) depends on the precipitation (P), the reference evapotranspiration (ET_o), and the soil-moisture (S) of each month. I calculated ET_o using FAO's Penman-Monteith equation [130], [146] using the same agrometeorological data retrieved from NASA POWER for AquaCrop's simulation. For any month i , if $P_i \geq ET_{o_i}$,

$$ET_{a_i} = ET_{o_i} \quad (Eq. B.5)$$

$$\Delta S_i = S_i - S_{i-1} \quad (Eq. B.6)$$

$$S_i = \min \{P_i - ET_{o_i} + S_{i-1}, STC\} \quad (Eq. B.7)$$

$$S_{i-1} = S_{i-1} * \exp\left(\frac{P_i - ET_{o_i}}{STC}\right) \quad (Eq. B.8)$$

The model assumes that monthly groundwater recharge (ΔR) occurs when P exceeds ET_o , and S is equal to STC . Otherwise, ΔR is zero. For any month i ,

$$\Delta R = \begin{cases} (P_i - ET_{o_i}) - (STC - S_{i-1}), & \text{if } P_i \geq ET_{o_i} \text{ and } S_i = STC \\ 0, & \text{otherwise} \end{cases} \quad (Eq. B.9)$$

This formulation assumes that the initial soil-moisture, S_0 , equals the soil-moisture storage capacity, STC [190]. Thus, the STC also serves as the baseline to initialize the calculation of the change in soil moisture between months. The following assumptions complete our model [140]:

- Recharge includes aquifers and non-aquifers and does not distinguish between them.
- The entire area of each district works as a recharge area.
- Land use and soil vegetation cover changes remain constant over the simulation period.
- The depth of root vegetation is constant at 750 mm (= 0.75 m).

Finally, the second part of the model measures water sufficiency by comparing the simulated irrigation from AquaCrop with our groundwater recharge estimates every year. This calculation requires the aggregation of the simulated irrigation over the dry and rainy seasons. However, it would be misleading to directly compare irrigation and recharge because irrigation occurs only on arable land, while groundwater recharges virtually over the entire surface of the country.

Then, I decided to assign weights to each variable to represent the ratio of arable land to the total surface area. Thus, I calculate the yearly water sufficiency (WS) through a weighted mass water balance of groundwater recharge (R) minus simulated irrigation (I) for year j .

$$WaterAvail_j = w_1 R_j - w_2 I_j \quad (Eq. B.10)$$

Roughly 15% of Ethiopia's area is arable land [143], so the ratio of arable land to total surface area is 1:6. Thus, I decided to allocate conservative weights for Ethiopia as $w_1 = 1$ and $w_2 = 1/5$. In Rwanda, about 50% of all the land area is arable land [144]. This ratio means that the weights for Rwanda are $w_1 = 1$ and $w_2 = 1/2$. While in Uganda, about 38% of total land area is arable land [145], which roughly represents a ratio of 1 to 3. Therefore, Uganda's weights are $w_1 = 1$ and $w_2 = 1/3$.

B.2. Additional Results

B.2.1. Demand for Inputs: Annual Electricity Requirements for Irrigation per Hectare

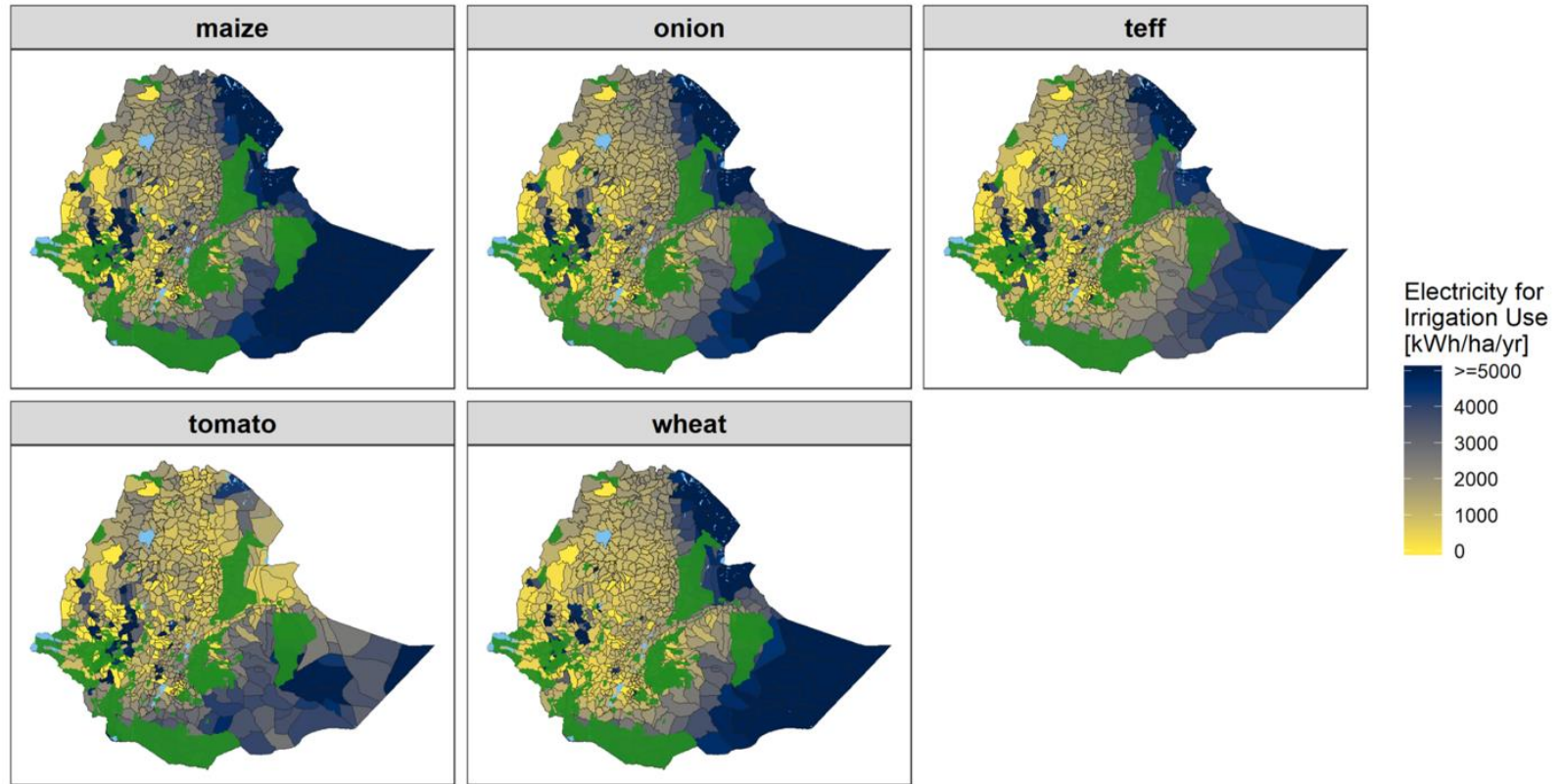


Figure B.2. Annual average electricity consumption for irrigation per hectare for five crops in Ethiopia. Green-filled areas represent protected areas not considered for agricultural production. Blue regions represent water bodies.

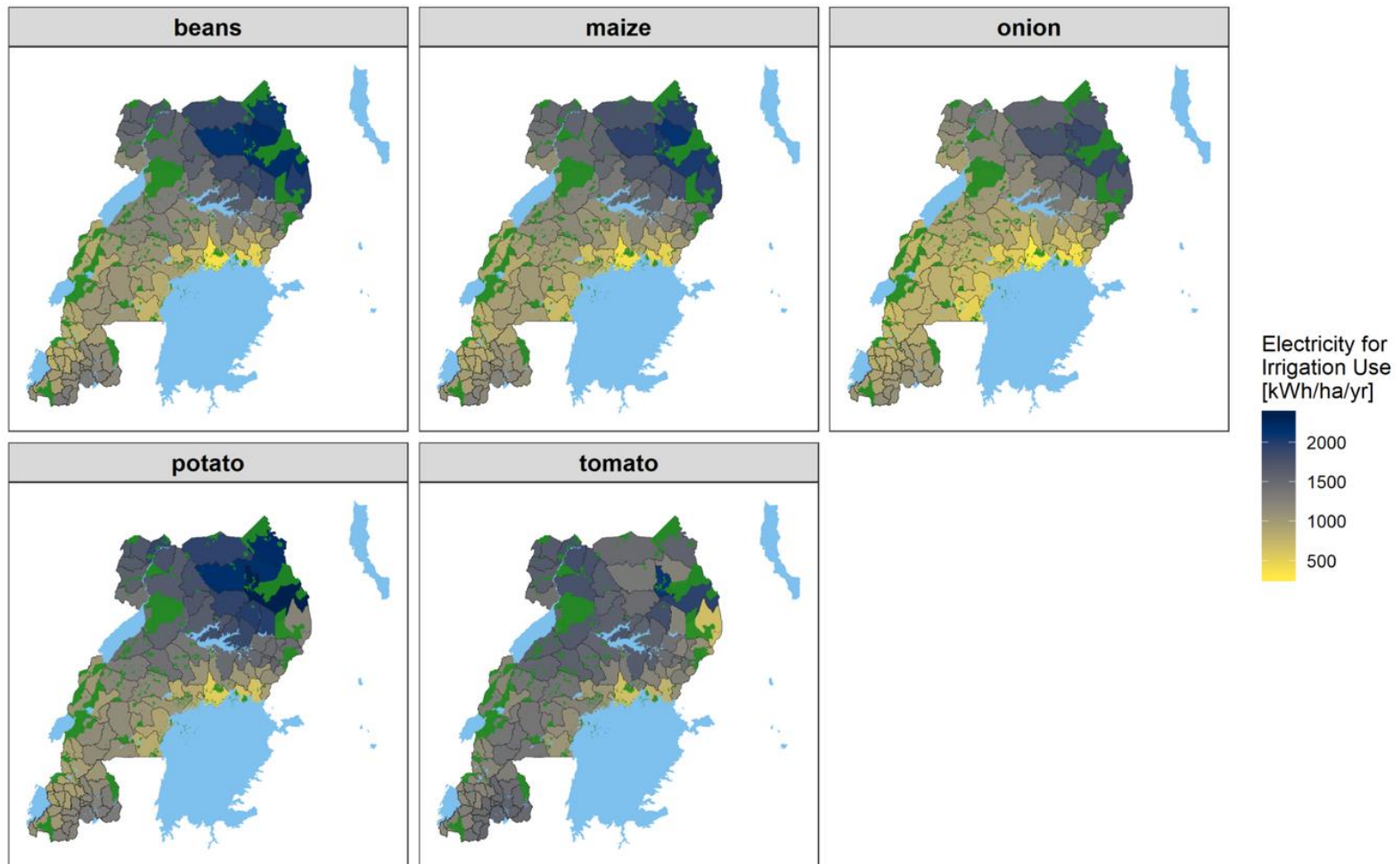


Figure B.3. Annual average electricity consumption for irrigation per hectare for five crops in Rwanda and Uganda. Green-filled areas represent protected areas not considered for agricultural production. Blue regions represent water bodies.

B.2.2. Hydrology model: Water Balance

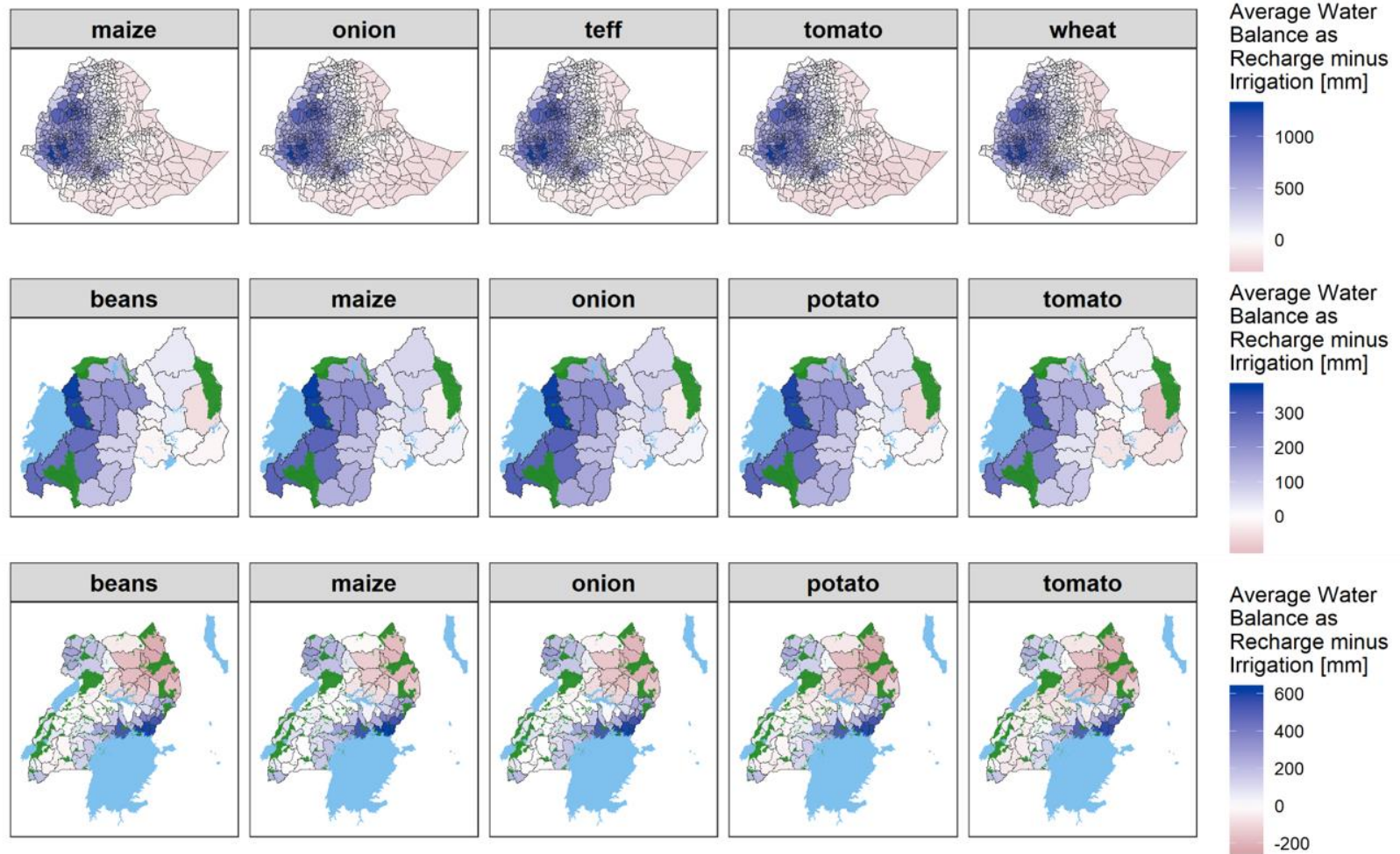


Figure B.4. Projected annual average water availability for Ethiopia (top row), Rwanda (middle row), and Uganda (bottom row). This water balance measures the weighted difference of water recharge minus simulated irrigation. Note that the size of the countries is not in the same geographical scale. Also, note that the ranges of our estimated average water values are different for each country.